12-2017

Live Load Distribution Factors and UHPC Shear Key Performance of SCDOT NEXT D Beam and Solid Slab Bridges

Francis Vincent Filosa
Clemson University

LIVE LOAD DISTRIBUTION FACTORS AND UHPC SHEAR KEY
PERFORMANCE OF SCDOT NEXT D BEAM AND SOLID SLAB BRIDGES

A Thesis
Presented to
the Graduate School of
Clemson University

In Partial Fulfillment
of the Requirements for the Degree
Master of Science
Civil Engineering

by
Francis Vincent Filosa
December 2017

Accepted by:
Thomas E. Cousins, Committee Chair
Brandon E. Ross
Weichiang Pang

ABSTRACT

For short to medium span bridges experiencing lower average daily traffic (ADT), the South Carolina Department of Transportation (SCDOT) currently utilizes both hollow core and solid slab precast concrete span bridge sections. The intended advantages of these bridge sections were that they could be built according to an accelerated bridge construction (ABC) schedule and have increased durability. Increasing a bridge's durability has economic advantages since they require less maintenance and have a greater lifespan.

Both the precast hollow core and solid slab spans have not met the SCDOT's durability requirements. Deterioration of the grout key between adjacent precast members has led to reflective cracking in both the bridge deck and bridge wearing surface. These cracks allow water and other corrosive materials to infiltrate the precast beam sections, and lead to the corrosion of the prestressing strands and reinforcement. Corrosion of prestressing leads to bridge repairs as well as a diminished life-span, both costly to the SCDOT.

Reflective cracking at the shear key also leads to a decreased ability for a bridge to share load among its adjacent members. Both hollow core and solid slab sections are designed to distribute load transversely across the bridge and longitudinally to the girder bearings. Individual girders resist only a portion of the loads on a bridge. If the shear key is degraded and its ability to share load lessened, a possible overload and catastrophic failure of a bridge member could occur.

These durability issues have proved to be problematic and have concerned the SCDOT. The SCDOT and Clemson University teamed up to conduct research in order to identify, modify, or develop a bridge type that was both more durable and could meet the schedule of ABC. The SCDOT and Clemson University settled on the northeast extreme tee (NEXT) beam, developed by the bridge technical committee of PCI Northeast.

The NEXT beam section is an advantageous bridge section for many reasons, including its geometric diversity, ability to meet an ABC schedule, utility accommodations, full deck option, and a wider shear key allowing for an easier concrete pour or grouting.

The NEXT beam cross section does not fall into an AASHTO LRFD category for simplified moment live load distribution factors. This project seeks to calculate live load distribution factors via live load test, and determine what, if any, category the NEXT section can fall under for simplified moment live load distribution factors. A future research project will assess the durability of the UHPC shear keys for both the NEXT D and solid slab span by monitoring the ability for girder sections to share load transversely over a period of two years. Results of this research will be given to the South Carolina Department of Transportation (SCDOT) so that they may be informed on how NEXT Beam transverse moment distribution behavior. Results on UHPC shear key performance and durability will also be given to the SCDOT.

ACKNOWLEDGMENTS

TABLE OF CONTENTS

TABLE OF CONTENTS (CONTINUED)

TABLE OF CONTENTS (CONTINUED)

TABLE OF CONTENTS (CONTINUED)

TABLE OF CONTENTS (CONTINUED)

TABLE OF CONTENTS (CONTINUED)

LIST OF TABLES

List of Tables (Continued)

List of Tables (Continued)

LIST OF FIGURES

List of Figures (Continued)

List of Figures (Continued)

List of Figures (Continued)

List of Figures (Continued)

List of Figures (Continued)

Chapter 1: Introduction

Every four years, the American Society of Civil Engineers (ASCE) produces a report card that grades America's infrastructure in sixteen different categories. Bridges are included within this report card. According to ASCE's 2017 report, of the 614,387 bridges in the United States, 9.1% are rated as structurally deficient (Bridges, 2017). Additionally, close to 40% of the nation's bridges are reaching their design life of 50 years. As many bridges approach the end of their design life, the report estimates that an additional $123 billion is needed for bridge rehabilitation projects. In the state of South Carolina, 964 of its 9,358 bridges are rated as structurally deficient. The Federal Highway Administration (FHWA) classifies a bridge as structurally deficient if "significant load carrying elements are found to be in poor condition due to deterioration" (Ahmad, 2011). When replacing these structurally deficient bridges, the state hopes that new technologies and materials can help build these bridges at an accelerated rate to promote safety and resilience so that longer design lives can be achieved.

For many of its bridges, The South Carolina Department of Transportation (SCDOT) commonly utilizes cast-in-place (CIP) construction, precast solid slab, or precast hollow core bridges. Hollow core bridge sections are precast prestressed concrete rectangular slabs with tubular voids located in the middle of the section that extend the length of the slab. Solid slab bridges are similar in shape and geometry to hollow core sections, but do not have the tubular voids. Time has shown that CIP bridges are durable, but have a long construction time. Hollow core flat slab bridges can be built according to

an accelerated bridge construction (ABC) schedule, however, several durability issues have occurred.

For short to medium span bridges carrying lower average daily traffic (ADT), SCDOT commonly implements either hollow core and solid slab precast concrete span bridge sections. The SCDOT has discovered that both the precast hollow core and solid slab spans present durability issues. As shown in figure 1, deterioration of the grout key between adjacent precast members has led to reflective cracking in both the bridge deck and bridge wearing surface. These cracks allow water and corrosive materials to infiltrate the precast beam sections which leads to the degradation of the concrete and eventually corrosion of the prestressing strands. Corrosion of prestressing strands can lead to bridge repairs, diminished life-span, and postings.
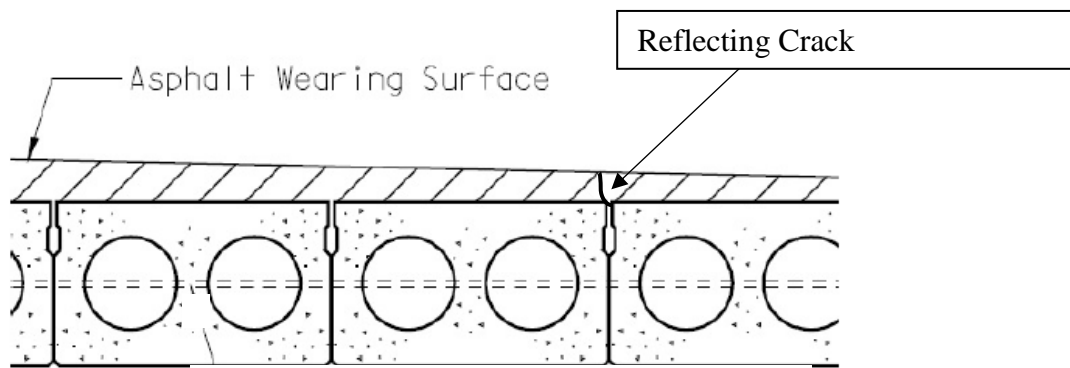
Figure 1: Section of Hollow Core Slab (Nielson et al., 2012)

Reflective cracking at the shear key is an indication of decreased transverse load distribution. Transverse load distribution is the ability of applied loads to be shared by adjacent members. If shear keys are degraded, transverse load distribution is decreased,

and load carrying capacity may be decreased. This can result in bridge postings and in extreme cases, overload and catastrophic failure of a bridge member.

These durability issues have proved to be problematic and have concerned SCDOT. In a past project, SCDOT and Clemson University teamed up to conduct research in order to identify, modify, or develop a bridge type that was both more durable and could lead to the schedule of ABC (Deery, 2010). SCDOT and Clemson University selected the Northeast Extreme Tee (NEXT) beam, developed by the bridge technical committee of PCI Northeast for further study and deployment on an SCDOT bridge (Culmo and Seraderian, 2010).

The NEXT beam is shaped like a double tee used in building construction (figure 2), but more robust, as shown in figure 3. The NEXT beam section was selected for many reasons, including geometric adaptability, ability to meet an ABC schedule, utility accommodations, full deck option, easier to inspect, and a full-depth wider shear key allowing for an easier concrete pour and greater bond between precast girder elements and shear key. One of the NEXT beam models (NEXT D), is precast with a full depth flange (8"). The NEXT D beam requires no CIP overlay and a bituminous asphalt overlay is optional. In other words, the NEXT D beam can carry traffic as soon as the girders are set, shear keys are poured, and guardrails are in-place.
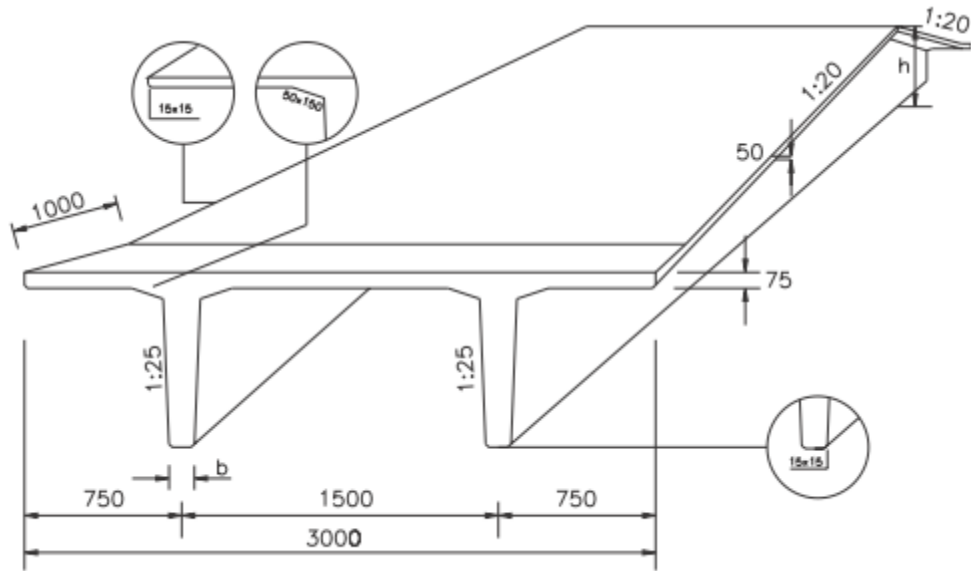
Figure 2: Typical Building Double Tee (Picture courtesy of Tekla Structures)
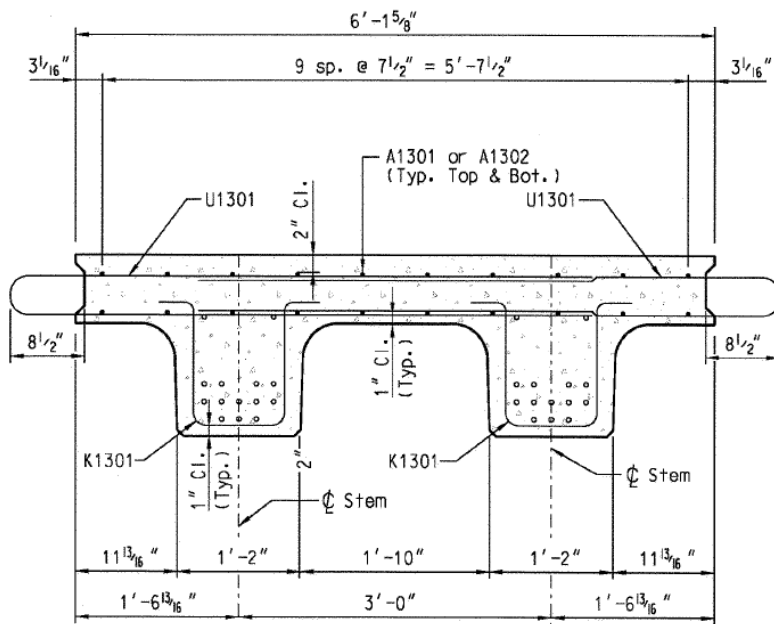
Figure 3: NEXT D Section Cut

Many states have started to use the different varieties of NEXT beam bridge girder systems as an alternate to CIP concrete or precast sections with great success. Additionally, some states have also replaced traditional shear key grout with ultra-high

performance concrete (UHPC). UHPC has very high compressive and tensile strength, and is extremely durable (Graybeal, 2010). Graybeal states that for a concrete to be considered UHPC, it must display compressive strengths greater than or equal to 21.7 ksi, and tensile strengths greater than or equal to 0.72 ksi (Graybeal and Russell, 2013). Additionally, UHPC bonds exceptionally well to precast bridge girder elements. The NEXT D bridge system that SCDOT is deploying includes UHPC as a replacement for grout in the shear keys. South Carolina and many other states are beginning to use UHPC as a replacement for grout in shear keys and other structural connections. Since NEXT beams and UHPC shear keys are beginning to see use by SCDOT and other state DOT's, research is needed to investigate the structural performance and durability of UHPC shear keys.

1.1 Hanging Rock Bridge

Hanging Rock Creek Bridge in Kershaw, SC, is an example of a short span low average daily traffic (ADT) bridge. The bridge consists of four simple spans: one 40' NEXT D span, two 70' hollow core slab spans, and one 40' solid core slab span. Hanging Rock Creek is the subject of this investigation.

A photo of the nearly completed Hanging Rock Bridge is shown in figure 4. The image displays four simply supported spans as well as the substructure beneath. Span 1 (far left and facing north) is a 40 ft. long NEXT-D beam span. Spans 2 and 3 are both 70 ft. long cored slab unit spans. Finally, span 4 is a 40 ft. long solid slab unit. The Hanging Rock Bridge utilizes Ductal Concrete as the UHPC shear key material. Ductal is the brand name of Lafarge Corporation's version of UHPC. Additionally, spans 2 – 4 are

transversely post-tensioned. The UHPC is fiber-reinforced: it contains steel fibers that increase both the concretes strength and ductility. Ductal concrete's strength is 6 to 8 times greater than standard concrete strength and has a lifespan 2 to 3 times longer (Ductal, 2015).

Figure 4: Hanging Rock Creek Bridge

The SCDOT chose to build a bridge with three different types of prestressed concrete girders so that a head-to-head comparison of the behavior of the three bridge types could be performed. Shear keys for the NEXT-D and solid and hollow slab spans are shown figures 5 and 7, respectively.

Figure 5: NEXT D Shear Key
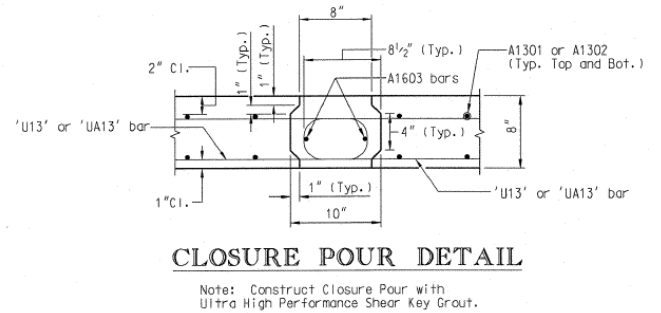
Figure 6: NEXT D Shear Key Detail
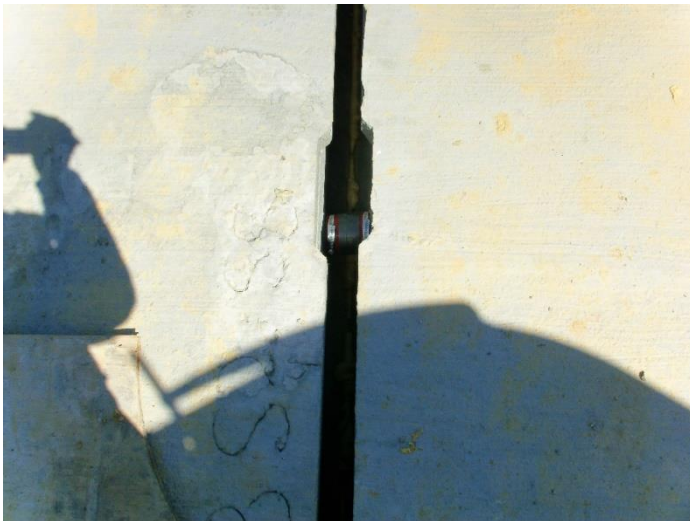
Figure 7: Solid Slab Shear Key
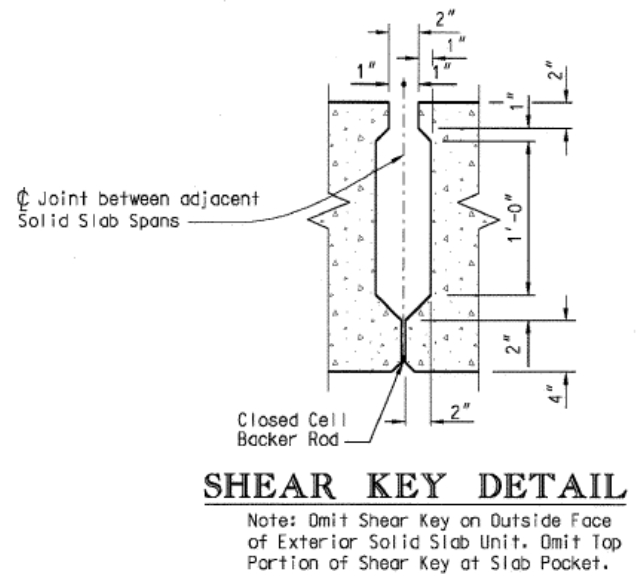
Figure 8: Solid Slab Shear Key Detail

Figures 9, 10, and 11 show the cross sections of spans 1, 2 and 3, and 4 respectively. Facing north, NEXT D beam bridge girders are numbered 1-6 while moving from left to right. Facing north, hollow core and solid slab bridges, girders are numbered 1 through 14 while moving from left to right.
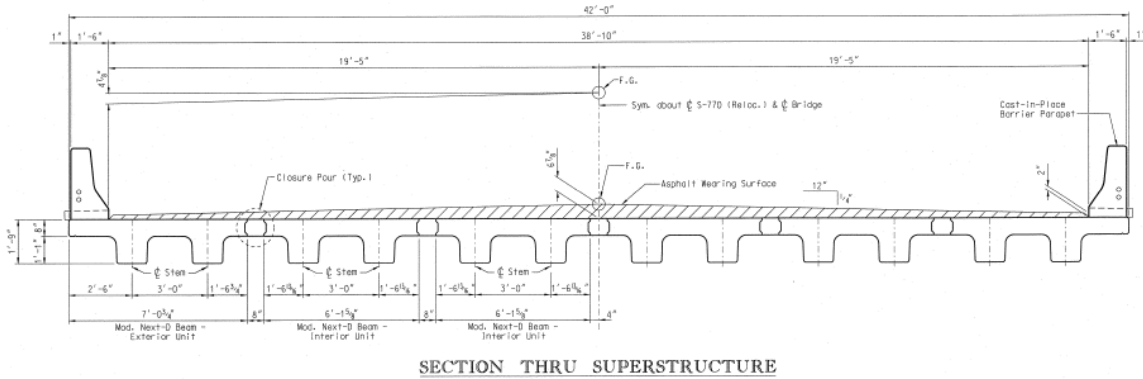
Figure 9: Cut through NEXT D Beam (Span 1)
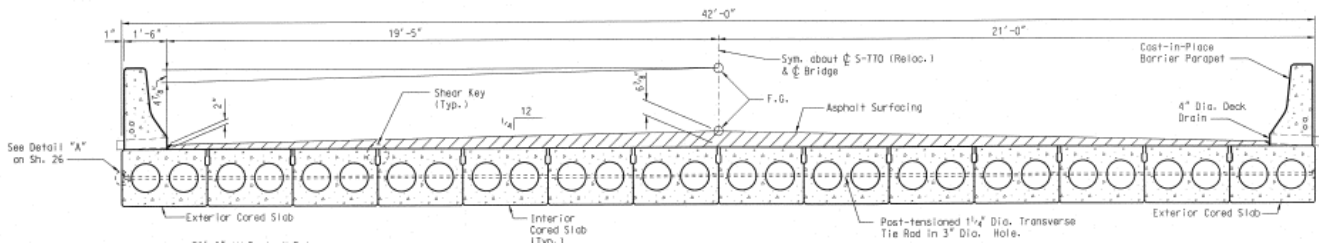
Figure 10: Section Cut through Hollow Core Slab Units (Spans 2 and 3)
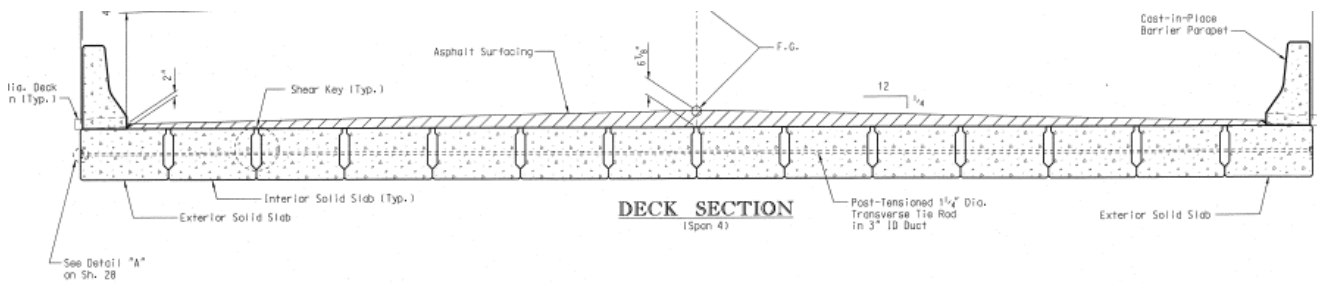
Figure 11: Section Cut through Solid Slab Unit (Span 4)

1.2 Load Distribution Factors

AASHTO LRFD uses distribution factors to account for transverse load sharing in many categories of bridges. The NEXT beam cross section does not neatly fall into an AASHTO LRFD category for calculating simplified moment live load distribution factors (DFM). It is a hybrid between type (i) and type (k) when referencing AASHTO LRFD (AASHTO LRFD 2010). Type (i) and (k) are shown in Figures 12 and 13 respectively. A Precast Concrete Institute (PCI) technical committee has recommended that engineers calculating DFM for bridges containing NEXT D beams can treat the bridge as type (k) (Guidelines, 2012). This project seeks to evaluate the accuracy of this recommendation via live load testing. Additionally, the durability of the shear key will be monitored over a period of two years. Durability monitoring will be a focus of subsequent thesis projects; the current thesis focuses on DFM. The purpose and scope are described in detail in the next section.

Supporting Components	Type of Deck	Typical Cross Section
Precast Concrete Double T Section With Shear Keys and With or Without Post Tensioning.	Integral Concrete	

Figure 12: Type (i) Girder (Double T Beam Bridge Section) [AASHTO LRFD]
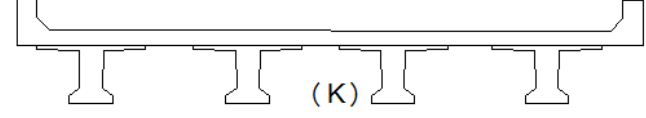
Supporting Components	Type of Deck	Typical Cross Section
Precast Concrete I or Bulb T section.	Cast in Place Precast Concrete	(K)

Figure 13: Type (k) Girder (Bulb T Beam Bridge Section) [AASHTO LRFD]

1.3 Purpose and Scope

The purpose of this entire project is threefold: 1) evaluate the transverse load sharing characteristics of the NEXT D beams via UHPC connection and determine the live load moment distribution factors, 2) to monitor and compare the health of the UHPC shear keys in both the NEXT-D beams and solid core slab over a two-year period, and 3) to perform material tests on UHPC samples. This thesis will focus on the initial live load test of Hanging Rock Creek Bridge and the UHPC specimen tests performed in the Clemson University laboratory. Two more live load tests (at 12 and 24 months from date of bridge opening) are scheduled and will be discussed in a thesis at a later date.

Truck weights and configurations for the live load tests were selected to generate the maximum bridge girder response. Bridge girder strains and deflections were recorded during the live load tests of the bridge spans containing NEXT D beams and solid core slab. Cube, split cylinder, and pull-off tests all were performed to obtain metrics of the UHPC found in Hanging Rock Bridge shear keys. Cube strength tests determined the compressive strength of the UHPC, split cylinder determined the tensile strength of the UHPC, and the pull-off test measured the bond strength between the precast concrete and UHPC. The results from this project are used to present recommendations for engineers

designing NEXT beam bridges, specifically live load distribution factors for moment and if UHPC shear keys are more durable than normal strength grout or concrete.

1.4 Objectives

The entirety of this research project set out to answer the four objectives below. This thesis will focus on objectives #1 and #4. The objectives are as follows:

1. How is load shared transversely between NEXT-D beams? What is the calculated DFM? How conservative is type (k) category, recommended by the PCI technical committee?

2. Does the transverse load behavior of NEXT-D beams and solid core units change over the next two years as the bridge ages?

3. How durable are the UHPC shear keys? Does the UHPC bond well to the precast? Is there a difference between the NEXT-D beam shear key (full-depth) and solid slab shear key (partial depth)? Are there any changes that would improve the joint detail?

4. What are the material properties of the UHPC? Specifically, what are the compressive, tensile, and bond strengths?

1.5 Organization

This Master's thesis is composed of five chapters. A literature review of NEXT beams, nondestructive bridge testing, and UHPC use in bridges is presented in chapter 2. Chapter 3 aims to present the setup and experimental procedure of the UHPC material tests and live load test. Results of the live load test are presented in chapter 4. Finally,

chapter 5 presents conclusions and recommendations based on the results found in

chapter 4.

Chapter 2:   Literature Review

2.1 NEXT Beam Background

The NEXT beam is an alternative to the typical box-beam girder used by many
state DOT's in short to medium span bridges. The NEXT beam addresses many of the
shortcomings of box beam girders including: accommodating utilities, construction
challenges, and difficulty grouting shear keys. There are three variations of the NEXT
beam, and they include NEXT D, NEXT E, and NEXT F (Seraderian, 2016). The NEXT
D has full flange thickness (8") with the top serving as a road surface. An optional
asphalt overlay may be added. The NEXT E has half flange thickness (4") and receives a
4" CIP concrete overlay. The NEXT F beam has a partial flange thickness, which serves
as formwork for an 8" CIP concrete overlay. Hanging Rock Creek Bridge span 1 is a
NEXT D bridge system. The geometry of the Hanging Rock Creek Bridge NEXT D
section cut is shown in figure 14.
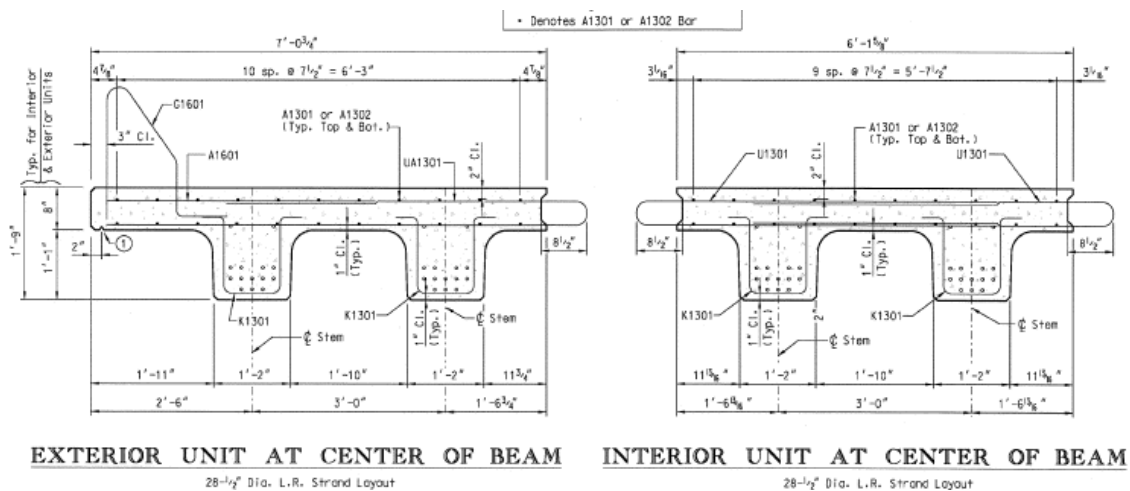
Figure 14: NEXT D Beam Section Cut

The idea for the NEXT beam came about in 2006 at the Rotondo Precast plant in Rehoboth, Massachusetts (Culmo and Seraderian, 2010). The Rotondo plant had developed a precast section that was used for high-level railroad platforms show in figure 15. The high-level railroad platform section exhibited many favorable characteristics for short and medium bridge span lengths. After some dimensional parameters were set by PCI, the NEXT beam was born.

Figure 15: High-Level Railroad Platform that Inspired NEXT Beam Design (Culmo and Seraderian, 2010)

The main issues that state DOTs face with flat slab and hollow core sections is their durability and load sharing abilities (Deery, 2010). The NEXT beams seeks to solve these durability issues a few ways. First, there are no voids in the NEXT beam bridge sections, which limits waters ability to infiltrate inside the precast section and corrode the prestressing steel. While NEXT beams limit corrosion, they are also much easier to

inspect for girder damage and strand corrosion in comparison to hollow core and solid slabs (Deery, 2010)

Additionally, NEXT beam shear keys are wider and full depth, unlike many box-beam solid slab and hollow core section shear keys. These modified shear keys should allow for a stronger more durable connection that are easier to grout. Shear key failures can often be attributed to inadequate grouting procedures, which are made difficult by shear key narrowness (El-Remaily et al., 1996).

Lastly, solid slab sections often do not have any reinforced concrete overlay to assist with load sharing. All NEXT sections have reinforced concrete flanges and/or overlay to assist with load sharing.

There are papers that have shown various ways to decrease reflective cracking some of which include using a full depth shear key and using a grout material with a high bond strength (Miller et al., 1999). The NEXT beams of the Hanging Rock Creek have implemented both of these strategies.

The remaining portion of the literature review aims to summarize relevant research completed and describe how the current study seeks to build off previous studies to answer the target objectives. Included in the literature review is a section on how transverse load distribution is accounted for by the AASHTO LRFD Bridge Design Specifications (2012). Another section contains background information on UHPC, how UHPC has been used in bridge connections by other state DOTs, and UHPC joint research conducted by Clemson University and Virginia Tech. The final section covers

research from the University of Massachusetts at Amherst on NEXT F beams, including their findings on transverse load distribution in NEXT beam bridges.

2.2 Dynamic Load Allowance

No road is smooth and perfectly flat. Roads all have different degrees of roughness. Additionally, approach slabs may settle, creating a ramp from approach slab to the bridge system. Road roughness and these ramps cause vehicles to oscillate, or to bounce up and down on their suspension systems as a vehicle crosses a bridge. As the vehicles bounce, the shocks compress. This downward compression force is greater than the weight of the vehicle alone. The increase in the force of the truck due to the bouncing and compression of the shocks is called the dynamic load allowance (IM) (Barker and Puckett, 2007).

Edgar Restrepo observed this ramp like effect in his thesis work at Virginia Tech (Restrepo, 2002). Figures 16 and 17 are the hypothetical versus actual bridge approach slab elevation views for the Route 601 Bridge. The actual approach slab has a slope due to poor soil compaction under the approach slab. For his thesis work, Restrepo performed two bridge tests, one in the fall of 2001 and one in the summer of 2002. During the fall 2001 test, the approach slabs were in poor condition as shown in figure 18. During the summer 2002 test, the approach slabs had been repaired as shown in figure 19. A comparison of IM factors from both bridge tests and AASHTO standards is shown in figure 20.
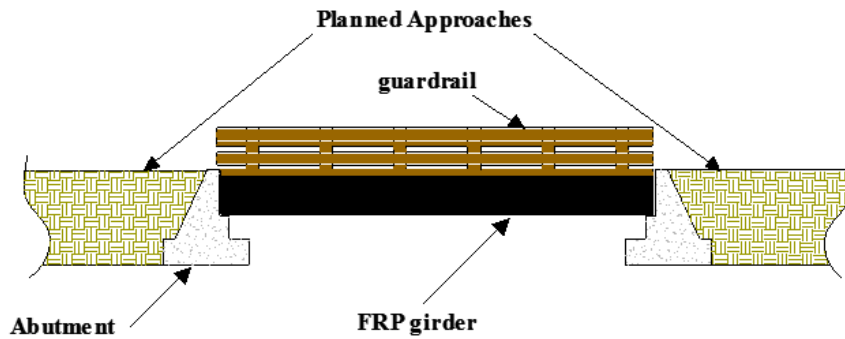
Figure 18: Elevation View of the Route 601 Bridge with Planned Approach Slabs (Restrepo, 2002)
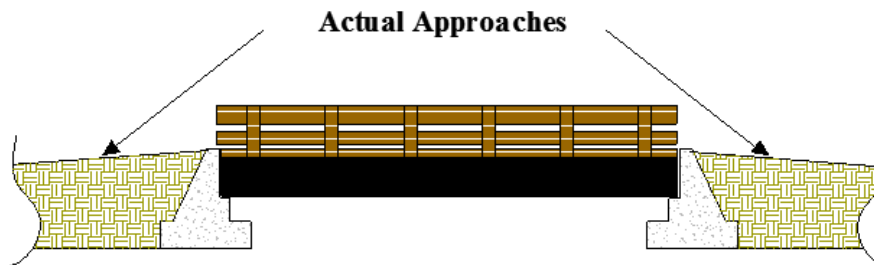
Figure 17: Elevation View of the Route 601 Bridge with Sloped Approach Slabs Due to Soil Settlement (Restrepo, 2002)

Figure 16: Approach Conditions of the Route 601 Fall 2001 Live Load Test (Restrepo, 2002)

Figure 20: Improved Approaches of the Route 601 Summer 2002 Live Load Test (Restrepo, 2002)
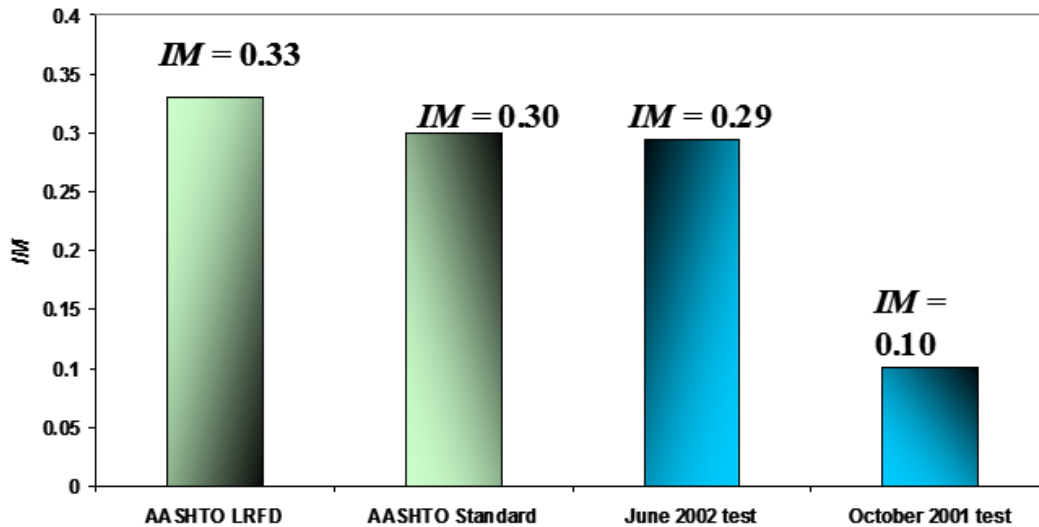
Figure 19: Route 601 IM Factor Comparison with AASHTO (Restrepo, 2002)

From the data shown in figure 20, it was concluded that the dynamic load allowance was affected by the settlement of the approaches. In this case, the approach slab improvements actually amplified the dynamic effects of the trucks. In the Fall 2001

test, the ramped approaches allowed for the truck to go slightly airborne during the live load test, resulting in smaller bridge responses and a lower IM factor. The repair of the bridge approaches did not allow the truck to go airborne in the summer 2002 test, resulting in greater bridge responses and an increased IM factor.

Figure 21 shows a bridge girder under static and dynamic loading for the US Route 15 Southbound bridge over Interstate 66. This bridge is a two span 244 ft. steel girder bridge. Figure 22 plots bridge displacement versus truck position since the static and dynamic tests operate on a different time scale. From figure 22, it is shown that the deflections are greater due to the dynamic response than the static response. These dynamic forces must be accounted for in bridge design. Factors that influence the IM include bridge stiffness, span length, truck weight, and road surface roughness.
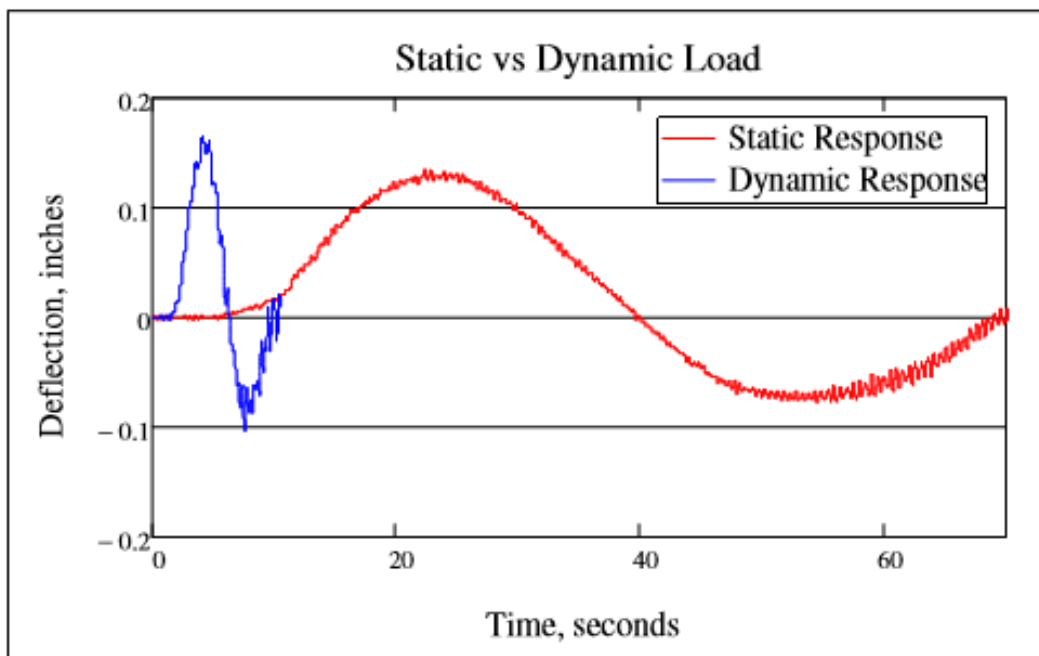
Figure 21: Static Versus Dynamic Load Effect (Collins, 2010)
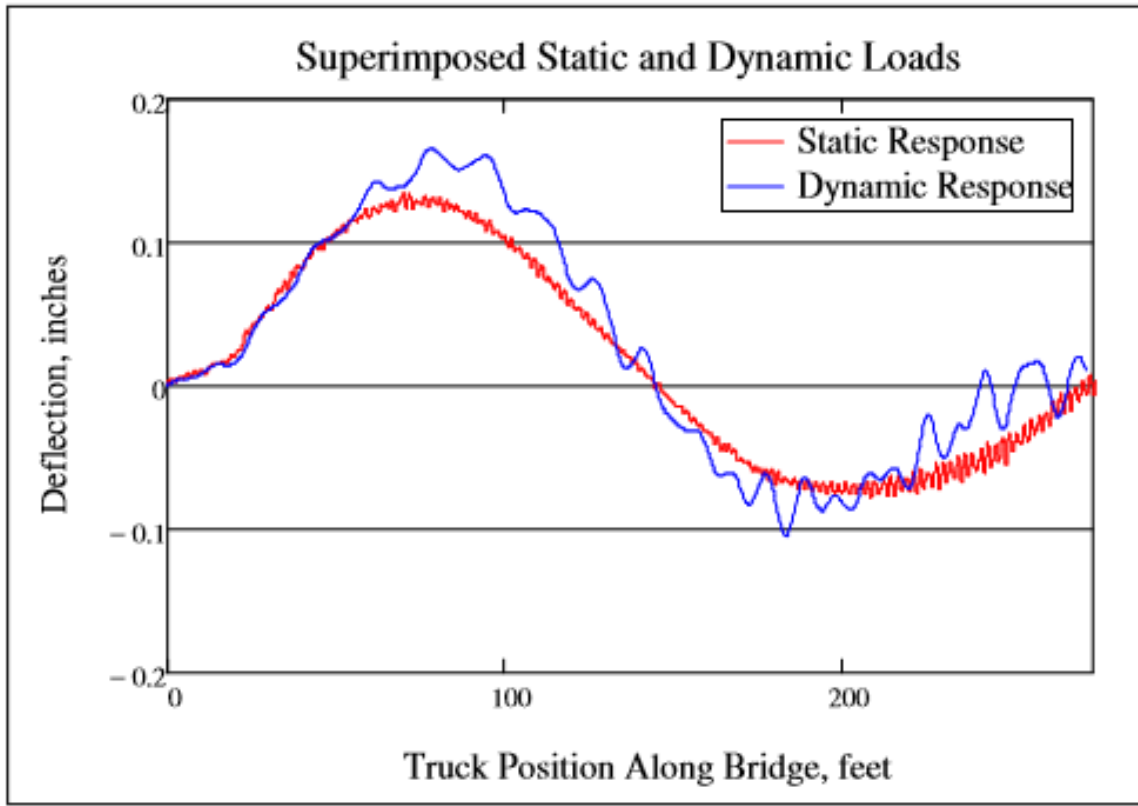
Figure 22: Dynamic Response Superimposed on Static Response (Collins, 2010)

2.2.1 AASHTO Dynamic Load Allowance

Rather than determining the IM analytically or experimentally, AASHTO has a table that guides engineers on how to design for the dynamic effect of a vehicular load. The table for the design IM of different bridge components is shown in table 1.

Table 1: AASHTO LRFD IM Factors (AASHTO LRFD 2012)

Component	IM
Deck Joints—All Limit States	75%
All Other Components:	
• Fatigue and Fracture Limit State	15%
• All Other Limit States	33%

In the case of Hanging Rock Creek Bridge, the bridge girders were designed used an IM of 1.33. This is a conservative value, which is illustrated in chapter 4 of this text.

2.2.2 Experimental Calculation of Dynamic Load Allowance

The dynamic load allowance is typically calculated using equation 1 below, where Dd_{yn} is the response (bending strain or deflection) due to dynamic loading, and D_{sta} is the response due to a static loading.

$$IM = \frac{D_{dyn}}{D_{sta}}$$ **Equation 1**

Once the IM is calculated, the dynamic loading is determined using equation 2, which converts the static loading into an appropriate dynamic loading:

$$P_{dyn} = P_{stat}(1 + IM)$$ **Equation 2**

2.3 Transverse Load Distribution in Slab-Girder Bridges

Bridges are designed to take vehicular loads and deliver them safely to the bridge foundation. Bridge decks and girders are designed to distribute load transversely across the bridge and longitudinally to the girder bearings. Individual girders resist a portion of the loads on a bridge. This portion or fraction of load is primarily a function of the transverse load distribution of the bridge.

The ability for bridge girders to share vehicular load transversely between adjacent bridge girders is predicted using moment distribution factors (DFM). Stiffness of bridge components, including but not limited to the concrete deck, diaphragms, bearings, and bridge geometry, all play a role in how vehicular loads are transversely distributed to each bridge girder (Barker and Pucket, 2007). After a live load distribution factor is obtained, axle loads are multiplied by the distribution factors. The product is equivalent to the vehicular design load, which is multiplied by a dynamic load allowance and then combined with other loads (i.e. deck weight, barrier rails, etc.) to produce the total design load. A large distribution factor means that less load is shared between adjacent girder members, and therefore, the girder directly beneath the axle load takes more load.

Figure 23 illustrates the concept of fair and poor transverse load distribution. Figure 23(a) is a picture of a slab-girder bridge and Figure 23(b) visually illustrates the load path of a point load distributed from the deck into the girders. As shown, the further away the girder is from the point load, the less load received. Figures 23(c) and (e), respectively, illustrate ideal load distribution, while Figure 23(d) illustrates that poor load distribution leads to excessive deflection in girders directly under load when compared to deflections of nearby girders.

Transverse load distribution is an important factor in the design of bridge girders to resist both applied shear and moment. Transverse load distribution for moment (or flexural) design of NEXT D beam bridges is the primary concern of this research, therefore, the following literature review will not address transverse load distribution as it relates to shear design of bridge girders.
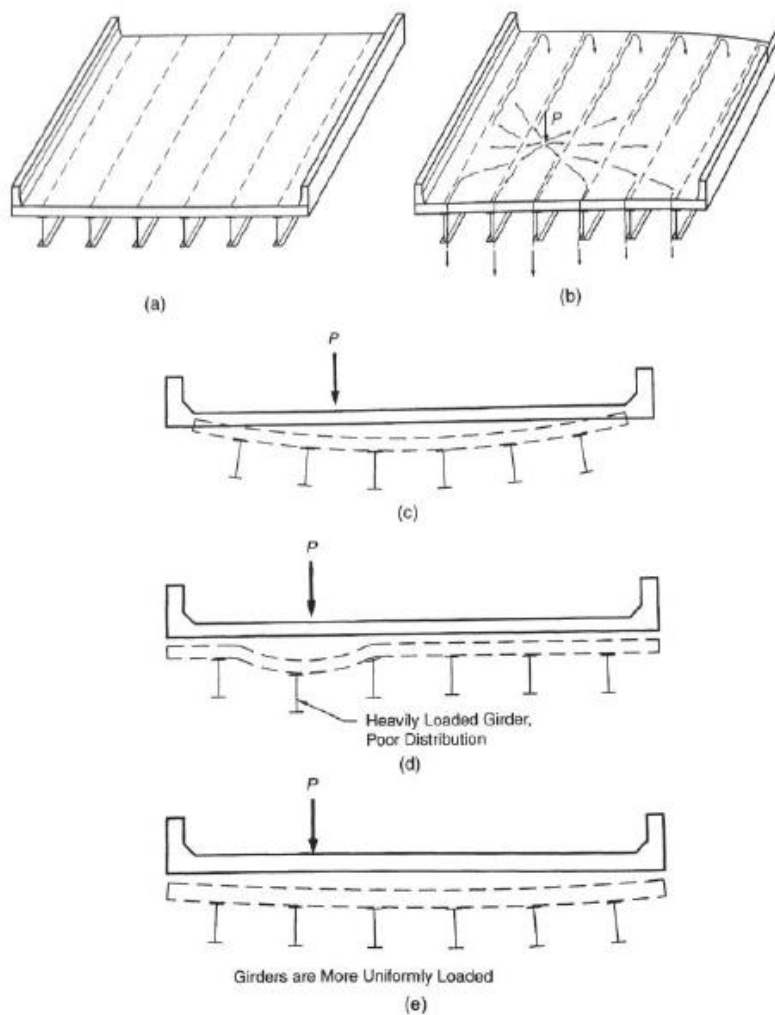
Figure 23: Illustration of Transverse Load Distribution (Barker and Puckett, 2007)

2.3.1 AASHTO LRFD Distribution Factors for Moment – NEXT Beam Bridges

Multiple factors are considered when calculating bridge girder distribution factors including girder spacing, length of span, girder geometry, and the modular ratio between girder and deck (Barker and Puckett, 2007). AASHTO LRFD presents a table of formulas (Table 4.6.2.2.1-1) that assists engineers in calculating distribution factors for single and multi-lane traffic loads for both interior and exterior girders. The empirical derivations of these formulas can be traced to NCHRP Project 12-26 (Zokaie and Imbsen, 1993). NEXT D girder bridges most closely resemble section types (i) and (k) from AASHTO LRFD 4.6.2.2.1-1, shown in figures 24 and 25, respectively.
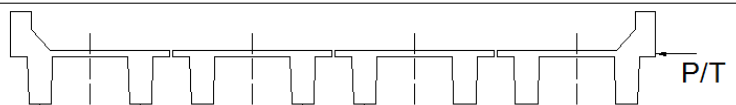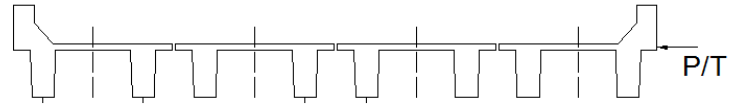
Supporting Components	Type of Deck	Typical Cross Section
Precast Concrete Double T Section With Shear Keys and With or Without Post Tensioning.	Integral Concrete	

Figure 25: Type (i) Girder (Double T Beam Bridge Section) [AASHTO LRFD]
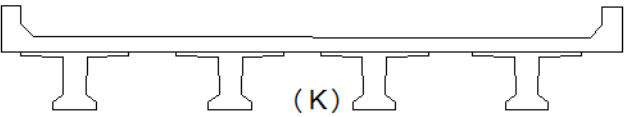
Supporting Components	Type of Deck	Typical Cross Section
Precast Concrete I or Bulb T section.	Cast in Place Precast Concrete	

Figure 24: Type (k) Girder (I Beam Bridge Section) [AASHTO LRFD]

Cross section (k) uses the following equations to calculate the DFM of an interior beam for single and multiple design lanes loaded:

$$gM_1{}^{i\text{-}} = 0.06 + \left(\frac{S}{14}\right)^{0.4} \cdot \left(\frac{S}{L}\right)^{0.3} \cdot \left[\frac{K_g}{\left(12 \cdot L \cdot t_s{}^3\right)}\right]^{0.1} \qquad \textbf{Equation 3}$$

$$gM_{2+}{}^{i\text{-}} = 0.075 + \left(\frac{S}{9.5}\right)^{0.6} \cdot \left(\frac{S}{L}\right)^{0.2} \cdot \left[\frac{K_g}{\left(12 \cdot L \cdot t_s{}^3\right)}\right]^{0.1} \qquad \textbf{Equation 4}$$

Where:

K_g = $n(I_{bs}+A_{bs}e_g{}^2)$

n = E_{Beam}/E_{Slab}

$gM_1{}^{i\text{-}}$ = DFM for interior girder with one lane loaded

$gM_{2+}{}^{i\text{-}}$ = DFM for interior girder with two or more lanes loaded

K_g = longitudinal stiffness parameter for the composite girder (in^4)

S = respective spacing between the girders (ft) for different approaches

L = spand of the bridge (ft)

t_s = thickness of deck slab (in)

n = modular ratio between the material of girder and material of deck

e_g = the distance between centers of gravity of stems and flange (in)

A_{bs} = cross sectional area of the stems (in^2)

I_{bs} = moment of intertia of the stems (in^4)

E_{Beam} = modulus of elasticity of NEXT beam (ksi)

E_{Slab} = modulus of elasticity of deck slab (ksi)

Similar equations for type (k) to calculate exterior girder DFM for one design lane load are not provided by AASHTO LRFD, rather, the lever rule is applied. The lever rule is outlined in AASHTO LRFD Section 4.6.2.2.2. Using the lever rule method, moments are summed about a hinge placed at the first interior girder. The reaction at the exterior girder is determined and then divided by the total truck load. The ratio of the exterior girder reaction by the total load is the calculated DFM for the exterior girders.

Equations to calculate type (k) exterior beam DFM for multiple lane loads are as follows:

$$g \quad = e * g_{interior}$$

$$e \quad = 0.77 + d_e/9.1$$

$d_e \quad$ = horizontal distance from the centerline of the exterior web of exterior beam at the deck level to the interior ede of curb or traffic barrier

Cross section (i) uses the following equations to calculate the DFM of an interior beam regardless of number of loaded lanes:

$$g \quad = S/D$$

$$C \quad = K(W/L) \le K$$

$$D \quad = 11.5 - N_L + 1.4 N_L (1 - 0.2C)^2$$

when $C \le 5$

$$D \quad = 11.5 - N_L \text{ when } C > 5$$

$$K := \sqrt{\frac{I \cdot (1 + \mu)}{J}}$$

$$g \quad = \text{distribution factor}$$

$$N_L \quad = \text{number of design lanes}$$

W   = edge-to-edge width of bridge (ft)

μ   = Poisson's ratio

J   = St. Venant torsional inertial (in^4)

Cross section (i) uses the lever rule (explained above) to calculate the DFM of an exterior beam regardless of number of loaded lanes. If a type (i) bridge is "sufficiently connected to act as a unit" (AASHTO, 2012) the bridge can calculate DFM values using the type (k) equations.

2.3.2 AASHTO LRFD Distribution Factors for Moment – Adjacent Box Beam Bridges

Adjacent box beam bridges most closely resemble section type (g) from AASHTO LRFD 4.6.2.2.1-1, shown in figure 26.

Precast Solid, Voided, or Cellular Concrete Box with Shear Keys and with or without Transverse Post-Tensioning	Integral concrete	
		P/T (g)
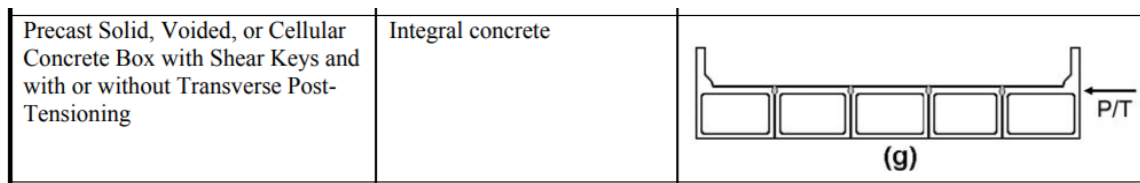
Figure 26: Type (g) Adjacent Box Beam Section [AASHTO LRFD]

Cross section (g) uses the following equations to calculate the DFM of an interior beam for a single and side-by-side truck load:

$$gM_1^{i\text{-}} = k \cdot \left(\frac{b}{33.3 \cdot L} \right)^{0.5} \cdot \left(\frac{I}{J} \right)^{0.25} \qquad \textbf{Equation 5}$$

$$gM_{2+}{}^{i\text{-}} = k \cdot \left(\frac{b}{305}\right)^{0.6} \cdot \left(\frac{b}{12 \cdot L}\right)^{0.2} \cdot \left(\frac{I}{J}\right)^{0.06} \qquad \textbf{Equation 6}$$

Where:

$$k = 2.5 \cdot \left(N_b\right)^{-0.2} \geq 1.5$$

N_b = Number of beams, stringers or girders

$gM_1{}^{i\text{-}}$ = DFM for interior girder with one lane loaded

$gM_{2+}{}^{i\text{-}}$ = DFM for interior girder with two or more lanes loaded

J = St. Venant torsional inertial (in^4)

L = spand of the bridge (ft)

b = width of beam (in)

I = moment of intertia about axis under consideration (in.^{4})

Cross section (f) uses the following equations to calculate the DFM of an exterior beam

for a single design lane loaded:

$$g = e \cdot g_{interior} \qquad \textbf{Equation 7}$$

Where:

$$e = 1.125 + \frac{d_e}{30} \geq 1.0$$

d_e = horizontal distance from the centerline of the exterior web of exterior beam at the deck level to the interior ede of curb or traffic barrier

$g_{interior}$ = distribution factor of interior beam

Cross section (g) uses same equations to calculate the DFM of an exterior beam for

multiple design lanes loaded except for one change:

$$e \quad = \quad 1.04 + \frac{d_e}{25} \geq 1.0$$

2.3.3 Experimental Calculation of Distribution Factors for Moment

The NEXT D bridge girder does not neatly fall into one of the AASHTO LRFD DFM categories, however, as previously stated, treating the section as type (k) may lead to higher, and therefore, more conservative calculated DFM's. Experimental DFM values can be calculated and can inform engineers how load is shared transversely between bridge girders. Through the use of a live load test, bridge girders can be instrumented to record the strain of the bridge girder. The maximum strain that a bridge girder experiences is used to calculate the DFM. Load may be applied to a bridge through the use of a slow driving truck. Using equation 8, bridge girder DFM values may be experimentally determined (Fu et al., 1996).

$$g_i = \frac{\varepsilon_i}{\sum_{j=1}^{n} \varepsilon_j} \qquad \textbf{Equation 8}$$

Where g_i is the distribution factor for girder "i", ε_i is the strain in girder "i", and ε_j is the strain in all of the other bridge girders taken at the same time that the maximum strain in girder "i" was measured.

An alternative equation (equation 9) has been proposed to experimentally calculate DFM values. This equation accounts for increased stiffness that is given by the barrier rails. The equation is as follows (Barnes et al., 2003):

$$g_i = \frac{w_i R_i}{\Sigma_{j=1}^{n} w_j R_j}$$

Equation 9

Where g_i is the distribution factor for girder "i", R_i is the response in girder "i", and R_j is the response in all of the other bridge girders taken at the same time that the maximum response in girder "i" was measured. Response (R) can be taken as either strain (ε) or displacement (Δ). W_i and W_j are the section moduli of girders i and j, respectively.

Figure 27 from Collins (2010), is a graphical displays the results of a live load test. The tested bridge contained 6 girders with equal spacing and stiffness. The results shown are for side-by-side truck crossing, which was meant to cause maximum load in girder 3. Two sets of data are displayed on the graph. The service strain is the greatest response experienced by each bridge girder, while the distribution strain is each girders response at the time when the greatest girder response is experienced by the maximally loaded girder, which in this case is girder 3. Girder strain is the highest in girders directly below wheel loads and dissipates as the girders get further away from the load. DFM values would be calculated by using the distribution data set in conjunction with Equation 9.
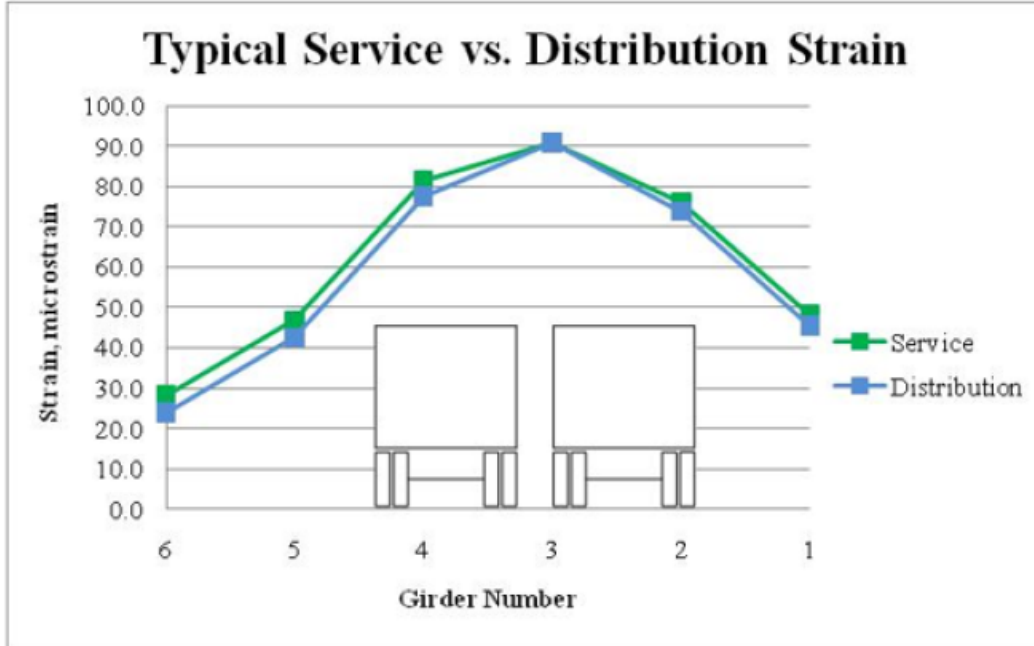
Figure 27: Live Load Distribution Factor for Moment Example (Collins, 2010)

2.4 Ultra-High Performance Concrete for Bridge Connections

Ultra-high performance concrete (UHPC) has been commercially available since about 2000 and is characterized by displaying compressive strengths of over 21.7 ksi and cracking tensile strengths above 0.72 ksi (Graybeal and Russell, 2013). Ingredients of UHPC include cement, fine sand, steel fibers, water, and other additives. The steel fibers in the mix are what gives UHPC its high tensile strength. UHPC is vastly more expensive than standard concrete (sometimes greater than 10 times as much) (Ultra-High Performance Concrete: Homeland Security), but is also more durable and needs less maintenance. Additionally, UHPC bonds well to cast-in-place (CIP) concrete and is resistant to fatigue cracking. Due to its durability and bond strength, UHPC is an

31

attractive option to use for connections between precast elements in bridges. Figure 28 is

a generic stress-strain curve of UHPC. The figure illustrates UHPC's remarkable tensile

strength and ductility, which is what makes it a viable material for bridge connections.
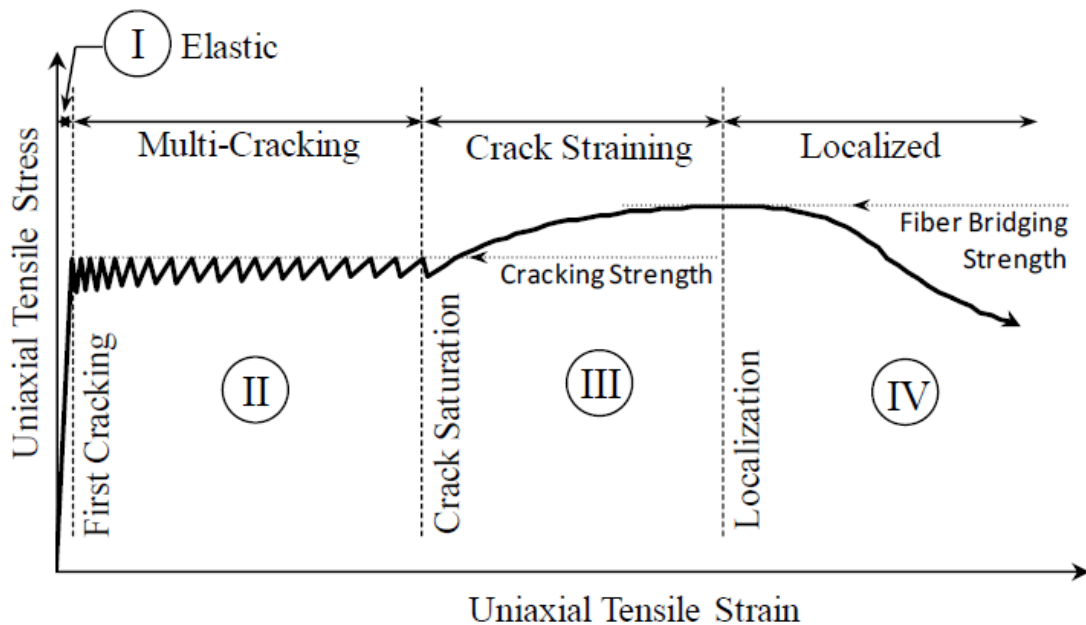
Figure 28: Generic UHPC Stress-Strain Graph (Picture courtesy of the FHWA)

2.4.1 Adjacent Box Beam Bridge Shear Key Connections

It has been well documented that adjacent box beam bridges (ABBB) have

durability issues, particularly in the shear key. In Kedar Halbe's dissertation from the

Virginia Tech (Halbe, 2014), he proposed new connection details to improve shear key

performance, reduce reflective cracking, and consequently, improve bridge durability.

Specifically, six different connection details between box beams were assembled and

tested. The research proposed two new connection details. The first proposed connection

made no change to an existing partial or full depth shear key, rather it added a Kevlar

sheet to reinforce the connection. The Kevlar sheet not only added strength to the

connection, but waterproofing as well. The detail for this connection is shown in figure 29.
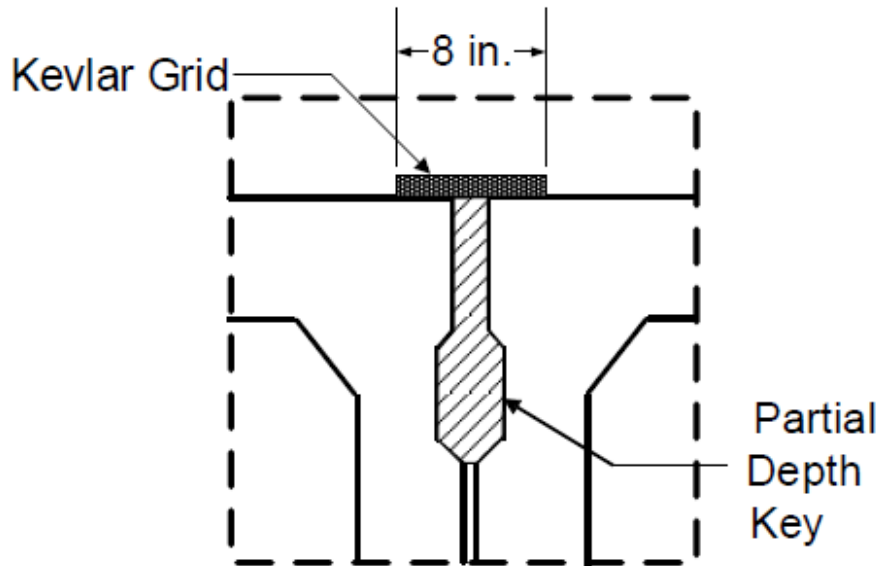
Figure 29: Typical Detail of Kevlar and Epoxy Connection (Halbe, 2014)

The second proposed connection detail is more complicated. Cracking in the ABBB shear keys was caused by the grout debonding from the concrete. The second connection, added a structural connection to improve the bond. This connection was a splice bar connecting the two adjacent beams at the top of the flange. UHPC or very high performance concrete (VHPC) replaced the shear key grout to keep the splice length of the bar short. UHPC and VHPC have a greater bond strength to rebar allowing for shorter development lengths. The detail for this connection is shown in figure 30.
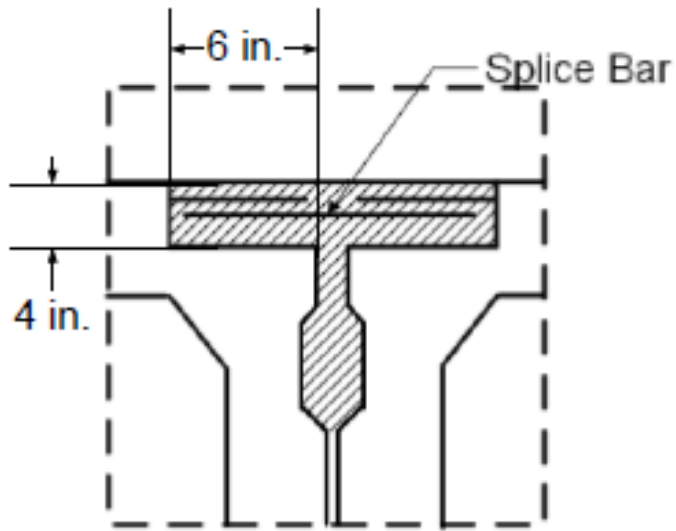
Figure 30: Top Flange Spliced Connection with UHPC (Halbe, 2014)

Two FE models of the specimens were created in ABAQUS to quantify responses of adjacent box bridges subject to truck loads. The first model used material properties shown in table 2, below, while the second model used the material properties measured from laboratory tests.

Table 2: Material Properties used in FE Model

Component	Unit Weight (pcf)	Modulus of Elasticity (ksi)	Poisson's Ratio
Topping Concrete	145	3644.1	0.2
Beam Concrete	145.5	4095.4	0.2
UHPC	147	6500	0.19
VHPC	147	5700	0.19
Grout	148	4415.2	0.2
Structural Steel	490	29000	0.3
Prestressing Strands	0.39*	28500	0.3

NOTE: * - indicates unit weight in lb/ft.

Of particular interest in the modeling was the horizontal opening of the joint, as shown in Figure 31. Joint displacement values for the sub-assembalge (SA) models and full scale bridge (FSB) models were recorded and measured as 0.0038 in and 0.00387 in., respectively. These predicted displacements serve as an order of magnitude value that the researchers can compare to to when performing a live load test on the solid slab section.
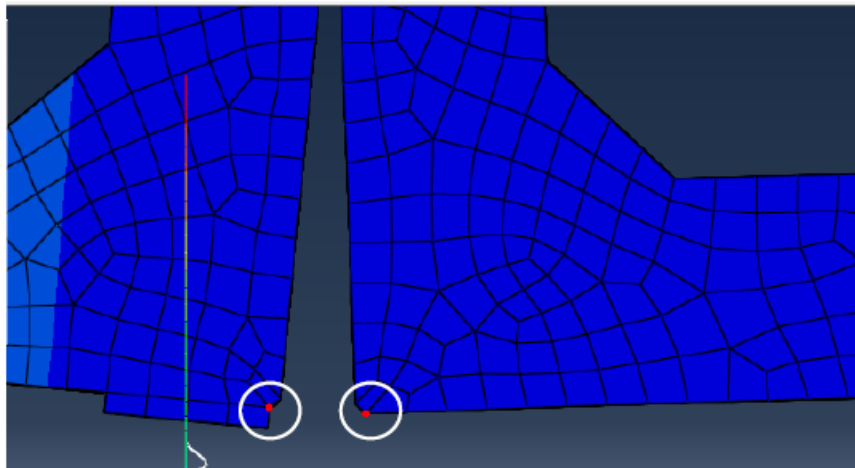
Figure 31: Joint Opening in the FE sub-assemblage Model (Halbe, 2014)

In addition to FE modeling, SA specimens using the two new proposed connection details were constructed and tested. The SA specimens were instrumented and recorded responses caused by fatigue and static strength tests. Relative gap displacements were measured by LVDTs to capture the joint behavior. The location of the instrumented LVDTs can be found in figure 32. Table 3 presents the concrete properties of the precast specimens.
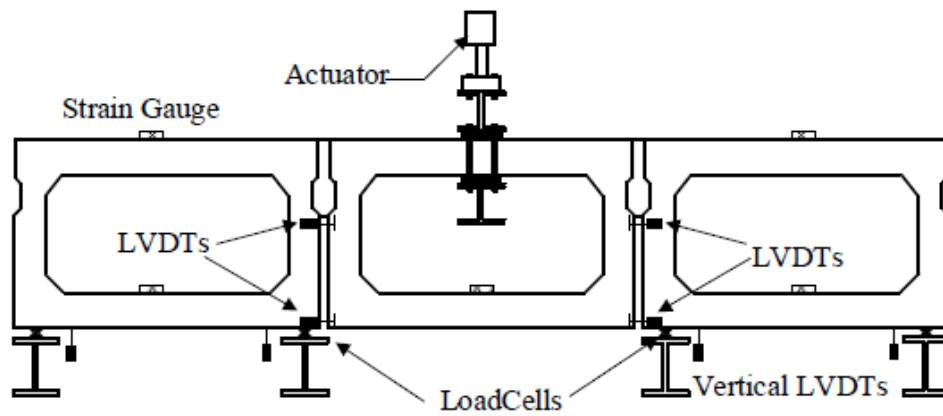
Figure 32: Test Setup for sub-assemblage Tests (Halbe, 2014)

Table 3: Concrete Properties in Precast Beam Specimens

Specimen Designation	Compressive Strength, (psi)	Splitting Tensile Strength, (psi)	Modulus of Elasticity, (ksi)
U-4-5-I-E	7360	816	4090
U-4-6-I-E	7360	816	4090
U-4-3-I	7360	816	4090
U-4-4-I	3900	-	3590
U-4-5-II	3900	-	3590
V-4-5-I	4700	-	-
V-4-6-I	4700	-	-
V-4-5-II	4640	-	-
V-4-3-I	4890	-	-
V-4-4-I	4890	-	-
V-4-4-II	4640	-	-
End of Test VHPC	4720	351	3400
U-6-5-I-E	7360	816	4090
U-6-6-I-E	7360	816	4090
U-6-7-I	3900	-	3590
U-6-8-I	3900	-	3590

Interface openings typically occurred before any cracks showed in the UHPC or VHPC pockets. Once the interface was completely opened, cracks either propagated diagonally below the grout pocket into the precast concrete, or, the interface would continue to delaminate along the bottom of the shear pocket. These failure forms are illustrated in figure 33.
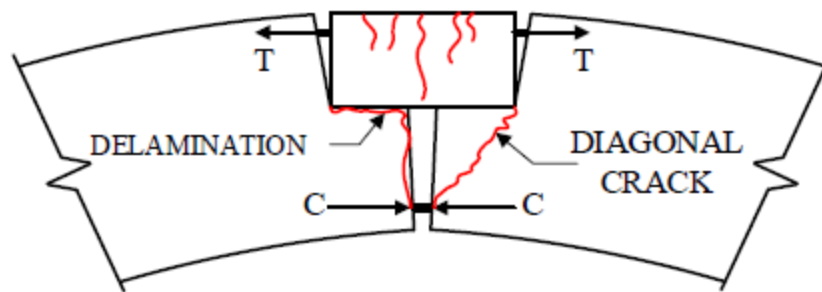
Figure 33: Crack Illustration in the Precast Joint Element (Halbe, 2014)

The interface measurements were plotted versus the applied load and can be seen in figures 34 and 35, respectively. Figure 34 shows displacements for all specimens with No. 4 reinforcing bars extending into the joint, while figure 35 has No. 6 bars. Interface displacements are significantly smaller in the No. 6 bar joint compared to No. 4 bar joint. For all test specimens, displacements are very similar up until debonding at the interface occurs, after which, displacements increase at different rates. The design capacity of the No. 4 bar specimens was 12.5 kips, and cracks began to occur at approximately 15 kips. The design capacity of the No. 6 bar specimens was approximately 27.5 kips, and cracks began to occur at approximately 30 kips. These figures and numbers allowed the researchers to learn about UHPC behavior under loading, and approximate values of when UHPC is expected to crack and move from the linear to the non-linear zone.
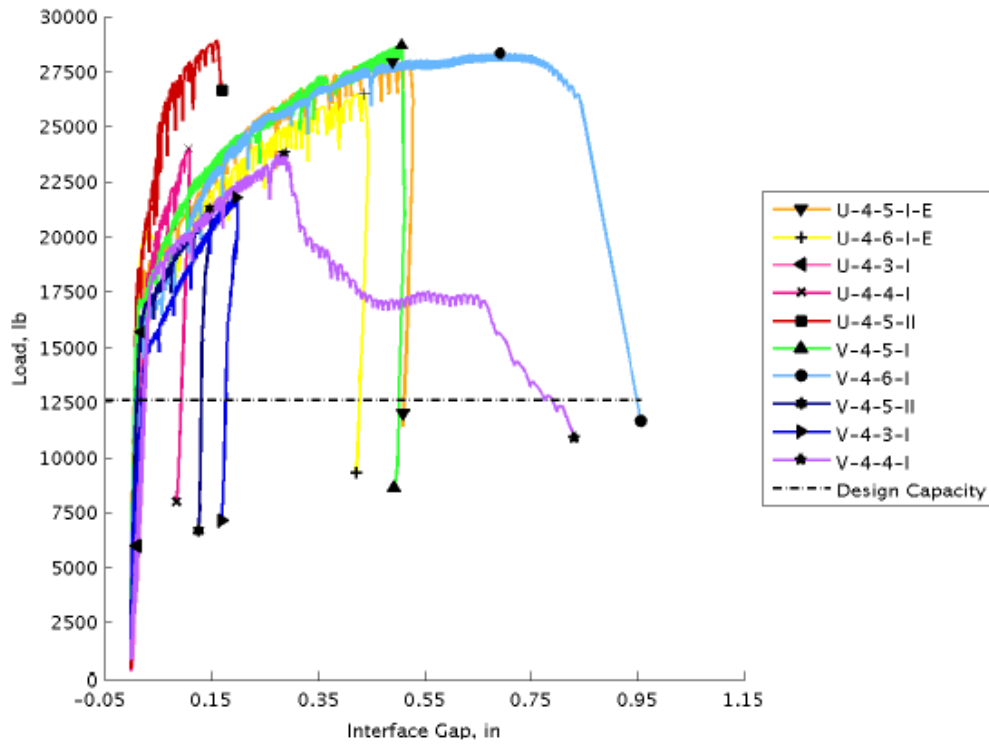
Figure 34: Load vs. North Interface Displacement for Specimens with No. 4 Bar (Halbe, 2014)
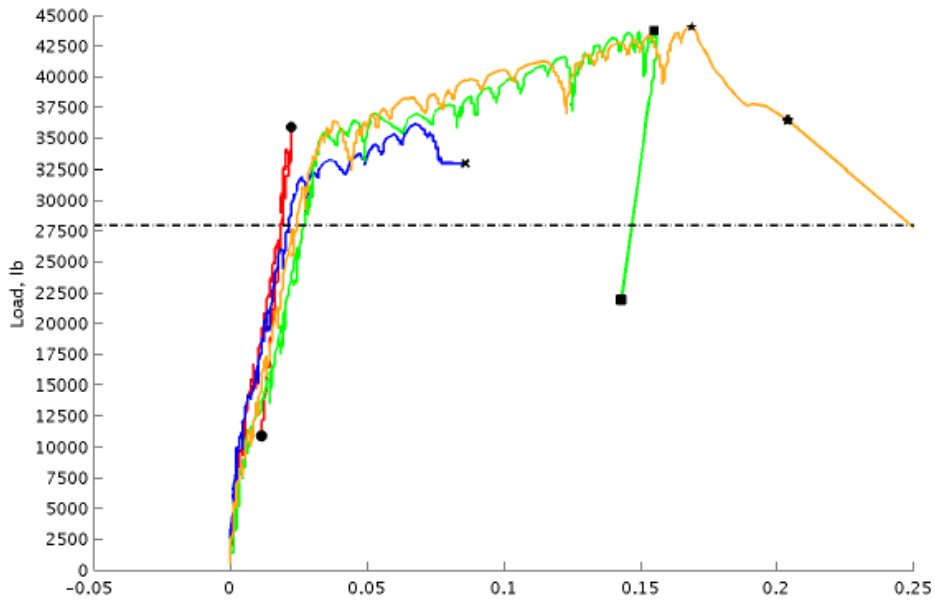
Figure 35: Load vs. South Interface Displacement for Specimens with No 6 Bar (Halbe, 2014)

2.4.2 Ultra-High Performance Concrete Compressive Strength

Table 4 contains UHPC tensile strength results from 3 different Virginia Tech researchers [(D'Alessandro, 2013), (Halbe, 2014), (Field, 2015), (Joyce, 2014)]. All of the Virginia Tech researcher's test results show that UHPC's compressive strength is significantly greater than compressive strength of conventional concrete.

Table 4: Virginia Tech UHPC Compressive Strength Test Results

Researcher	Specimen ID	Specimen Age	Average Compressive Stress (ksi)	Number of Specimens Tested
Halbe	1		17.6	3
	2	13 Days	17.2	3
Field	3	7 Days	16.0	3
	4	28 Days	19.9	3
Joyce	5	7 Days	11.3	2
	6	11 Days	15.5	2
	7	7 Days	11.6	2
	8	11 Days	14.3	2
D'Alessandro	9	4 Days	14.5	3
	10	7 Days	18.7	3
	11	14 Days	19.5	3
	12	21 Days	20.3	3
	13	28 Days	20.8	3
	14	104 Days	24.9	3

2.4.3 Ultra-High Performance Concrete Tensile Strength

Table 5 contains UHPC tensile strength results from 3 different Virginia Tech researchers [(D'Alessandro, 2013), (Halbe, 2014), (Field, 2015)]. Fields concluded that the due to the steel fibers, UHPC exhibited strong splitting tensile strength and post

cracking behavior. Additionally, the UHPC was much more durable (scaling surface tests), making it a good option for shear keys where durability is key.

Table 5: Virginia Tech UHPC Tensile Strength Test Results

Researcher	Specimen ID	Specimen Age	Average Tensile Strength (ksi)	Number of Specimens Tested
Halbe	1	13 Days	2.04	3
	2	13 Days	2.20	3
Field	3	7 Days	1.81	2
	4	28 Days	2.40	2
D'Alessandro	5	7 Days	2.35	3
	6	14 Days	2.79	3
	7	196 Days	3.44	2

2.4.4 Ultra-High Performance Concrete Bond Strength

In 2014, Graybeal submitted a report and guidance on how field-cast UHPC connections should be constructed to provide a stronger and more durable connection between precast girders. Since the bond strength between UHPC and the precast concrete is much stronger than conventional grout, shorter rebar development lengths are allowed (Graybeal, 2014). Figure 36 from (Joyce, 2014) illustrates the bond strength of UHPC, very high performance concrete (VHPC), and conventional grout to precast concrete, respectively. The UHPC was named Ductal and produced by Lafarge. The VHPC mix was developed at Virginia Tech. It is similar to UHPC, but has less strength.

Bond strength was measured via the pull-off test. In addition to UHPC, a mix labeled "VHPC Large" was used in the research. VHPC-Large takes the original mix design of VHPC and substitutes the small aggregate for large aggregate. VHPC-Large mix design is shown in Table 6. Figure 37 shows UHPC and VHPC-Large's significant

bond strength compared to conventional grout, making it a useful substitute for grout in bridge joints.
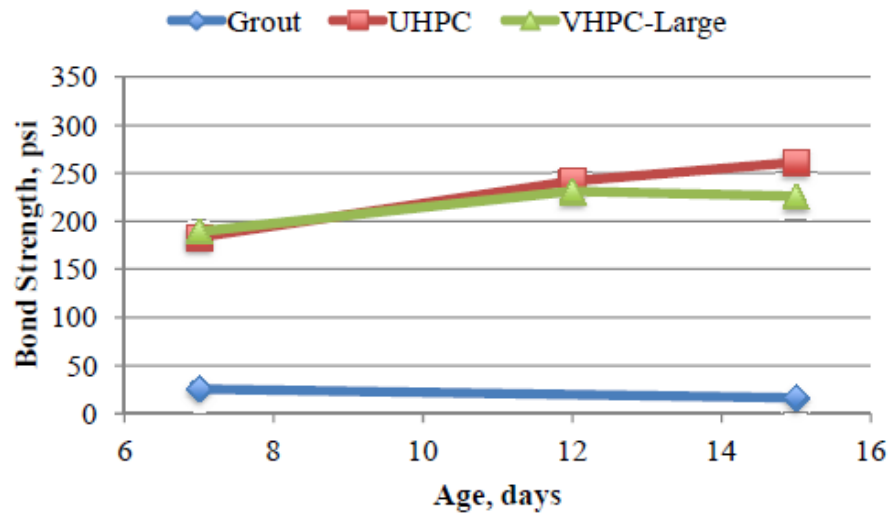
Figure 36: Bond Strength to Precast Concrete (Joyce, 2014)

Table 6: VHPC-Large Mix Design (Joyce, 2014)

Constituent	lb/yd^3
Water	319
Cement	1121
Fly Ash	240
Silica Fume	240
Sand	1450
¼ in. Limestone	621
1.2 in. Steel Fibers (2%)	265
HRWR	22-26 oz/cwt.
w/cm	0.20

Table 7 from Halbe (2014) illustrates the bond strength of UHPC, very high performance concrete (VHPC), and conventional grout to precast concrete, respectively. A schedule of the specimen types can be found in table 8. Mix designs for the UHPC and VHPC are shown in Table 9.

Table 7: Bond Strength to Precast Concrete (Halbe, 2014)

Specimen	Type	Bond Strength (psi)		Age (Days)
		Test Start	Test End	
1	Grout	N/A	N/A	76
2	UHPC	195	204	96
3	UHPC	79	93	128
4	Grout	68	74	170
5	VHPC	35	86	187
6	VHPC	97	93	211

Table 8: Specimen Test Schedule (Halbe, 2014)

Specimen	Type
1	Existing Detail
2	UHPC Top Connection
3	UHPC Top Connection with Topping
4	Existing Detail with K&E
5	VHPC Top Connection
6	VHPC Top Connection with Topping

43

Table 9: UHPC and VHPC Mix Proportions (Halbe, 2014)

Constituent	UHPC (lb/cu. ft.)	VHPC (lb/cu. ft.)
Cement	44.44	41.50
Silica Fume	14.44	8.90
Fly Ash	NA	8.90
Ground Quartz	13.15	NA
Fine Sand	63.7	53.70
¼ in. max coarse aggregate	NA	23.00
water	6.82	11.80
superplasticizer	1.92	0.75 – 1.05
Steel fibers	9.74	9.80
Water/cementitious	0.12	0.20

2.4.5 Ultra-High Performance Concrete in Joint Connections

In a study funded by the FHWA, UHPC deck connections between six different precast deck panels were tested under cyclic and static loadings (Graybeal, 2010). UHPC was used in both transverse and longitudinal connections between precast members. The specimens were first loaded to an amount below cracking strength for 2 million cycles, then 5 million cycles to a load larger than cracking strength. Finally, the specimens were statically loaded until failure.

Two of the six specimen tests were loaded in order to test the longitudinal joint. Figures 37 and 38 below, show the joint reinforcement details for the two longitudinal joint specimens. The average compressive strength of UHPC in the joint was 31.8 ksi. The concrete panels were fabricated using a high performance concrete (HPC) with 28-day compressive strength of 6.5 ksi.
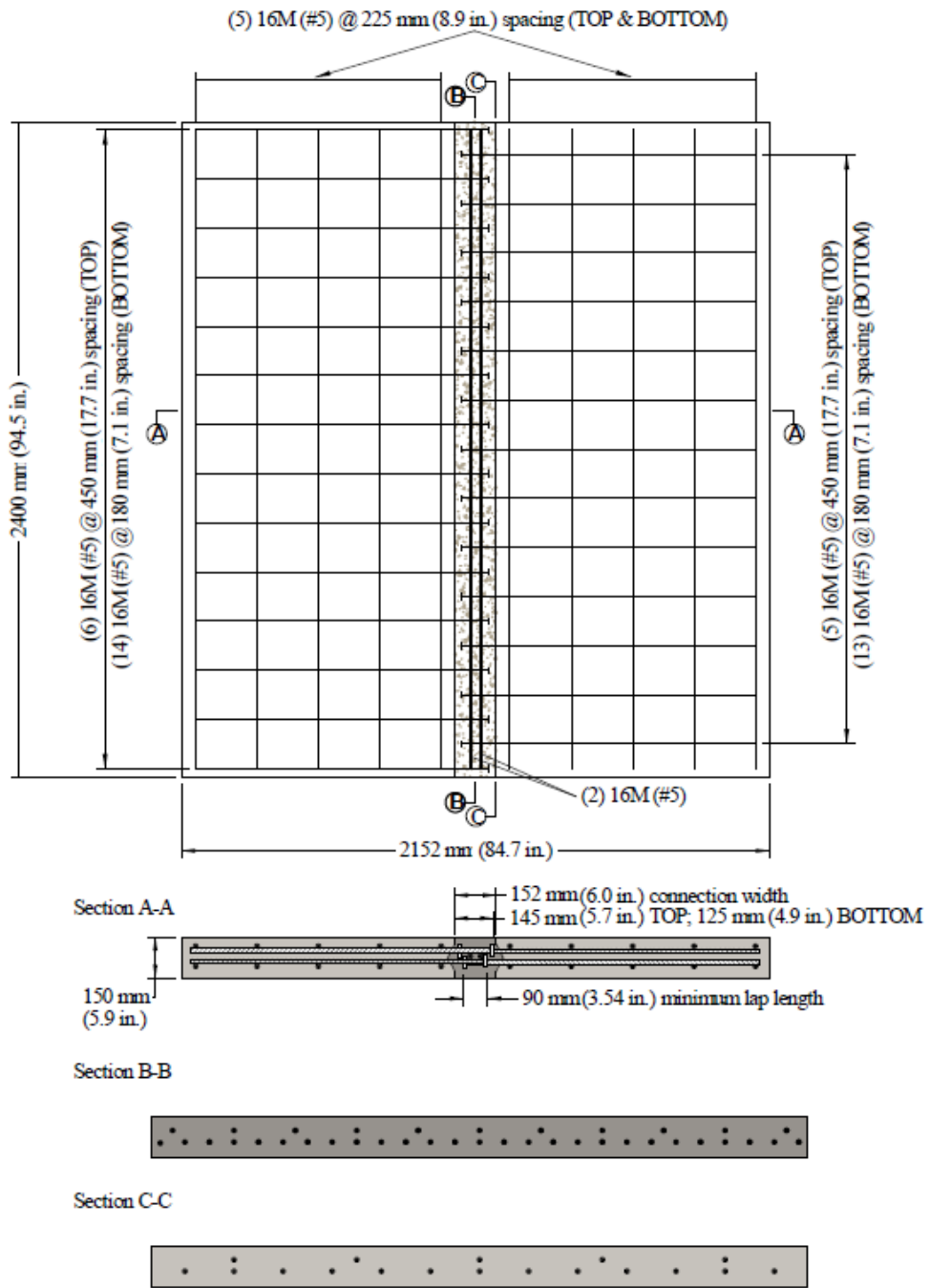
Figure 37: Layout and Rebar plan for Concrete Panel 6H (Graybeal, 2010)

(5) 16M (#5) @ 225 mm (8.9 in.) spacing (TOP & BOTTOM)

2400 mm (94.5 in.)

(6) 16M (#5) @ 450 mm (17.7 in.) spacing (TOP)
(14) 16M (#5) @ 180 mm (7.1 in.) spacing (BOTTOM)

(5) 16M (#5) @ 450 mm (17.7 in.) spacing (TOP)
(13) 16M (#5) @ 180 mm (7.1 in.) spacing (BOTTOM)

(2) 16M (#5)

2152 mm (84.7 in.)

Section A-A

152 mm (6.0 in.) connection width

150 mm
(5.9 in.)

150 mm (5.9 in.) lap length

Section B-B

Section C-C
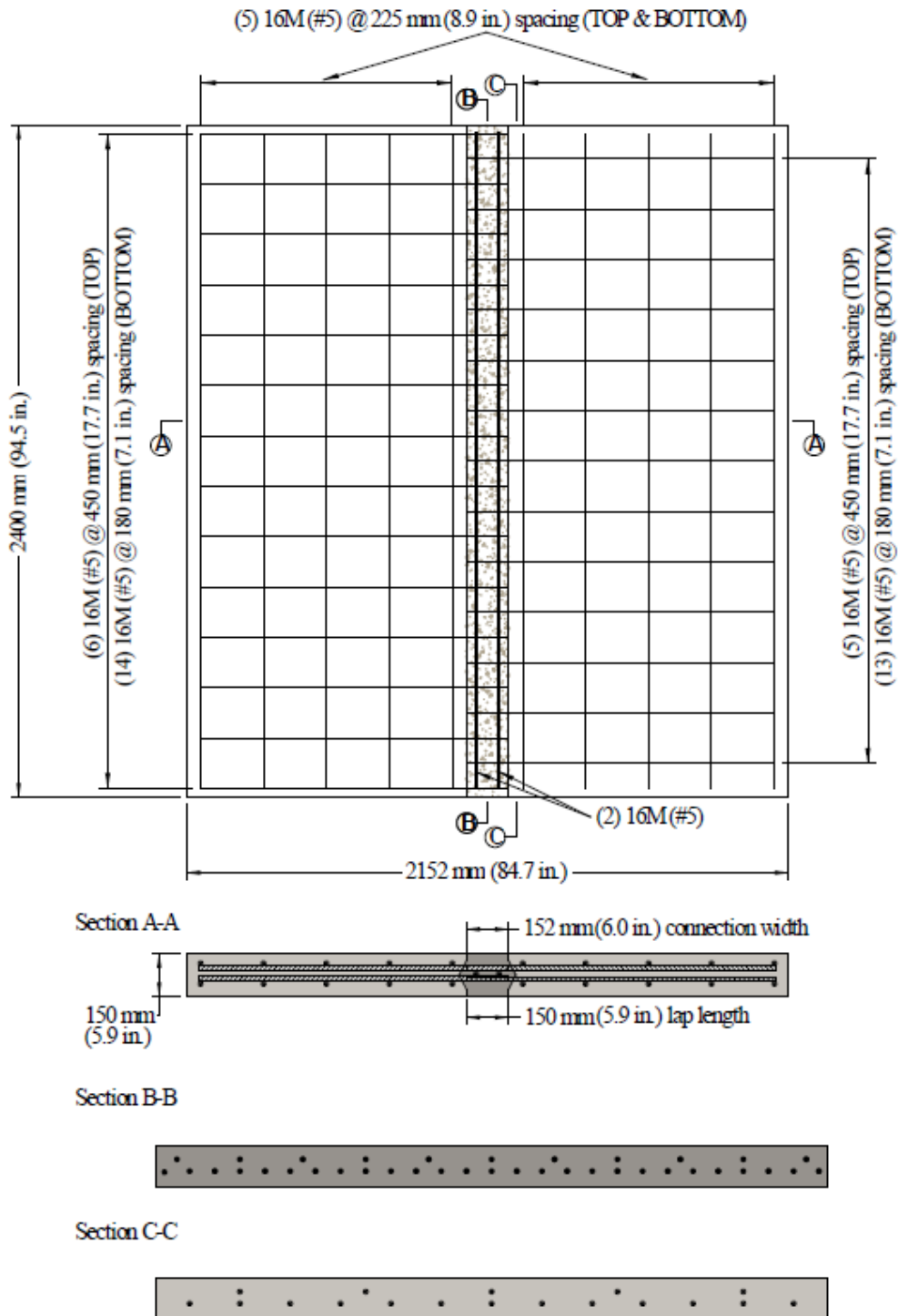
**Figure 38: Layout and Rebar plan for Concrete Panel 6B
(Graybeal, 2010)**

The deck panels were designed and fabricated in a way to simulate a longitudinal joint connection between the top flanges of adjacent bridge girders. The test specimens were loaded in three-point bending to induce flexural stresses in the longitudinal joint, as shown in Figure 39.
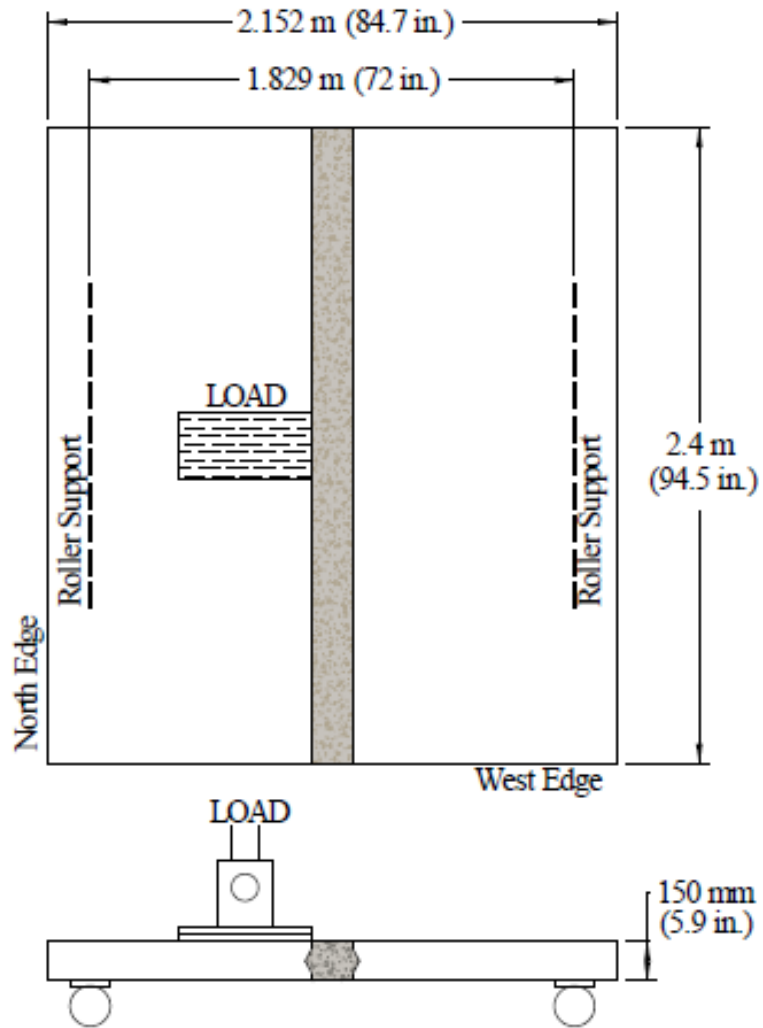
Figure 39: Test setup for Cyclic Loading (Graybeal, 2010)

The panel specimens were instrumented with both strain gauges and LVDTs, as shown in Figure 40. The LVDT was instrumented in such a way to capture any opening at the UHPC joint. Figure 41 shows a graph of the joint opening data as the test specimen went through the cyclic load test. 10,154,101 cycles were performed at a load range between 3 and 21.5 kips. 1,118,000 amount of cycles were performed between 3 and 32 kips. Minimal joint deflection was detected during the first two cyclic load phases as shown in figure 41. The final cyclic phase loaded the test specimen from 3 to 40 kips for 343,399 cycles, at which point the specimen failed along the joint interface. In the final loading phase, a joint opening of approximately 0.28 in. was detected before failure of the specimen. This data will be used as a reference to compare with the Hanging Rock Bridge LVDT test data measuring relative horizontal displacement at the joints.
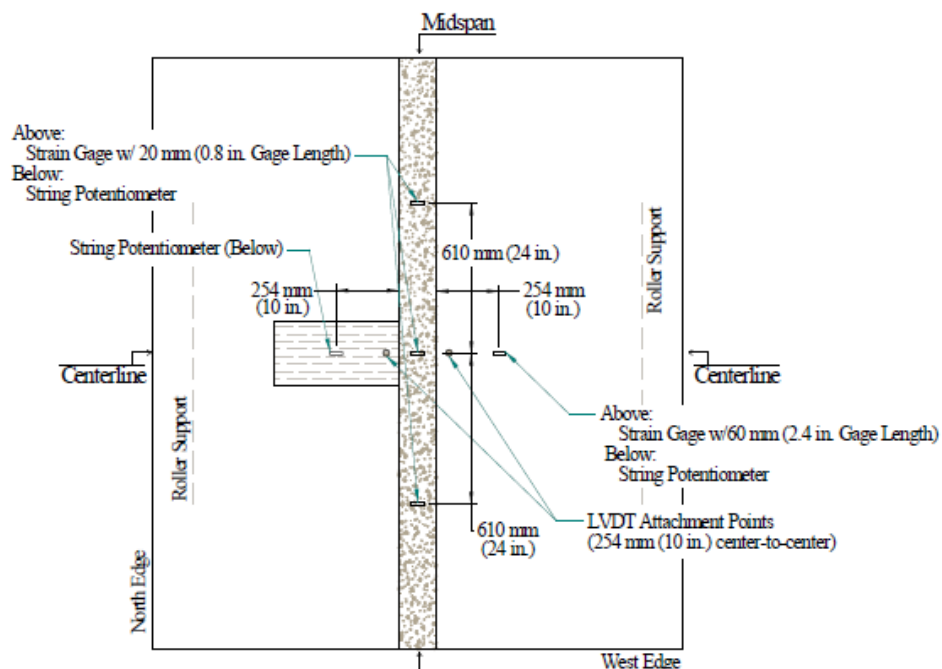
Figure 40: Concrete Panel with UHPC Joint Instrumentation Setup (Graybeal, 2010)
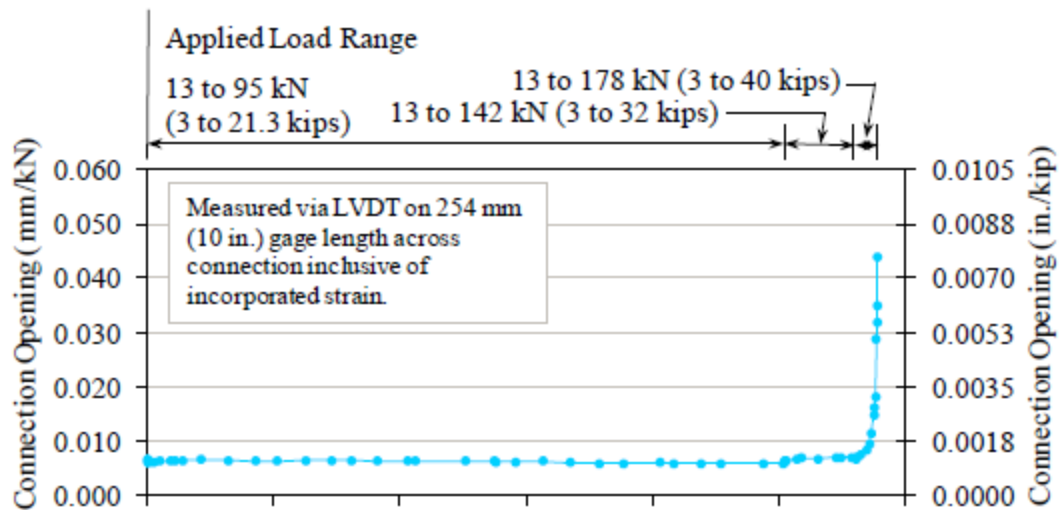
Figure 41: Graph of Load vs. Joint Opening for test specimen 6B (Graybeal, 2010)

Figure 42 is a picture of Graybeal's recommended UHPC detail for adjacent box beams. This structural connection allows the transfer of shear, moment, and axial forces across the joint. Additionally, no transverse post-tensioning or concrete overlay is needed. Graybeal (2014) states that this connection can easily be applied to the flange tips of NEXT beams. The connection is very similar to Kedar Halbe's flange spliced connection from his Virginia Tech dissertation mentioned in Literature Review section 2.3.1. It is important to research and observe how different connection details can positively influence the bond between precast concrete elements. These same tactics could later be applied to help NEXT D connection design.
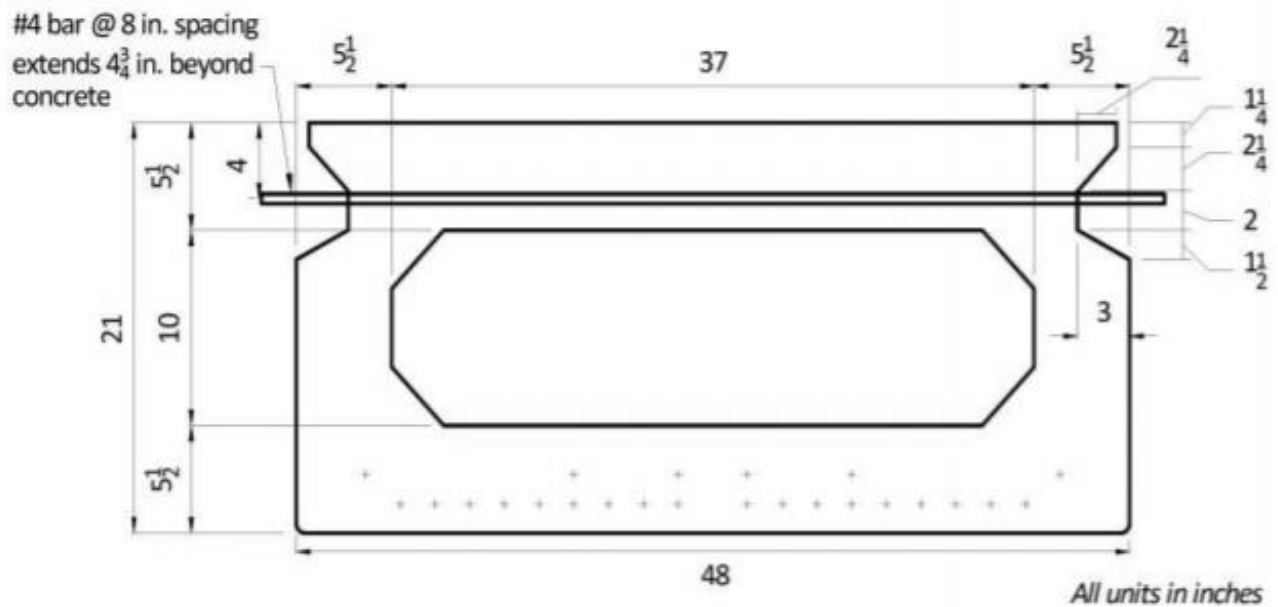
Figure 42: UHPC Adjacent Box Beam Connection (Graybeal, 2014)

Figure 43 from a PCI bridge technical committee displays several different options for NEXT D beam joint detailing. There are options for both UHPC and non-shrink grout shear keys. Vermont Agency of Transportation (VAOT) has built several bridges with the non-shrink grout and hooked bars and has not noted any issues with the joints (Culmo Email September 22, 2016).
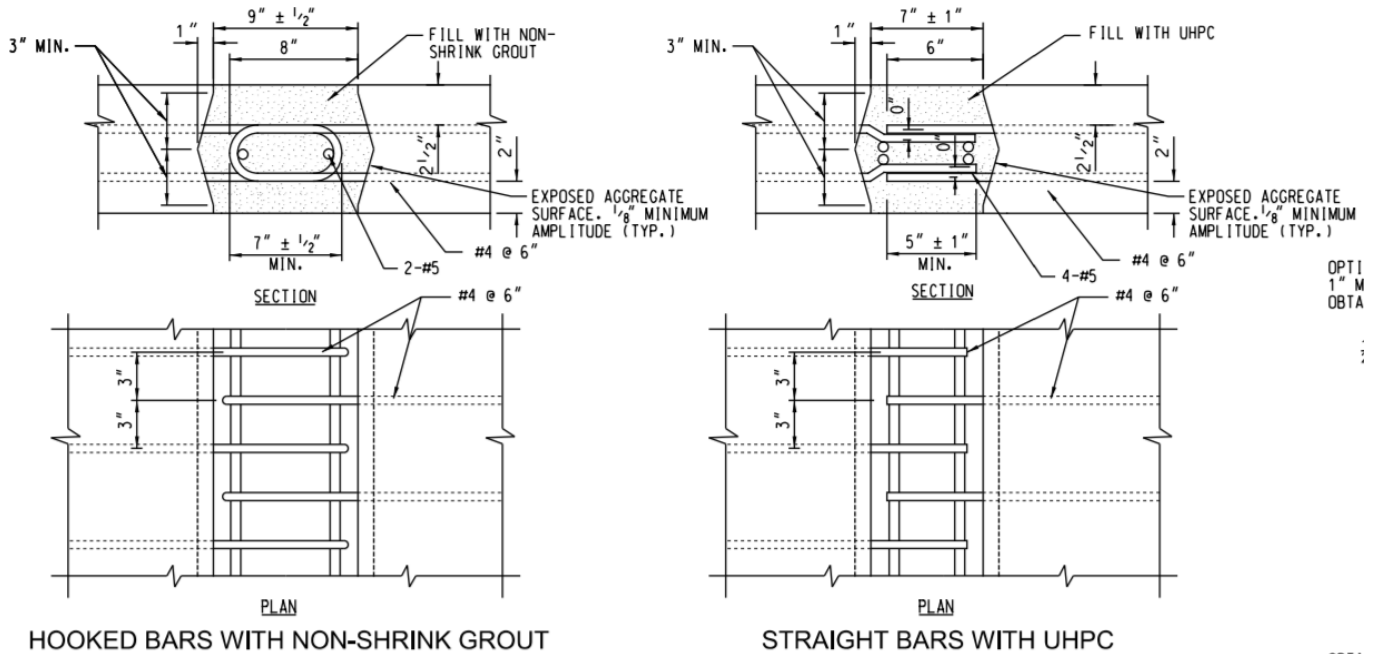
**Figure 43: NEXT D Joint Details for Non-shrink Grout and UHPC
(Culmo Email September 22, 2016)**

Researchers at Clemson University tested a joint very similar to the hooked bar detail from figure 43. The purpose was to evaluate the performance of the proposed shear key configuration that SCDOT was hoping to use for NEXT D beam joints. Figure 44, shows the shear key detail of the 11 specimens tested.
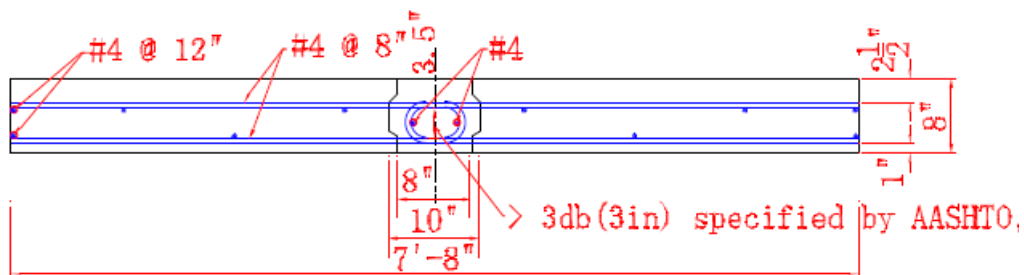
Figure 44: Hooked Bar Shear Key Detail (Sheng et al., 2013)

Three different materials were used for the shear key: Grout with polyvinyl alcohol (PVA) fiber, UHPC with steel fiber, and UHPC with PVA fiber. Two precast panels were connected via joint and then instrumented with gauges. After instrumentation, specimens were loaded both statically and cyclically. Instrumentation layout can be seen in figure 45. Table 10 shows different specimens and their respective shear key mixtures.
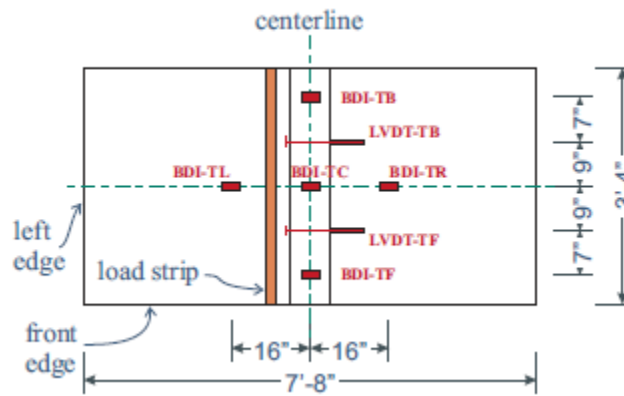
Figure 45: Strain Gauge and LVDT Layout for Shear Key Test (Sheng et al., 2013)

Table 10: Test Matrix for Static Tests (Sheng et al., 2013)

Shear Key Mixture	Moment to Shear Ratio	Specimen ID
Quikrete Non-Shrink Precision Grout + Nycon-PVA-RECS15	43 (HM)	STA-01 MONO-01 MONO-01(redo)
Lafarge UHPC + steel fiber	43 (HM)	STA-02 MONO-02
Lafarge UHPC + Kuraray PVA	43 (HM)	STA-03 STA-04 MONO-03
	12 (HS)	STA-05 STA-06 MONO-04

During the static tests, bond interface cracks were recorded as 121 kip-in., 277 kip-in., 183 kip-in., 247 kip-in., 285 kip-in., and 285 kip-in. for specimens STA-01 to STA-06, respectively. These values were determined from the moment-curvature curves taken from LVDT readings. The max moment capacities for these specimens were 763.5 kip-in, 742.5 kip-in, 736.6 kip-in, 738 kip-in, 650 kip-in, and 634.1 kip-in, respectively. Fatigue/service load capacities for specimens FAT-01 through FAT-04 were 5.3 kip (110 kip-in of internal moment), 8.7 kip, 4.9 kip, and 8.1 kip respectively. No relative horizontal displacements were included in the report. A main conclusion from the report was that UHPC was the recommended NEXT D shear key material since it was adequately strong, ductile, and stiff.

2.5 Field Test of Adjacent Beam Bridges

2.5.1 Suck Creek Bridge

Researchers at Clemson University performed a live load test at the Suck Creek Bridge in South Carolina in order to understand the bridge's load-sharing abilities and behaviors (Sheng et al., 2013). Specifically, the goal of the testing was to analyze the data and explain why reflective cracking was forming on the wearing surface of the bridge. Figure 46, shows a cross section of the bridge deck.
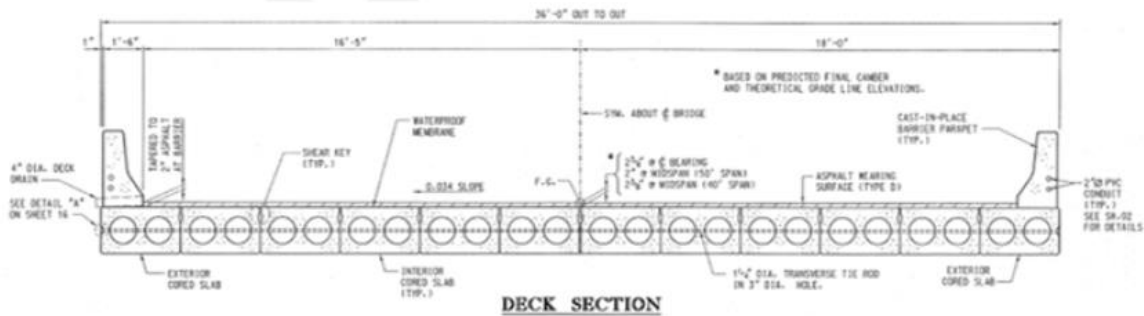
Figure 46: Cross Section of Suck Creek Bridge (Sheng et al., 2013)

LVDTs and strain gauges were used in bridge instrumentation. LVDTs captured the global displacements of the bridge and local displacements across the shear key. The LVDT instrumentation setup is shown in figures 47 and 48.
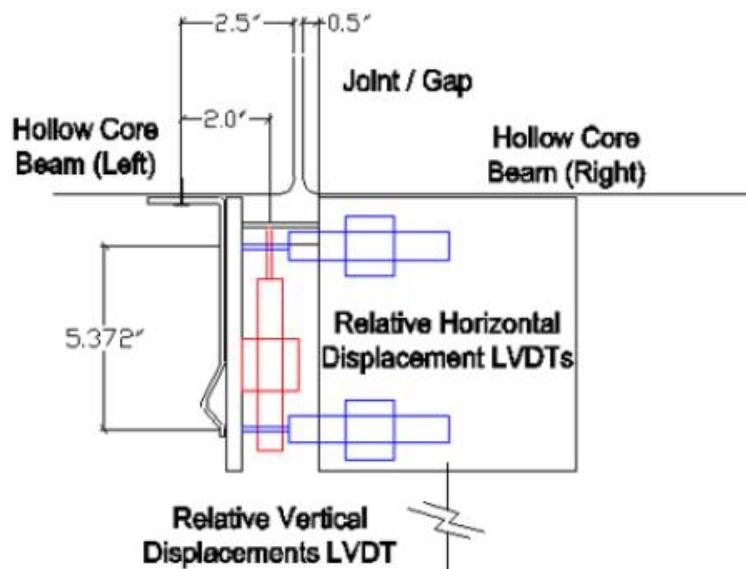
Figure 47: LVDT Mounting Schematic (Sheng et al., 2013)
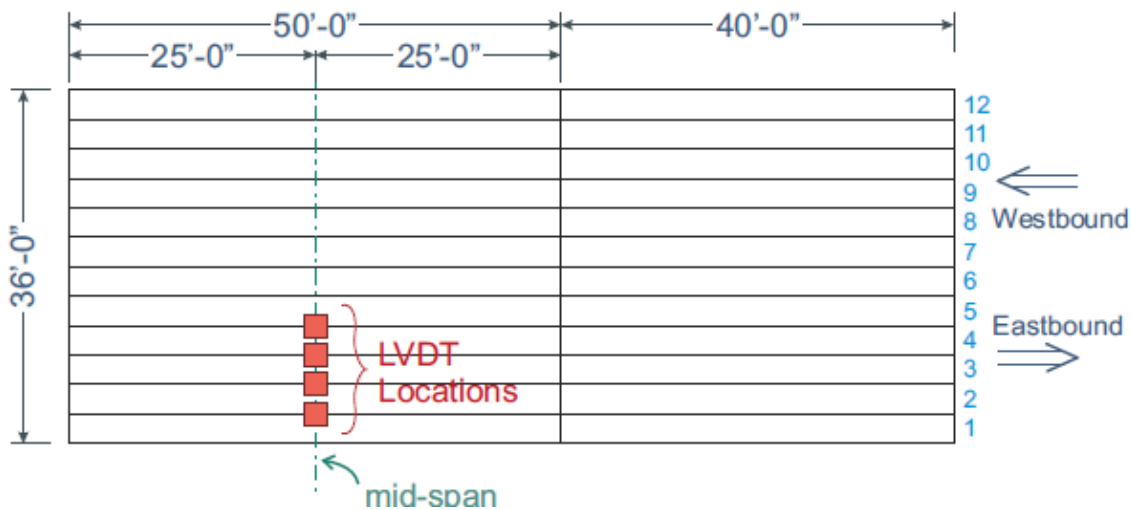
Figure 48: LVDT Locations for First Test (Sheng et al., 2013)

A weighted dump truck was driven over the bridge (figure 49) and data was recorded. Joint displacement can be seen in table 11. The relative deflections were fairly large, and it was determined that these relative vertical and angular displacements were causing reflective cracking. The relative deflections have been included to compare with deflections measured from the solid slab span live load test of the Hanging Rock Creek Bridge.
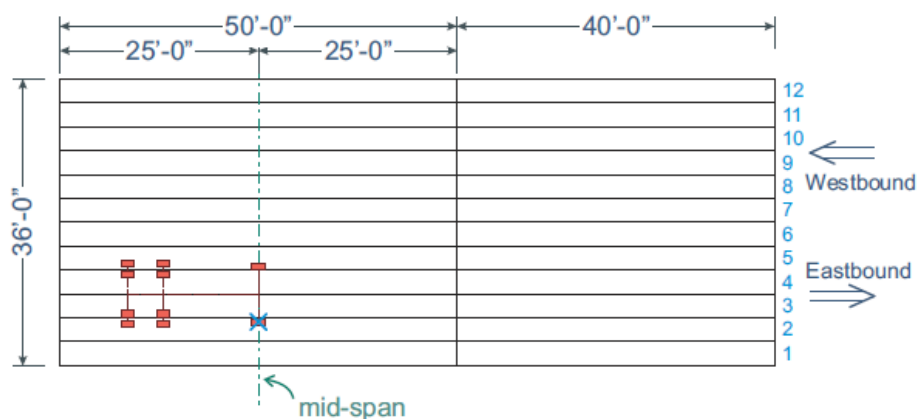
Figure 49: Truck Position for First Live Load Test (Sheng et al., 2013)

Table 11: Displacement Values from First Bridge Test (Sheng et al., 2013)

Joint	LVDT	Mean (in.)	COV of Displacement
	Relative Displacement Measurements		
	Relative Vertical	-0.0171	0.010
1	Horizontal Top	0.0032	0.019
	Horizontal Bottom	0.0037	0.010
	Relative Vertical	-0.0004	0.003
2	Horizontal Top	0.0064	0.013
	Horizontal Bottom	0.0079	0.006
	Relative Vertical	-0.0004	0.021
3	Horizontal Top	-0.0002	0.210
	Horizontal Bottom	-0.0003	0.030
	Relative Vertical	0.0050	0.005
4	Horizontal Top	0.0056	0.010
	Horizontal Bottom	0.0058	0.016
	Global Displacement Measurements		
1	Global Vertical	-0.063	0.032
2	Global Vertical	-0.071	0.003
3	Global Vertical	-0.067	0.006
4	Global Vertical	-0.063	0.001

2.5.2 Arden Road Bridge

Researchers at Virginia tech performed a live load test at the Arden Road Bridge in Nokesville, VA to understand the bridge's load-sharing abilities and behaviors (Halbe, 2014). Specifically, the goal of the testing was to analyze the data and analyze the bridge's load sharing capabilities. Figure 50, shows a cross section of the bridge deck.
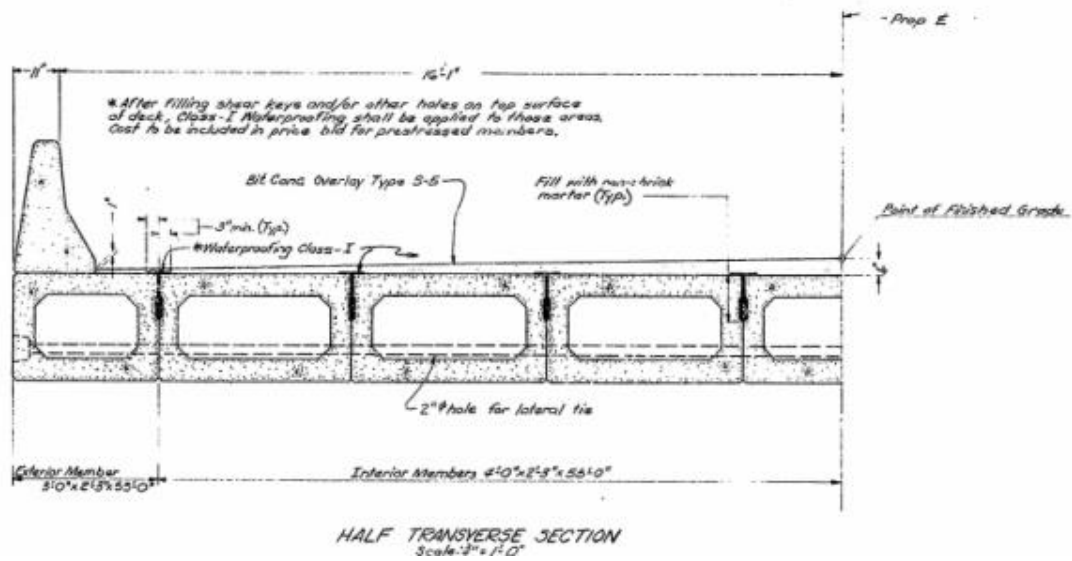
Figure 50: Cross Section of Arden Road Bridge (Halbe, 2014)

LVDTs and strain gauges were used in bridge instrumentation. LVDTs captured

the global displacements of the bridge and local displacements across the shear key. The

bridge instrumentation is shown in figure 51.
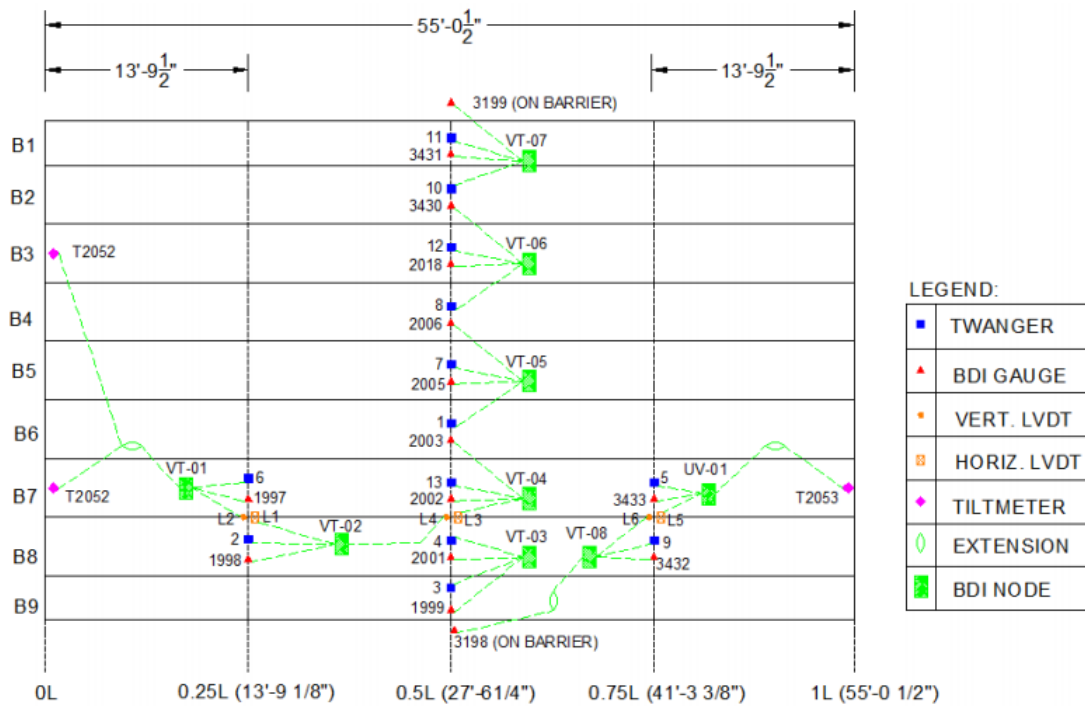
Figure 51: Arden Road Bridge Layout and Instrumentation (Halbe, 2014)

A weighted dump truck was driven over the bridge and data was recorded. Joint displacement can be seen in figure 52. The relative deflections have been included to compare with deflections measured from the solid slab span live load test of the Hanging Rock Creek Bridge. It should be noted that lots of reflective cracks were present in the bridge's wearing surface.

58
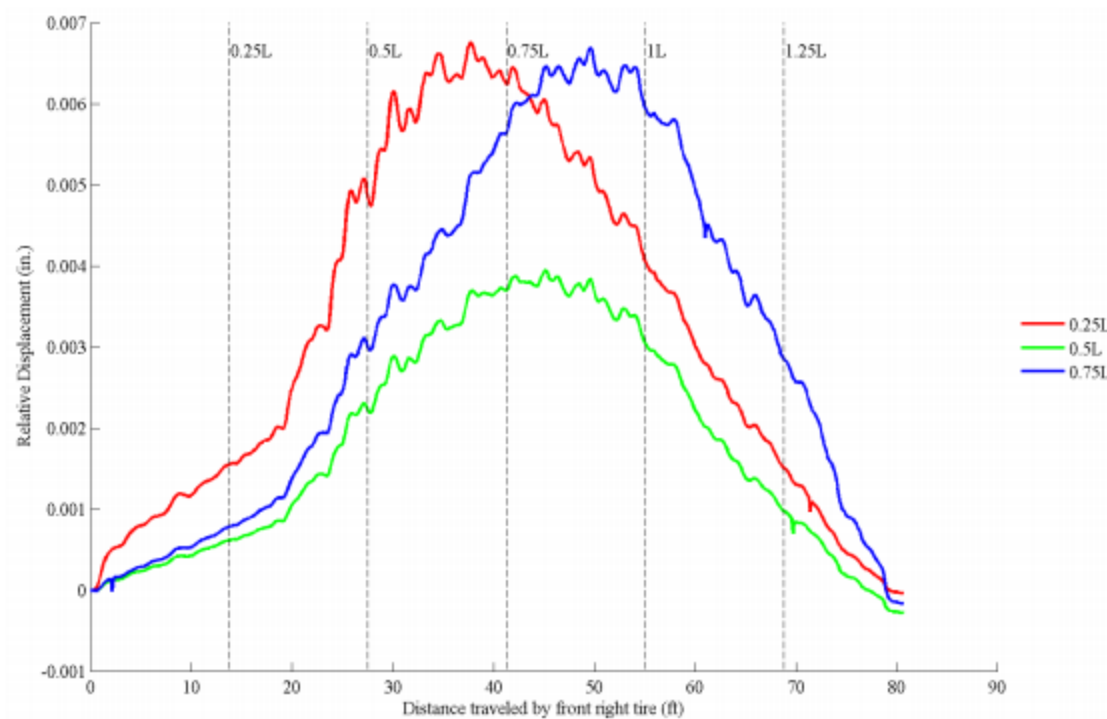
Figure 52: Typical Horizontal joint displacement (Halbe, 2014)

2.6 NEXT Beam Case Studies and Investigations

NEXT Beam bridges have successfully been used for bridge construction by many state DOTs across the country. Additionally, live load testing and finite element modeling has been performed on the NEXT F beam section in order to evaluate live load distribution factors for both moment and shear.

2.6.1 New Bridge Case Study

NEXT beam bridges are being used across the United States by many state DOT's. States that have accepted the use of NEXT beams include Massachusetts, Vermont, Maine, Rhode Island, New Hampshire, New York, New Jersey, Delaware, Pennsylvania, and Virginia (Seraderian, 2016).

The New Bridge, located in York, Maine, was the first NEXT beam bridge designed and constructed in the United States (figure 53) (Gardner and Hodgdon, 2013). It is seven-span concrete bridge that takes Route 103, 500 feet across the York River. The original bridge was a steel girder system built in 1957. It was quite narrow (24 feet roadway width) and also in poor condition due to the coastal climate. Additionally, the original bridge had to be closed during construction, thus detouring traffic. As a result, accelerated bridge construction (ABC) was a must in addition to an increased roadway width.

Contractors bidding on the bridge were presented with two bridge designs including one utilizing the New England Bulb Tee (NEBT) and one utilizing the NEXT 36 (36 inch depth) beam. The NEBT beam was an attractive option since contractors are very familiar with it, and the price was driven down due to the presence of multiple manufactures. However, of the five contractors that bid, four decided to bid on the NEXT beam design option. The NEXT beam and NEBT superstructures were roughly the same cost in materials. The contractors discovered that the NEXT beams could be erected more quickly leading to project savings. Each span consisted of four NEXT beams and no deck formwork was required. It was estimated that the NEXT beam system saved the project seven weeks of construction time in comparison to the NEBT beam system.

Figure 53: The New Bridge in York, ME (Gardner and Hodgdon, 2013)

2.6.2 NEXT F: AASHTO Equations, FE Modeling, and Live Load Testing

Researchers at the University of Massachusetts at Amherst calculated NEXT F DFM

values using AASHTO LRFD equations, FE modeling, and live load testing. Research

was conducted in a three phase project as follows:

1. Phase one occurred in 2012 and was a parametric study of how changing span

   length and skew angle affected DFM values of NEXT F bridges using type (i) and

   type (k) AASHTO LRFD equations. Additionally, these results were compared to

   those of the FE model

2. Phase two occurred in 2014 when a live load test was conducted on the NEXT F

   Brimfield Bridge. DFM values were determined and compared to the AASHTO

LRFD DFM values. DFM values from the live load test were then used to

recalibrate the FE model from phase one.

3. Phase three was a final report where conclusions and recommendations were

made.

In phase one, researchers at the University of Massachusetts at Amherst

calculated NEXT F DFM values using two different stem spacings and bridge categories

(Singh, 2012). The first method, called the double stem approach (DST/Type (i)), took

the stem spacing as the spacing between NEXT F beams, as shown by the value S_2 in

figure 50. The second method, called the single stem approach (SST/Type (k)), calculated

the stem spacing as the average stem spacing of two adjacent NEXT F beams, displayed

as the value S^* in figure 54. S^* is the DFM for a single web, and was thus multiplied by

two to reach a DFM for the entire NEXT F unit. The SST approach was applied to type

(k) bridges, while the DST approach was applied to type (i) bridges. Research concluded

that either spacing method could be safely used to calculate the NEXT F DFM (Ericson

et al.), but the SST (type k) approach was more conservative (Singh, 2012).
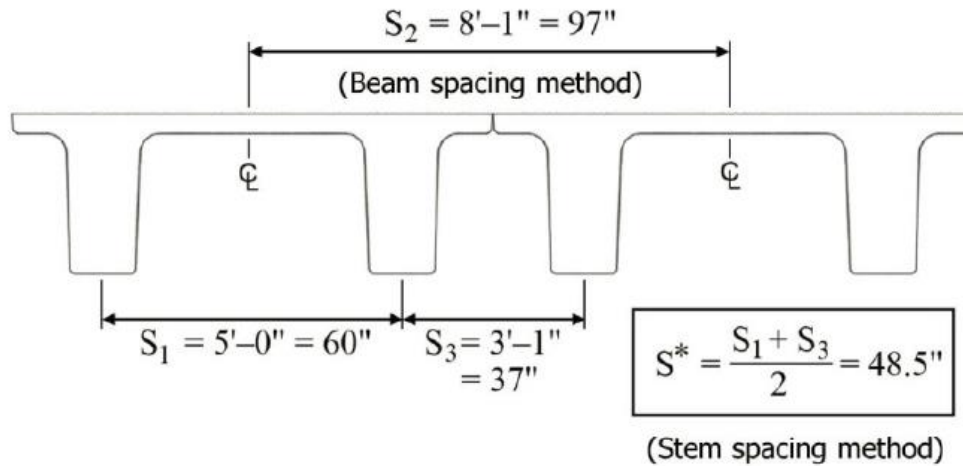
Figure 54: Differential Stem Spacing of the NEXT F Beam (Singh, 2012)

A parametric study was performed using the AASHTO type (i) and type (k) equations and a finite element model in order to see how different parameters affected the DFM values. Specifically, skew angle and span length were varied. By changing the span length and skew angles, different DFM values for interior and exterior girders were generated from AASHTO equations. The results are found in tables 12 13 below (Singh, 2012). Results show that the single stem method (type k) from AASHTO is the most conservative in calculating DFM values for interior girders, while double stem method (type i) is more conservative in calculating DFM values for exterior girders. The finite element model produced the least conservative DFM values.

Table 12: DFM Values with Differing Span Lengths - (Skew Angle = 0⁰) [Singh, 2012]

Beam Location	Span Spacing or Analysis Method	50 ft			66.7 ft			80 ft		
		SSM	BSM	FE	SSM	BSM	FE	SSM	BSM	FE
Interior	$gM_{i\text{-}1L}$	0.66	0.53	0.51	0.63	0.50	0.42	0.61	0.49	0.40
	$gM_{i\text{-}2}^{+}$	0.83	0.71	0.58	0.82	0.70	0.57	0.80	0.68	0.55
Exterior	$gM_{e\text{-}1L}$	0.71	0.82	0.64	0.71	0.82	0.62	0.71	0.82	0.60
	$gM_{e\text{-}2}^{+}$	0.63	0.74	0.64	0.62	0.73	0.63	0.61	0.72	0.62

Table 13: DFM Values with Differing Skew Angles - (Span = 66.7 ft) [Sing, 2012]

Beam Location	Angle Spacing or Analysis Method	0⁰ skew			30⁰ skew			45⁰ skew		
		SSM	BSM	FE	SSM	BSM	FE	SSM	BSM	FE
Interior	$gM_{i,\,1L}$	0.63	0.50	0.42	0.61	0.48	0.42	0.59	0.46	0.39
	$gM_{i,\,2}^{+}$	0.82	0.70	0.57	0.79	0.66	0.57	0.77	0.63	0.52
Exterior	$gM_{e,\,1L}$	0.71	0.82	0.62	0.69	0.79	0.65	0.67	0.74	0.64
	$gM_{e,\,2}^{+}$	0.62	0.73	0.63	0.60	0.69	0.66	0.58	0.65	0.65

In a second follow up study performed at the University of Massachusetts at Amherst, DFM values were calculated from a live load test and compared with DFM values calculated from AASHTO LRFD equations (Bahjat et al., 2014). The live load test occurred at the Brimfield Bridge of Brimfield, MA. The bridge was a single span bridge constructed to replace the aging bridge that was located over Mill Brook. The superstructure of the bridge consisted of six NEXT 32-F beams (figure 55) with an 8 in. CIP deck. The bridge was 66.7 ft. and had a 30 ° skew.
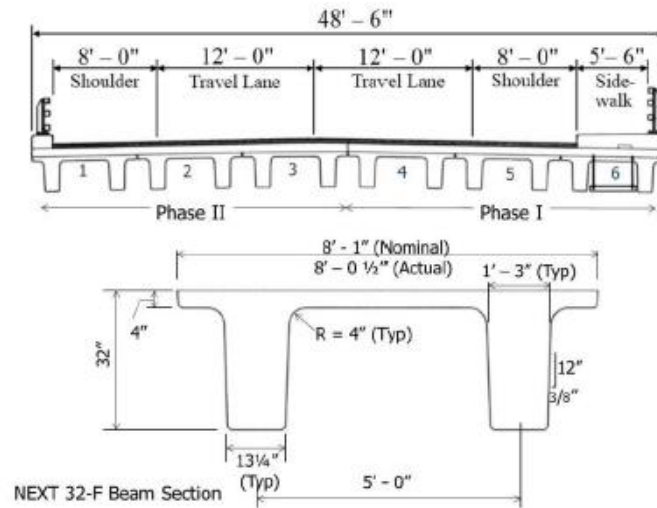
Figure 55: NEXT 32-F Dimensions and Bridge Cross Section (Bahjat et al., 2014)
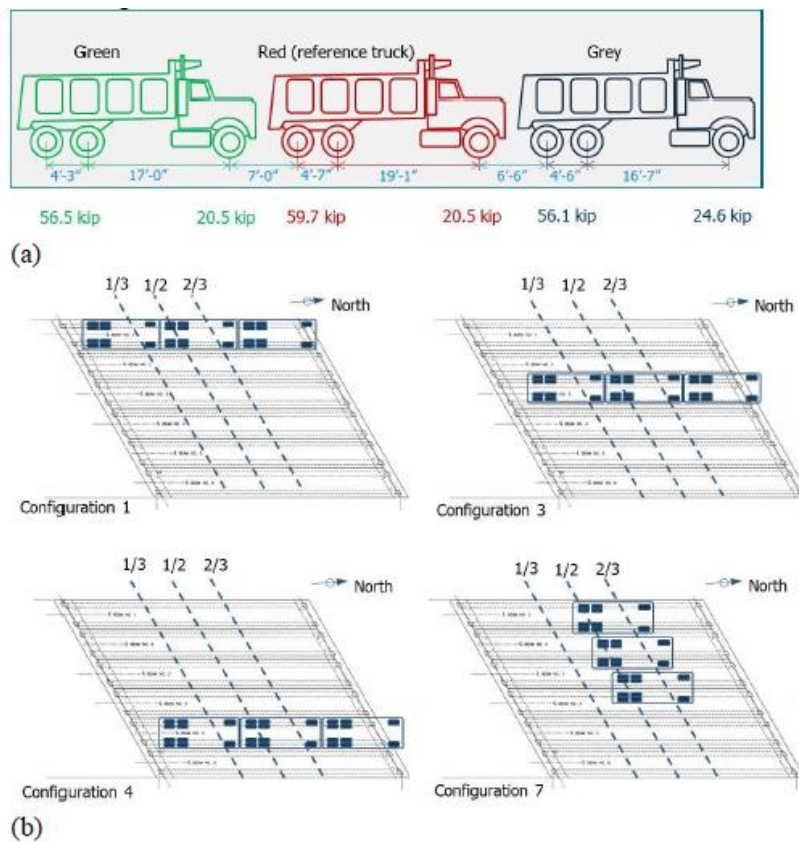
Figure 56: Weighted Trucks and their Respective Positions. (a) Truck Dimensions and axle weights; (b) Truck Configurations used in Load Test (Bahjat et al., 2014)

Single and multiple lane load configurations were used and are shown in figure 56 and 57. The moments experienced by each bridge girder for each of the 10 different truck configurations are shown in table 14. DFM values were calculated from this table. From the single lane loaded live load test, the DFM was calculated to be much lower than the moment DFM when using AASHTO LRFD (0.53 versus 0.61) (Bahjat et al., 2014). When multiple lanes were loaded, the live load test had a calculated DFM of 0.75 and the AASHTO LRFD calculated value was 0.78.
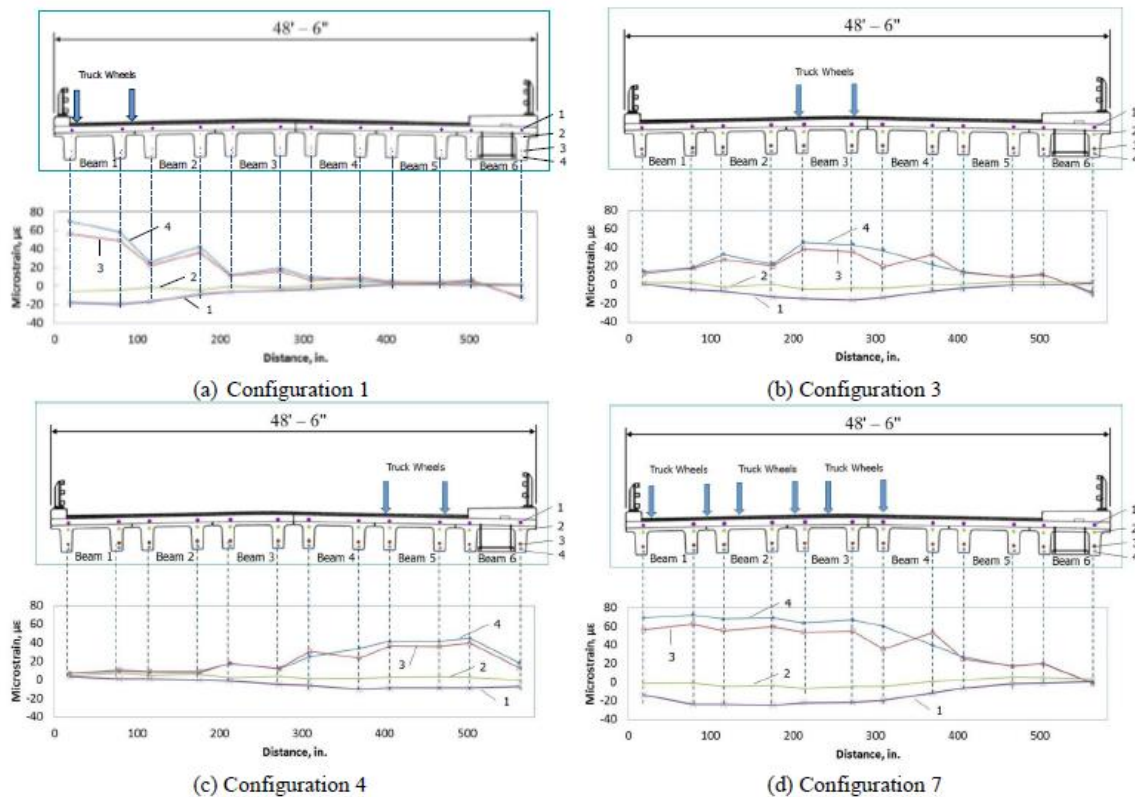
Figure 57: Strain Distribution for Multiple Live-Load Loading Conditions (Bahjat et al., 2014)

Table 14: Maximum Moments Experienced During Load Test (Bahjat et al., 2014)

Load test[a]	Moment (Kip-ft)							M_{max}/M_{total}[b]
	Beam 1	Beam 2	Beam 3	Beam 4	Beam 5	Beam 6	Total	
1N	346.05	182.04	82.21	42.30	18.67	-17.03	654.24	0.53
1S	170.08	90.02	83.74	35.87	15.83	-3.86	391.67	0.43
2N	203.36	236.45	144.07	75.29	33.54	-0.33	692.38	0.34
2S	195.56	228.99	130.37	57.11	25.53	-7.35	630.21	0.36
3N	90.58	148.10	236.40	160.12	62.03	10.43	707.66	0.33
3S	91.64	149.67	224.12	143.79	55.97	5.52	670.71	0.33
4N	44.03	41.93	79.74	159.47	223.48	168.85	717.48	0.31
5N	293.10	210.83	106.12	58.80	23.23	-8.02	684.06	0.43
5S	277.11	213.84	104.30	49.71	22.01	-13.70	653.27	0.42
6N	144.39	211.93	193.99	105.11	40.58	3.46	699.47	0.30
7N	381.76	365.98	345.54	270.30	119.26	51.28	1534.11	0.75
8N	107.53	190.66	340.26	389.69	313.84	221.26	1563.24	0.75
9N	191.40	189.32	190.49	170.82	99.17	46.54	887.73	0.65
10N	80.55	99.01	162.83	207.17	175.97	165.36	890.90	0.70
FE-7N[c]	399.04	357.61	334.36	332.50	117.50	80.63	1621.64	0.74
FE-8N[c]	94.40	254.74	332.50	396.30	404.41	163.76	1646.10	0.74

[a]Number indicates configuration number and letter indicates facing direction of trucks.
[b]The total moment in Configurations 7 through 10 was divided by three to calculate the live-load distribution factor for a single loading lane.
[c]Live-load distribution factors from FE models were only computed for variable soil conditions (see FE section in paper).

A final report drew conclusions and made recommendations from the two studies performed at the University of Massachusetts at Amherst (Ericson et al.). Conclusions drawn were that the live load test DFM values were more conservative that than those calculated in the original FE model (from phase one), but less conservative than AASHTO LRFD equation DFM values.

2.6.3 Clemson University NEXT D Beam FE Modeling and AASHTO Equation Parametric Study

Using AASHTO LRFD equations and FE modeling, researchers at Clemson University performed a parametric study on the NEXT-6 D beam (a NEXT D beam with 6' wide flange), specifically on how span length and lanes loaded affected the DFM values (Sheng et al., 2013). For AASHTO LRFD equations, the NEXT-6 D beam was

analyzed as a type (i) cross section. Results from the FE model were much less conservative than the AASHTO equations. A table of the calculated DFM values is shown in table 15. The Hanging Rock Creek NEXT D span is very similar to the NEXT-6 D. Results between the two studies will be compared.

Table 15: Load Distribution Factors for NEXT-6 D Beam (Sheng et al., 2013)
.

Span length (ft)	Girder location	Number of lanes loaded	Positive moment		Shear	
			3D FEM	AASHTO	3D FEM	AASHTO
40	Exterior	1	0.250	0.683	0.652	0.683
		2	0.271	0.480	0.626	0.464
		3	0.255	0.480	0.545	0.464
	Interior	1	0.291	0.431	0.527	0.600
		2	0.437	0.552	0.694	0.671
		3	0.475	0.552	0.608	0.671
30	Exterior	1	0.203	0.683	0.633	0.683
		2	0.192	0.519	0.591	0.464
		3	0.167	0.519	0.504	0.464
	Interior	1	0.351	0.478	0.523	0.600
		2	0.472	0.596	0.735	0.671
		3	0.506	0.596	0.637	0.671
22	Exterior	1	0.345	0.683	0.619	0.683
		2	0.294	0.565	0.554	0.464
		3	0.239	0.565	0.465	0.464
	Interior	1	0.395	0.535	0.614	0.600
		2	0.534	0.649	0.779	0.671
		3	0.519	0.649	0.668	0.671

2.7 Accelerated Bridge Construction

America's bridges are in need of repairs and replacements. Many bridges have been rated structurally deficient and many are reaching their design life of 50 years. There is a great need for these bridges to be constructed in both a safe manner and at a faster rate. Construction activity creates traffic congestion, which impedes the nation's

productivity and safety (Chen, 2014). Accelerated bridge construction (ABC) is a method of construction that can accelerate the rate at which bridges in the United States are built and repaired. ABC utilizes prefabricated bridge element systems (PBES), which can allow contractors to erect bridges in a manner of hours compared to months. PBES parts fit together like an erector set and need only to be bonded together.

Traditional simple bridges can take months to construct. The foundation, pier columns and caps, and superstructure all must be formed and poured. ABC bridges are built at a very high quality. Conventional concrete decks have a life span of 25 years. Using high performance concrete (HPC), the life span of the bridge deck is projected to be up to 75-100 years. Thus, using HPC in ABC, the product is potentially a higher quality more durable bridge constructed at an accelerated rate. Additionally, there are fewer traffic delays and the work zone is safer to both workers and motorists.

Box beams have certain limitations that hinder their ability to be built according to an ABC schedule. If a reinforced concrete overlay is needed much time and money is spent for and on the formwork. Additionally, shear key grouting is slow due to the limited workspace. While the box beam falls shorts in these two cases, the NEXT beams thrive. NEXT F beams are built with a 4 inch flange that acts as a concrete overlay form. NEXT D beams are built with an 8 inch flange and only require an optional asphalt overlay. Also, NEXT beam shear keys are much wider, which allows for a quicker and higher quality shear key grouting (The NEXT Beam, *High Bridge Team* Powerpoint). Finally, NEXT sections are wider than solid slab and hollow core slabs. Fewer bridge girders can be used to provide traffic lanes, which saves construction time.

2.8 Nondestructive Load Testing (Definition and Objectives)

The manual from the 1998 USA Transportation Research Board defined nondestructive load testing as the following:

"*Non-destructive load testing is the observation and measurement of the response of a bridge subjected to controlled and predetermined loadings without causing changes in the elastic response of the structure. The principle of load testing is simply the comparison of the field response of the bridge under test loads with its theoretical performance as predicted by analysis. Basically, two types of non-destructive load tests are available: diagnostic and proof.*" (Casas et al., 2009)

"When determining a safe and accurate load-carrying capacity for a bridge, the best model of the structure is to use the bridge itself" (Chajes et al., 2000). Testing performed on bridges over the years has shown that sometimes bridges resist loads in ways that are not always considered in design or in modern engineering codes (Hiens and Galambos, 1972). Additionally, theoretical models are not always able to predict bridge behavior either due difficult to find parameters or because of difficulties modeling soil-structure interaction. It is, therefore, very beneficial to conduct nondestructive load testing on certain bridges to gain insight into bridge behavior. Some main objectives of load testing are the refinement of structural modelling, looking for possible bridge damage and bridge deterioration, determination of the bridge load carrying capacity, and to verify bridge behavior of non-standard structural types that do not neatly fall into a typical bridge category. Useful information that can be obtained from nondestructive load

tests includes experimental influence lines, load distribution, and dynamic amplification factors.

2.8.1 Types of Nondestructive Load Testing

The three types of nondestructive bridge loading include soft load testing, diagnostic load testing, and proof load testing (Casas et al., 2009). Soft load testing uses bridge weigh-in-motion (WIM) instruments to weigh live traffic as it crosses the bridge. Simultaneously, the WIM system measures important structural parameters including influence lines, load distribution, and impact factors. Soft load testing is advantageous because no road closures or pre-weighed vehicles are needed.

Diagnostic load test objectives are similar to those of the soft load test. They serve to verify and adjust analytical models if needed. Trucks of known weights are used in the diagnostic load tests. The trucks are heavier than live traffic used in soft load testing, but not as heavy as those used in proof load testing. Roads are closed as the trucks cross the bridge at varying speeds and configurations. Properties determined from this test include live-load distribution, support restrain, and the effect of impact (Chajes et al., 2000).

Proof testing uses the largest loads of the three nondestructive tests and seeks to calculate the bridge capacity from a large loading that keeps the bridge within the linear elastic zone.

2.8.2 Diagnostic Testing Candidates

Diagnostic load tests can be relatively expensive and are only recommended when the benefits of the gathered data are higher the costs of performing the load test. Good bridge candidates for this type of testing include bridges that have unique geometries and

71

whose analytical models are in needed of verification and possible modification. Other candidates include bridges that lack as-built documentation or unknown material properties. The cost of diagnostic testing can be of great value; diagnostic testing may provide information that keeps an existing bridge in service, thus saving the cost of replacement.

2.8.3 Diagnostic Testing Instrumentation and Procedure

Before live load testing can commence, one must orchestrate proper bridge instrumentation in order to gather useful data from the bridge responses. Bridge responses that are tested frequently include midspan girder deflection, girder strain, bearing rotation, and girder relative displacement. Maximum deflection and strain values are extremely useful because of their direct use in the calculation of dynamic load allowance and distribution factors.

Strain values can be recorded using various types of strain gauges and attachment methods. In the Hanging Rock Creek experiment, BDI stain gauges were attached with epoxy to concrete on the underside of the bridge girder. Girder deflections were measured with differing instruments, depending on whether absolute or relative displacement is being sought. For example, linear variable differential transformers (LVDTs) are mounted on the underside of adjacent girders to measure relative horizontal displacement. String pots are used to measure absolute displacement. String pots stay stationary and are attached to the underside of bridge girders at any desired point along the length of the girder. All of these bridge instruments are connected to a wireless data acquisition system where recorded data is saved (Cai and Shahawy, 2017). The sampling rate of this system

can be adjusted for tests that require many data points in a short time frame, such as dynamic test where trucks cross bridges at highway speeds.

Once a bridge has been properly instrumented it is ready for live load testing. Trucks of known weights are driven across the bridge and follow the paths of clearly marked lanes (Neely et al., 2004). These trucks can be filled to weight up to the 72 kip range, equivalent with that of the AASHTO HL-93 design truck (Sartor et al., 1999). If multiple trucks are present, different arrangements can be used, such as trucks side by side, to produce maximal bridge responses (Chajes et al., 2000). Speeds of the trucks may also be varied, from a crawling speed all the way to a highway speed to produce dynamic loading effects.

2.9 Literature Review Summary

A literature review of each of the above topics was combined for the purposes of this project. The knowledge gained from NEXT beam research helped the author to understand the shortcomings of precast solid slab and hollow core girders and the problems that NEXT beams aim to fix. Research on AASHTO transverse load distribution helped the author understand how these values are calculated depending of bridge geometry and how the values are used in bridge design. Research on ultra-high performance concrete helped the author understand how it differed from normal concrete and how it could be applied to enhance the performance of modern bridges, particularly in the shear key. Research on accelerated bridge construction helped the author understand the country's current need of bridge repairs and a safe effective way to solve this issue. Research on NEXT beam testing familiarized the author with research that has

been already done to further understand the behavior of NEXT beam and how this project

differed from research previously conducted. Finally, research on nondestructive load

testing helped the author understand the purpose, goal, and process of the nondestructive

live load test. The goal of the research on the Hanging Rock Creek Bridge is to combine

the information gained from author's nondestructive load test, UHPC materials tests, and

literature review, and combine them to display a clear depiction of NEXT D beam

behavior and in service performance.

Chapter 3: UHPC Tests and Nondestructive Live Load Test

The project's goals were to investigate the behavior of NEXT D bridge girder and solid slab spans with a UHPC shear key. To accomplish these goals a live load test of the Hanging Rock Creek Bridge was conducted. Specifically, the UHPC material properties were determined through material testing and the bridge transverse load distribution behavior and joint movement was measured during a live load test. This chapter details the procedures for the tests performed for this project. The first section lays out UHPC material tests executed. The second section illustrates the live load test conducted at Hanging Rock Creek Bridge.

3.1. NEXT D and Solid Slab Span Material Properties

Table 16 displays the NEXT D and Solid Slab Span's specified material properties. SCDOT personel performed material testing on the precast concrete, cement, aggregate, prestressing steel, and steel reinforcement. SCDOT performed the concrete compressive testing according to ASTM C-39/C-1231 and SC 701 standards. Tables 17, 18, 19, and 20 give the results for the class 6500 (concrete with specified strength of 6.5 ksi used in NEXT D and solid slab spans) cylinder compressive test, class 8000 (concrete with specified strength of 8 ksi used in cored slab spans 2 and 3) cylinder compressive strength, reinforcing steel tests, and prestressing steel tests, respectively. Class 8000 concrete was not directly involved in this research project, but will be relevant in subsequent research projects. Class 8000 concrete was used in the cored slab spans (spans

2 and 3) not with the NEXT D span or solid slab span. Specifications for Class 6500 and

8000 concrete can be found in the SCDOT 2007 structural concrete table 701.2.12.2.

Table 16: Specified NEXT D and Solid Slab Span Material Properties

Material	Specified Properties
Class 6500 Concrete	$f`_c$ = 6.5 ksi
Class 8000 Concrete	$f`_c$ = 8.0 ksi
Prestressing Steel with 0.5" Diameter	Low Relaxation Strands
	Area = 0.153 in^2
	f_{pu} = 270 ksi
Prestressing Steel with 0.6" Diameter	Low Relaxation Strands
	Area = 0.217 in^2
	f_{pu} = 270 ksi
Reinforcing Steel	f_y = 60 ksi

Table 17: Class 6500 Concrete Cylinder Compressive Test Results at 28 Days

Specimen	Strength (ksi)
1	10.4
2	11.2
3	12.5
4	12.7
5	11.3
6	11.9
7	10.1
8	11.7
9	10.9
10	11.3
11	12.4
12	11.9
13	10.3
14	10.4
15	10.0
16	10.1
17	9.6
18	9.4
19	9.8
20	9.7
Average Compressive Strength = 10.9 ksi	

Table 18: Class 8000 Concrete Cylinder Compressive Test Results at 28 Days

Class 8000 Compressive Cylinder Test	
Specimen	Strength (ksi)
1	11.5
2	11.5
3	11.7
4	11.1
5	11.8
6	11.2
7	11.2
8	11.3
9	11.3
10	11.7
11	11.3
12	11.0
13	11.9
14	11.5
15	11.1
16	10.7
17	11.0
18	11.5
19	11.3
20	11.6
Average = 11.3 ksi	

Table 19: Grade 270 Prestressing Test Results for 0.5" and 0.6" Diameter Strands

Prestressing Cable Breaking Strength Testing	
Specimen (Diameter)	Breaking Stress (ksi)
1 (0.5")	298
2 (0.5")	286
3 (0.6")	283
4 (0.6")	293
5 (0.6")	285
6 (0.6")	288
Average Tensile Strength = 289 ksi	

Table 20: Grade 60 Steel Reinforcement Test Results

Specimen	Specimen Size	Yield Strength (ksi)	Tensile Strength (ksi)
1	#4 Rebar	85.0	109
2	#4 Rebar	74.5	99.0
3	#4 Rebar	69.5	101
4	#4 Rebar	64.5	97.5
5	#5 Rebar	64.0	96.0
6	#5 Rebar	65.0	98.0
Average Yield Strength #4 = 76.3 ksi Average Yield Strength #5 = 64.5 ksi			

To conclude this section, all SCDOT tested materials met the given specifications. The average concrete class 6500 compressive strength was 10.9 ksi and met the specified strength of 6.5 ksi. The average breaking stress of the grade 270 low-relaxation prestressing steel strands was 292.0 ksi met the specified strength of 270 psi. The grade 60 reinforcing steel's average yield strength of 70.1 ksi met the specified strength of 60 ksi.

3.2 UHPC Materials Tests

A summary of the materials tests conducted by Clemson University researchers is provided in Table 21. Procedures for the tests are described in the subsequent subsection.

Table 21: Material Test Summary

Test	Specimen	ASTM Standard	Reference
Compressive Strength	2 in. Cubes	C109	ASTM (2013)
Splitting Tensile Strength	3. in. x 6 in. Cylinders	C496	ASTM (2011)
Pull-off Test	2 in x 2.5 in Cylinders	C1583	ASTM (2013)

3.2.1 UHPC Mix Design

The UHPC mix design was created by Ductal. It contains Ductal ready mix (cement, silica fume, and sand), high range water reducer, and steel fibers. A common Ductal UHPC mix design can be found below in table 22**.** The mixing of the UHPC was handled by Lafarge employees.

Table 22: Typical Ductal UHPC Mix Design

Constituent	lb/yd³
Ductal Premix	3700
Water	219
Premia 150 (Superplasticizer)	51
1/2 in. Steel Fibers (2%)	263
w/cm	0.06

3.2.2 Compressive Strength

Compressive strength tests were performed with 2 in. x 2 in. cubes in accordance with ASTM C109. The cubes were tested in groups of five at ages of 28 days, 90 days, and 6 months, respectively. Figure 58 shows a cube that is about to be tested.

Figure 58: 2" x 2" Cube Compressive Strength Test

3.2.3 Split Tensile Strength

Split tensile strength tests were performed with 3 in. x 6 in. cylinders in accordance with ASTM C496. The cylinders were tested in groups of five at ages of 28 days, 90 days and 6 months, respectively. Figure 59 shows a schematic drawing of a split tensile test. Cylinders were placed in between thin wooden strips to assist with loading alignment.
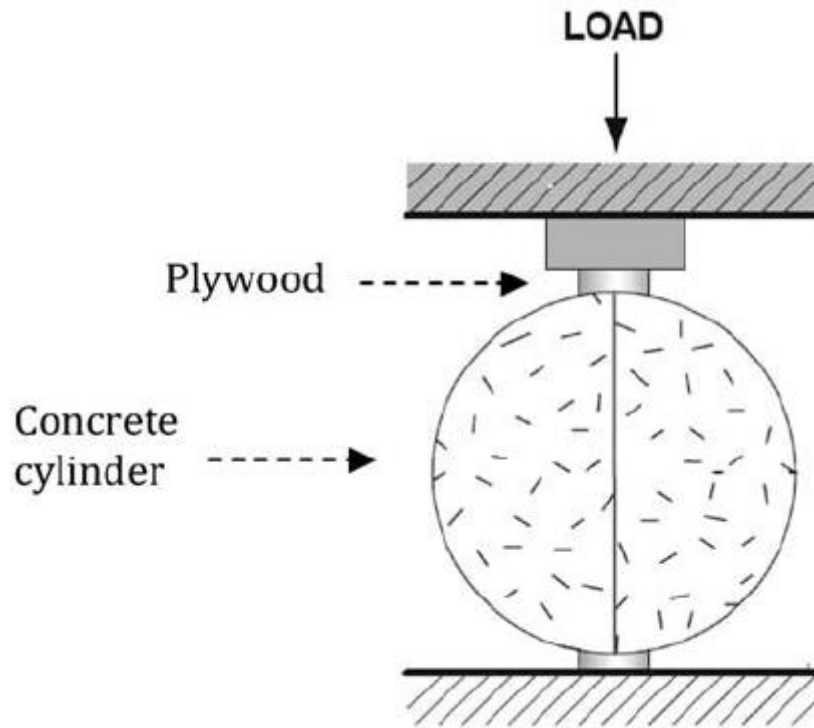
Figure 59: Schematic Drawing of Split Tensile Test (Courtesy of Roohollah Bagherzadeh)

3.2.4 Bond with Concrete

Bond strength of the UHPC to the precast concrete was measured by performing

pull-off test in accordance with ASTM C1583. Figure 60 is a picture of the test specimen.

The test specimen was prepared at the precast yard. To prepare the specimen, a form was

built at the precast concrete yard. Then 6" of the concrete with the concrete mixed used to

make the precast bridge girders was poured into the form. The specimen cured for 28

days before being transported to the bridge site. At the bridge site, 1.5" of UHPC topping

was poured on top of the 6" specimen. That same day, the Clemson Bridge team picked

up the specimen. Figures 61 and 62 show the top and section views of the test specimen, respectively.

Figure 60: 2' x 2' UHPC to Precast Test Specimen
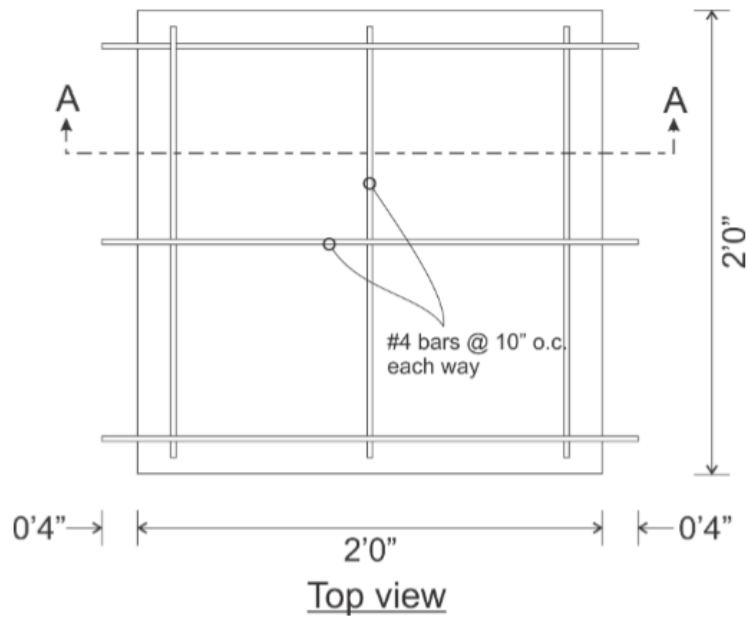
Figure 61: Schematic Top View of Pull Off Test Specimen
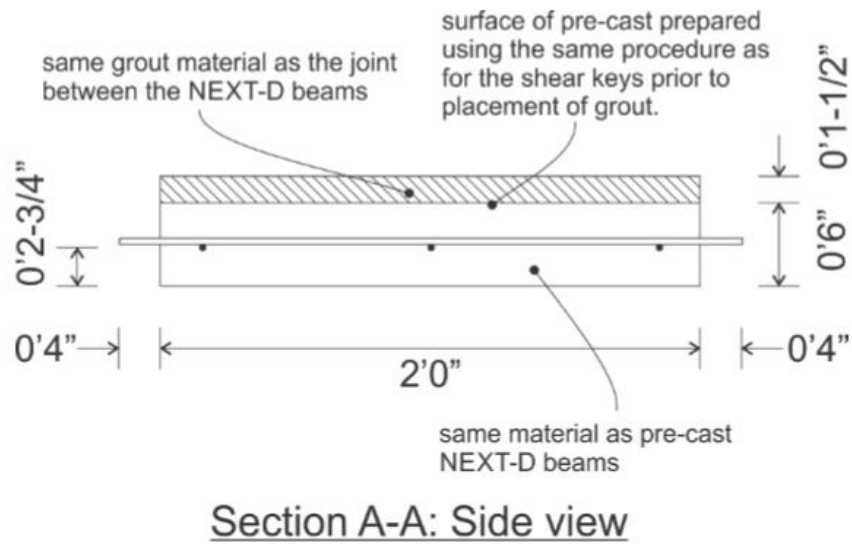
Figure 62: Schematic Side View of Pull Off Test Specimen

Multiple 2 in. x 2 in. core holes were drilled in the test specimen, as shown in figure 63. The holes were drilled 2" deep to meet the ASTM specification that the core must be drilled at least a ½" below the transition between concrete layers.
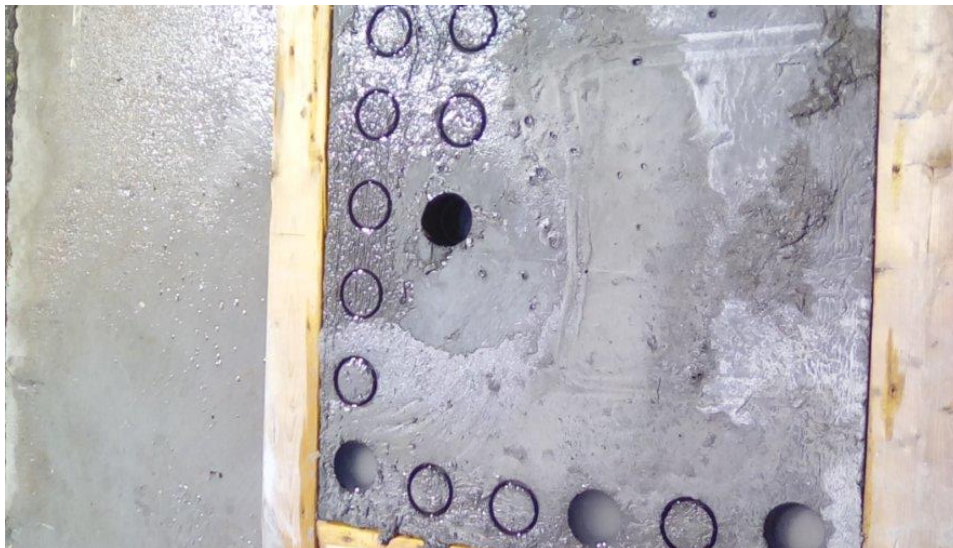
Figure 63: Test specimen with cored holes

Using a high strength epoxy and the Proceq DYNA pull-off tester, pull-off tests were conducted when the 1.5" UHPC overlay was 6 months old. Figure 64 shows a schematic drawing of the pull-off test, and figure 65 shows a specimen after a failure between the UHPC and precast concrete connection.
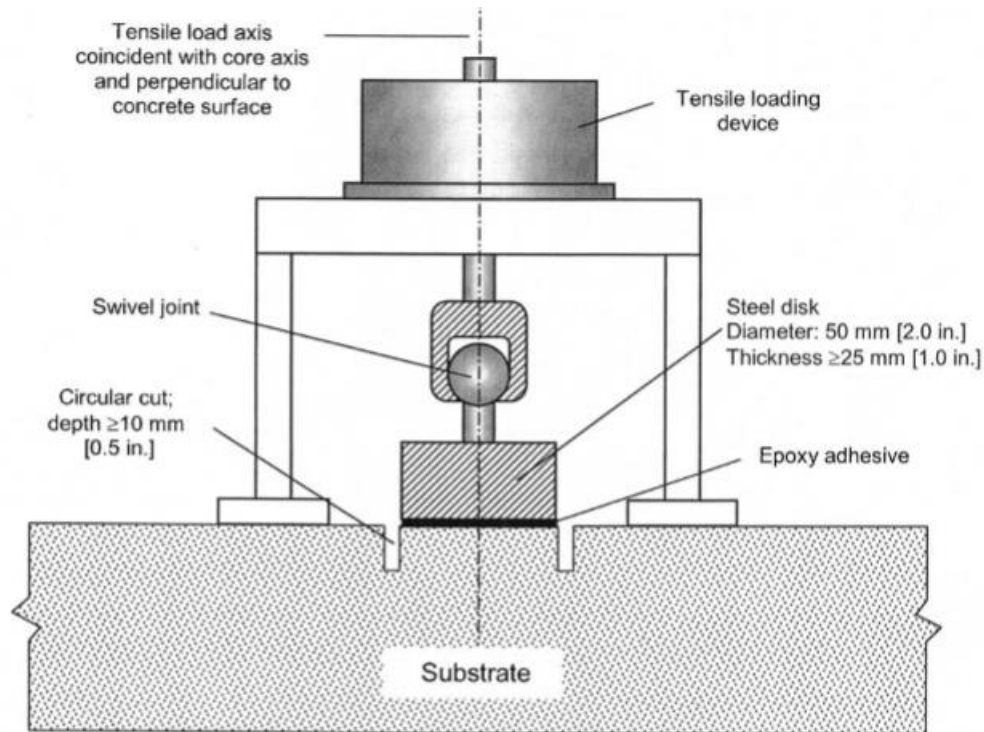
Figure 64: Schematic Drawing of Pulloff Test (Courtesy of ASTM C1583)

Figure 65: Failure of Test Specimen at the UHPC to Precast Interface

By providing torque to the hand crank, the steel cylinders, which were fastened to the concrete with epoxy, were pulled until one of four failures occurred: a) Failure in the substrate (precast concrete) b) Bond Failure at the precast concrete to UHPC connection c) Failure in the UHPC d) Failure at the epoxy bond. These four failure modes are illustrated in figure 66 below.
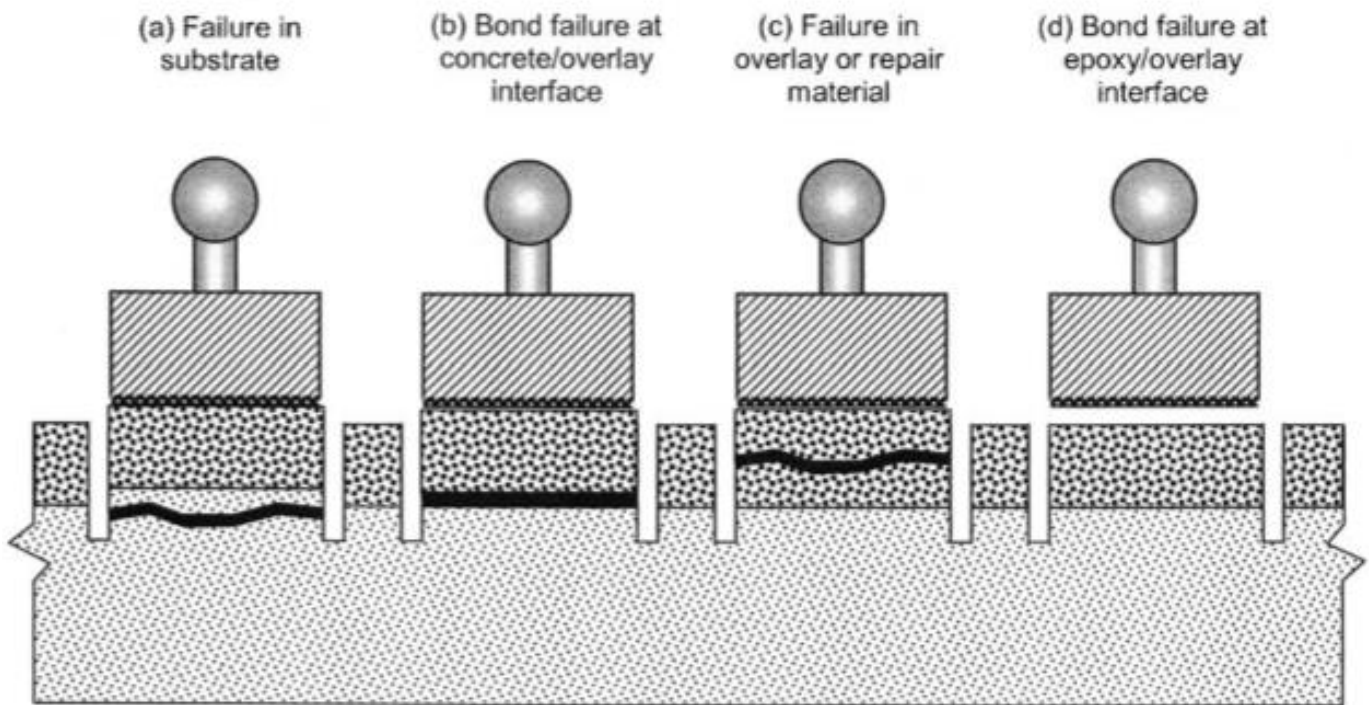
Figure 66: Schematic Drawing of Pulloff Test Failure Modes (Courtesy of ASTM C 1583)

3.3 Live Load Test

The purpose of the live load tests was to determine transverse load distribution of the NEXT D and solid slab spans, and to investigate the performance of the longitudinal joints between girders under service loads. To accomplish these goals, concrete surface strains and joint movements under load was measured.

The live load test of the Hanging Rock Creek Bridge took place over two days in July of 2017. The first test day, July 26, consisted of attaching the instruments to the NEXT D span of the bridge, setting up the data acquisition system, and conducting live load testing. The bridge instruments were removed that evening. On the second day of the

test, July 27, the solid span of the bridge was instrumented and tested in the same fashion as the NEXT D span.

3.3.1 Data Collected

A live load test was performed to measure many different bridge responses and behaviors. Only a few bridge responses were required to be measured at the Hanging Rock Creek Bridge, however. The main objectives of the live load test were to determine the transverse load distribution of both the NEXT D and solid spans, respectively, and the UHPC shear key bond and durability. The bridge responses measured to determine transverse load distribution included strain in the girders, while relative girder displacements were measured to assess the health of the UHPC shear key.

3.3.2 Bridge Instrumentation

Based on the data needed, it was concluded that strain transducers would measure the precast concrete surface strain, and linear variable differential transformers (LVDTs) would measure girder relative horizontal displacements.

3.3.3 Data Acquisition

BDI provided the data acquisition (DA) system in addition to the bridge instrumentation. The DA system's role is to collect, record, and save all data from the live load test. Strain transducers and LVDTs were connected to a 4-channel DA device called a node. The node had 4 channels, which meant that 4 different instruments potentially could be connected to the node. The node receivers are wirelessly connected

to a central base station. The base station data receives data wirelessly from all node

receivers. Data was then saved to a laptop running STS software.

3.3.4 Truck Descriptions

SCDOT provided two three-axle dump trucks that were used for the Hanging

Rock Creek Bridge field test. The trucks were filled with gravel and then had their front

and rear wheel tandem axles weighed separately at the quarry. They had total weights of

43.8 kips and 47.7 kips, respectively.

The trucks' dimensions were measured at the bridge site. Figures 67 through 70

show the trucks' respective axle weights and dimensions.

11.0 kips   32.8 kips
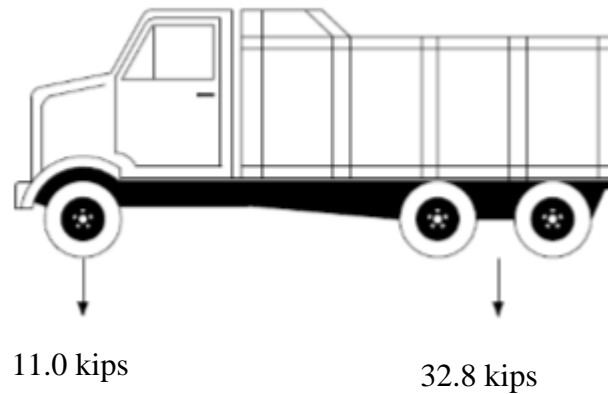
Figure 67: Truck #1 Weight

Figure 68: Truck #2 Weight

11.6 kips   36.1 kips

6'-11"   6'-11"

12'-2"   4'-7"
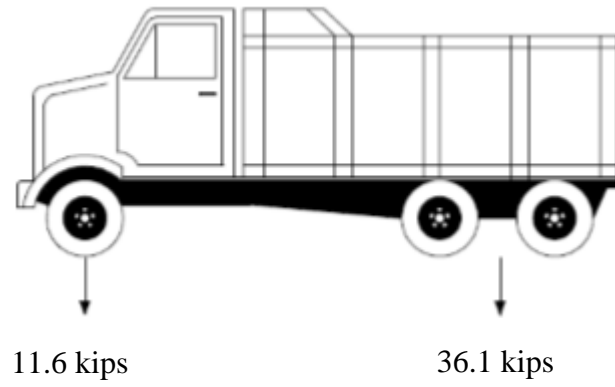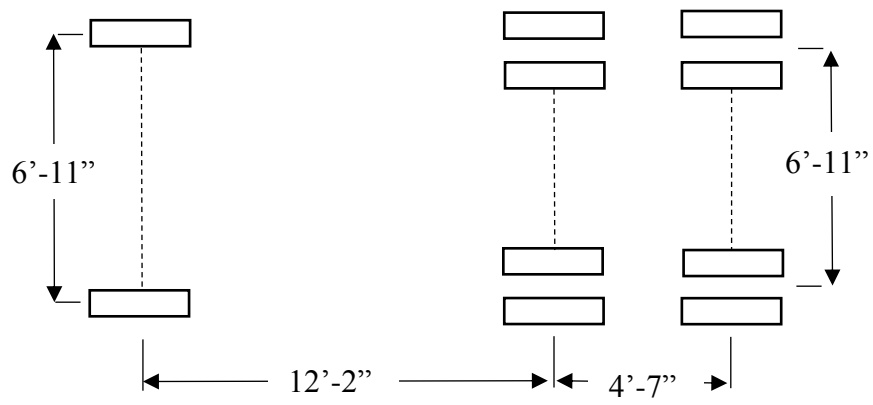
Figure 69: Truck #1
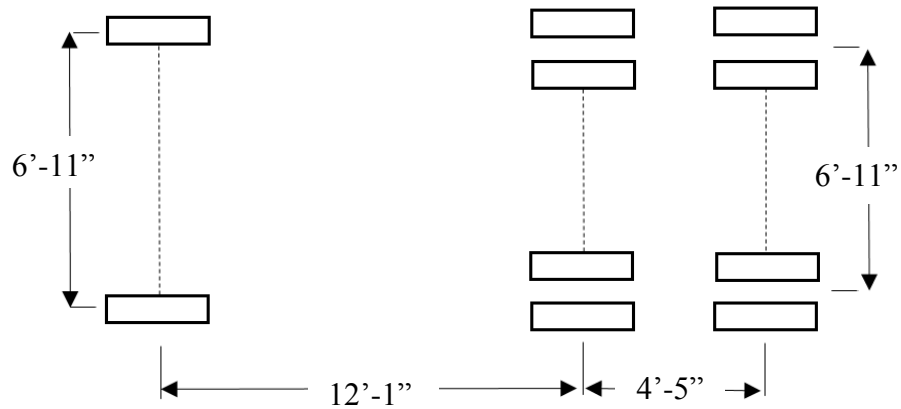
Figure 70: Truck #2

3.3.5 NEXT D Span

3.3.5.1 Strain Transducers

Twelve strain transducers manufactured by Bridge Diagnostics Incorporated (BDI) measured concrete surface strain on the NEXT D span. Strain transducer calibrations were provided by BDI. Strain transducers measured longitudinal bending strain of the bottom flanges at the mid-span of the bridge girders. Figure 71 shows where the strain transducers were physically attached to girders. Strain transducers were mounted at mid-span because this location is close to the section of maximum moment and bending strain. Figure 72 below shows 3 strain transducers attached to a NEXT D girder. Figure 73 is a close-up of a strain gauge mounted to the NEXT D span.
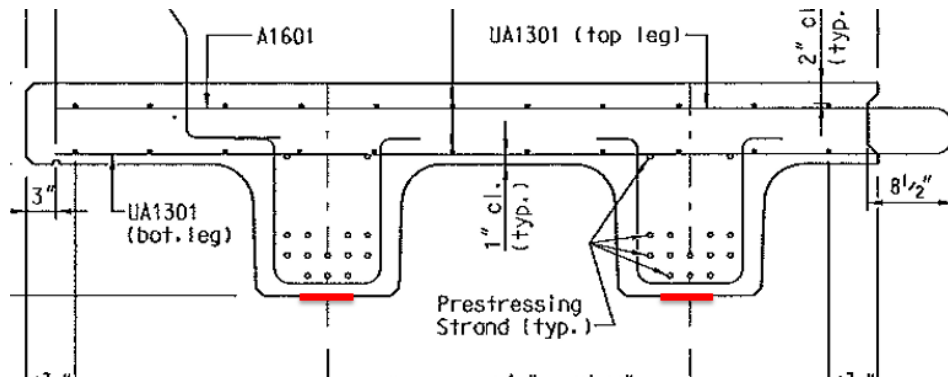
Figure 71: Strain Transducer attachment to NEXT D Girder

Figure 72: BDI Strain Gauges on NEXT D Span

Figure 73: Close-up of NEXT D BDI Strain Gauge

Strain transducers were mounted to the concrete by first attaching the metal feet to the strain transducer and locking them down with nuts. These metal feet were then covered with adhesive and then sprayed with accelerant. After the accelerant was sprayed, the metal feet were quickly pressed and held on the concrete face for five seconds before a strong bond was formed. Figures 74 and 75 show the adhesive and accelerant used.

Figure 74: Loctite Adhesive (Picture courtesy of Robert Gunter)

Figure 75: Loctite Accelerant (Picture courtesy of Robert Gunter)

3.3.5.2 Linear Variable Differential Transformers

Six LVDTs and their calibrations were provided by BDI for this project. LVDTs were recalibrated by the author. Four LVDTs were instrumented on the NEXT D span. LVDTs measured the girder relative horizontal displacement by recording the movement of the arm relative to the body of the transformer. Six custom made cases were created to hold and attach the LVDTs to the girders. A LVDT in its case rigged to a NEXT D girder can be seen in figure 76.
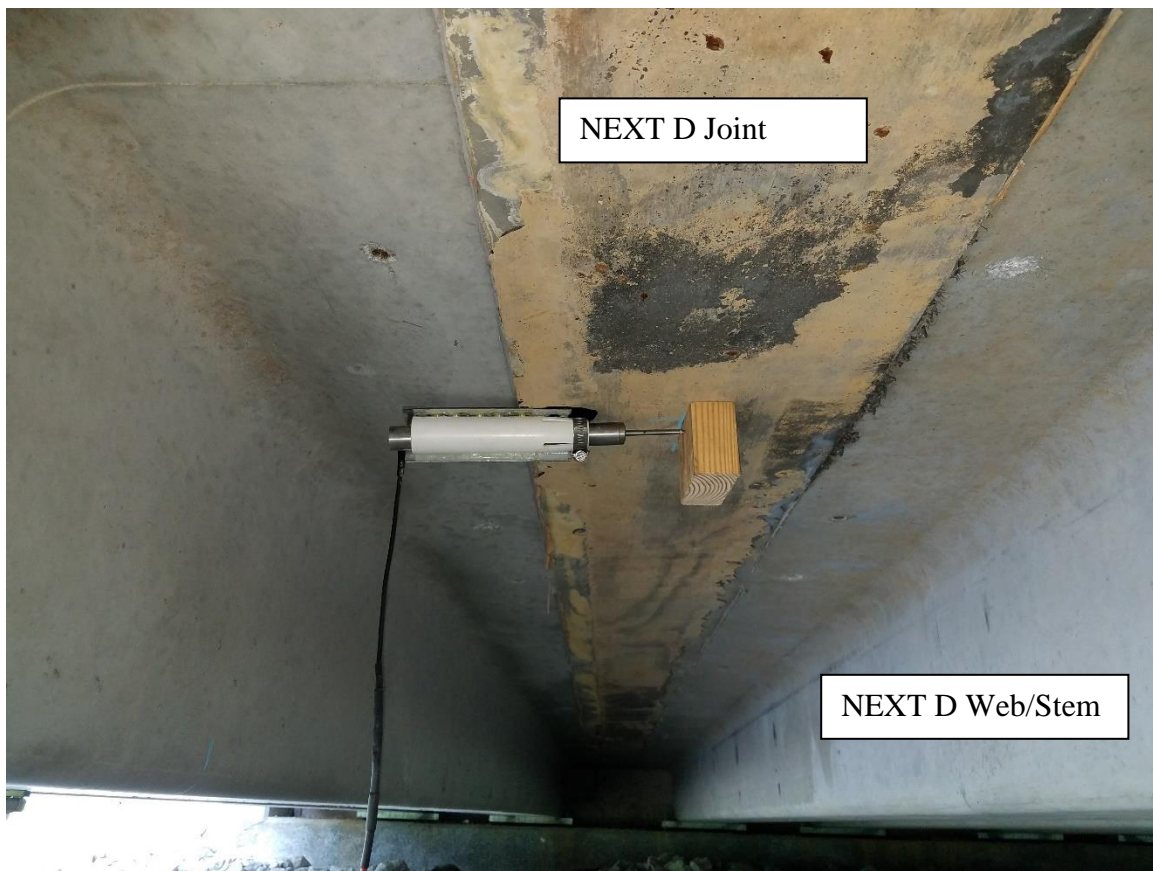
Figure 76: LVDT Rigged to measure Relative Horizontal Displacement on NEXT D Girder

The relative horizontal displacements between bridge girders was a point of interest in this project since displacement is an indication of the health of the shear key. Horizontal deflections indicate an opening at the longitudinal girder joint (Gunter, 2016). Additionally, these displacements help researchers determine if transverse post-tensioning rods are assisting with transverse load distribution. Excessive movements at the joints can cause reflective cracking in the asphalt roadway surface. LVDTs were able to capture displacement at the joints. The first live load test was conducted when the bridge was healthy and brand new. These relative displacements will be the baseline. If these horizontal displacements increase for future tests, this is a strong indication of a damaged shear key.

To measure the horizontal displacement, the LVDT was placed in the custom case and glued to the bottom of the concrete girder. The custom case allowed the LVDT to be easily attached to the underside of the bridge. The arm of the LVDT was pointed perpendicular to the flow of traffic. Across the joint, a wooden block was glued to the bottom of the concrete girder as well. The wooden block provided a point of contact for the LVDT arm.

3.3.5.3 Instrumentation Plans

The NEXT D bridge instrumentation plans for strain gauges and LVDTs can be seen in figures 77 and 78. Figure 77 shows the layout of the strain gauges and figure 78 shows the layout for the LVDTs. Table 23 lists each strain gauge and LVDT with its corresponding BDI gauge number. This table is included to help read graphs found in the appendix. The numbers on both layouts are the sensors' respective BDI identification

numbers. The layout utilizes 12 strain transducers and 4 LVDTs across the entire width

of the span. The goal of this setup was to analyze the transverse load distribution of the

NEXT D section and detect horizontal joint movements.

North: Out of Page

Strain Transducer
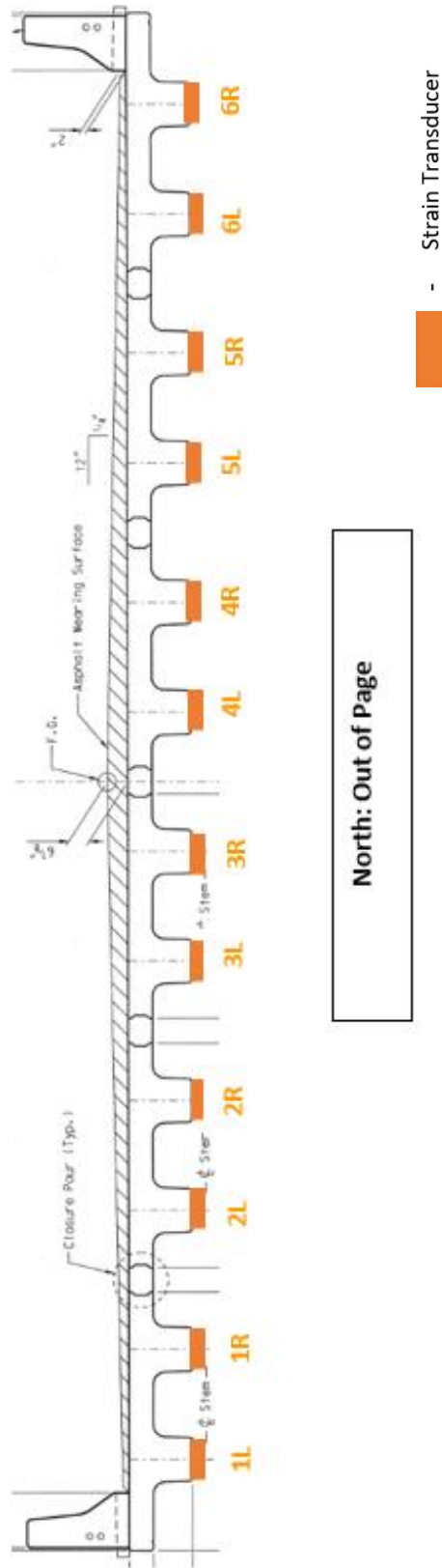
Figure 77: NEXT D Strain Gauge Layout

98
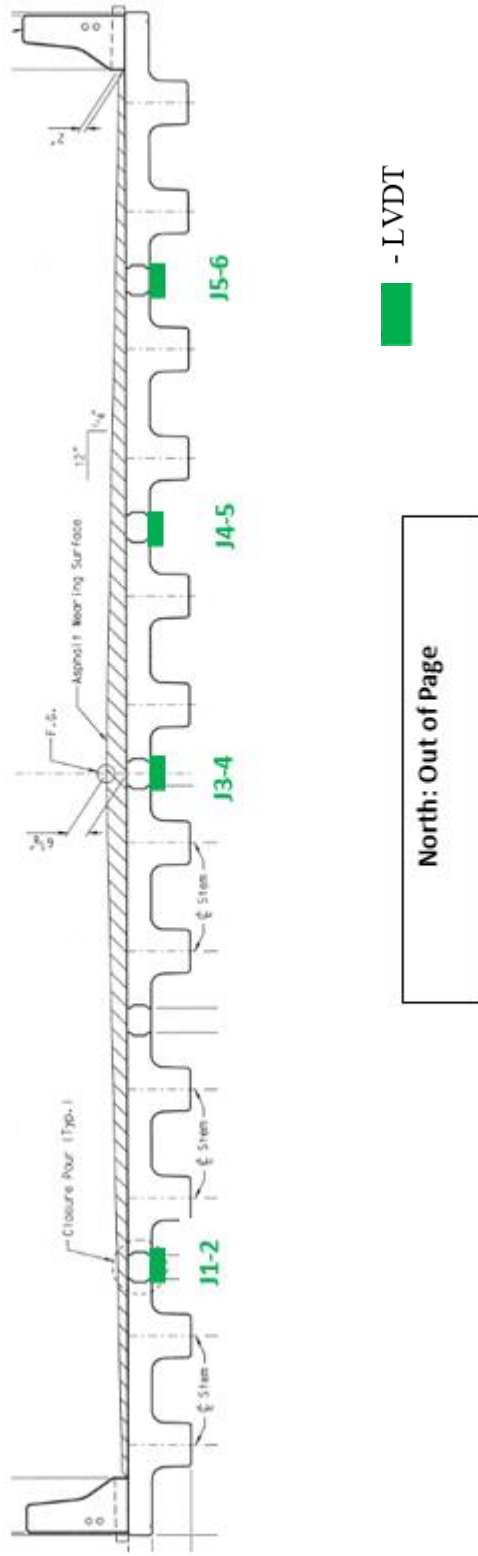
Figure 78: NEXT D LVDT Layout

Table 23: NEXT D BDI Gauge List

Instrument Layout Identifier	Sensor Type	BDI Gauge Number
1L	Strain Gauge	5334
1R	Strain Gauge	5332
2L	Strain Gauge	5325
2R	Strain Gauge	5338
3L	Strain Gauge	5329
3R	Strain Gauge	5337
4L	Strain Gauge	5333
4R	Strain Gauge	5336
5L	Strain Gauge	5326
5R	Strain Gauge	5328
6L	Strain Gauge	5335
6R	Strain Gauge	5323
J1-2	LVDT	1030
J3-4	LVDT	1028
J4-5	LVDT	1029
J5-6	LVDT	1770

3.3.5.4 Loading Configurations

Eight different load scenarios were used during the field test on the NEXT D span. Certain loading configurations used one truck, while others used two trucks. Scenarios 1-7 were pseudo-static tests, meaning the trucks travelled across the bridge at less than 5 mph. The trucks travelled slowly across the bridge to eliminate bouncing and dynamic effects. Scenario 8 was a dynamic test, meaning trucks drove across the bridge at approximately the posted speed limit. The purpose of the dynamic test was to see if a truck traveling at highway speeds caused greater bridge bending strains. Table 24 provides a loading summary for the solid slab live load test. Figures 79-85 illustrate the truck alignment for each load scenario.

Table 24: NEXT D Load Configuration Summary

Loading Scenario	Trucks Used	Trials	Truck Speed (mph)	Primary Purpose
1	Truck 2	4	< 5	Maximum load in exterior girder
2	Truck 2	3	< 5	Maximum load interior girder adjacent to exterior girder
3	Both Trucks (Truck 2 on outside)	3	< 5	Maximum load in exterior girder with side by side trucks
4	Both Trucks (Truck 2 on outside)	3	< 5	Maximum load in interior girder with side by side trucks
5	Truck 2	3	< 5	Wheel line over joint to cause maximum horizontal displacement
6	Truck 2	3	< 5	Maximum load in exterior girder (symmetric with loading 1)
7	Truck 2	3	< 5	Maximum load outside in interior girder (symmetric with loading 2)
8	Truck 2	7	≈ 45	Dynamic Load Allowance
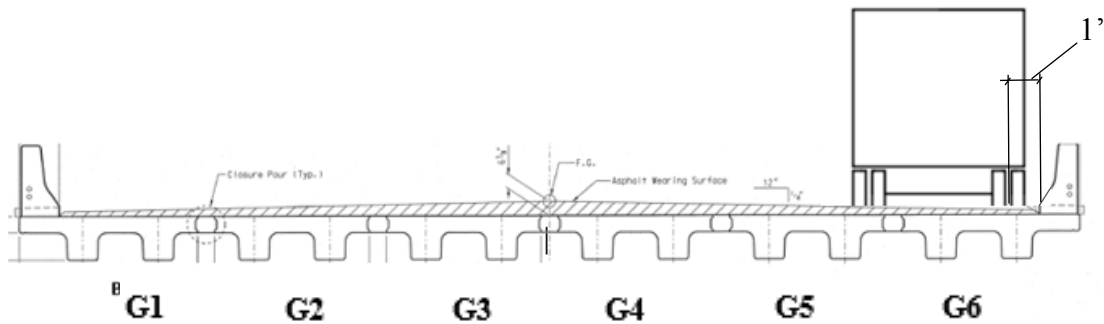
Figure 79: Load Configuration 1 (Exterior Girder Single Truck)
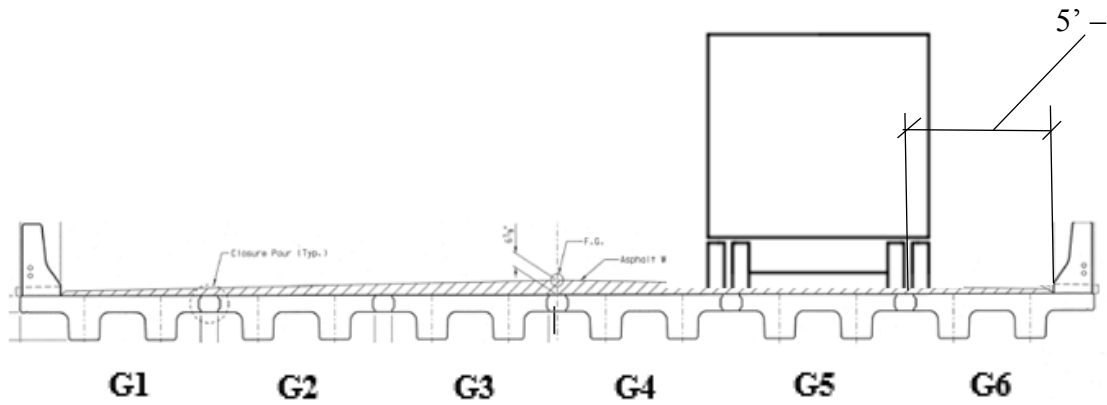
Figure 80: Load Configuration 2 (Single Truck on Interior Girder)
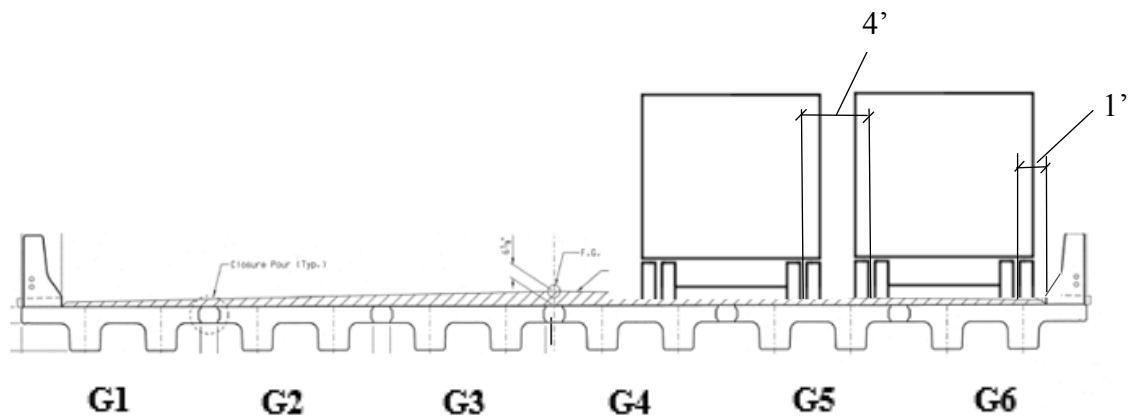
Figure 81: Load Configuration 3 (Two Trucks Max Loading Exterior Girder)
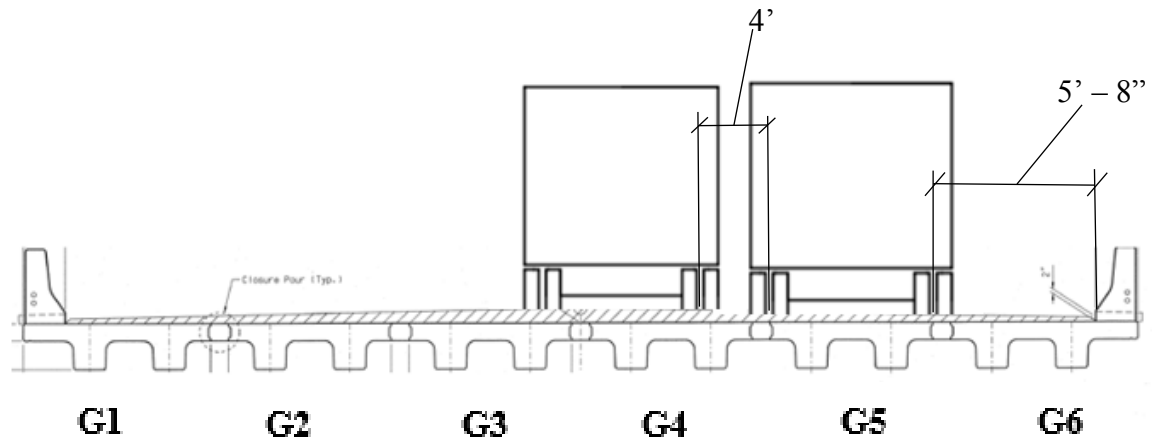
Figure 82: Load Configuration 4 (Two Trucks Max Loading Interior Girder – One wheel line directly over Joint)
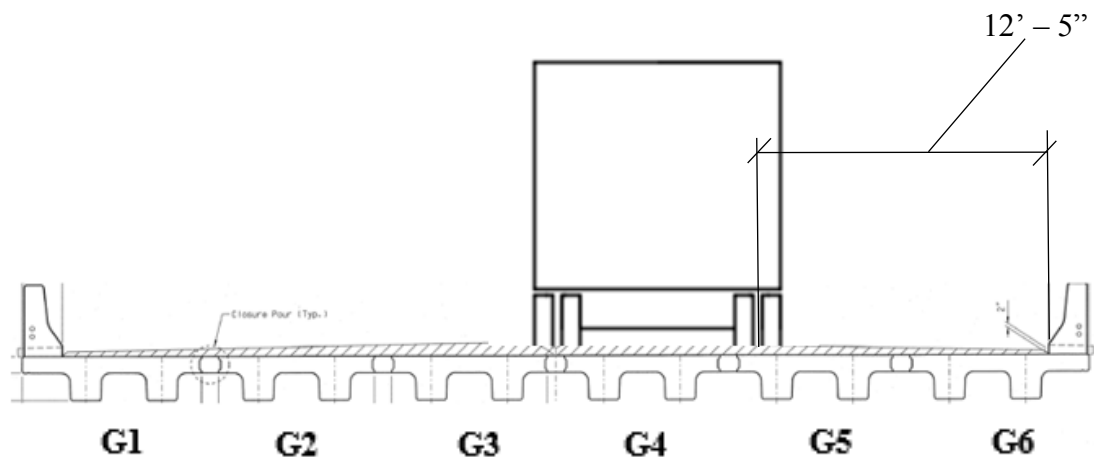
Figure 83: Load Configuration 5 (Single Truck on Interior Girder – Wheel Line over Middle Joint)
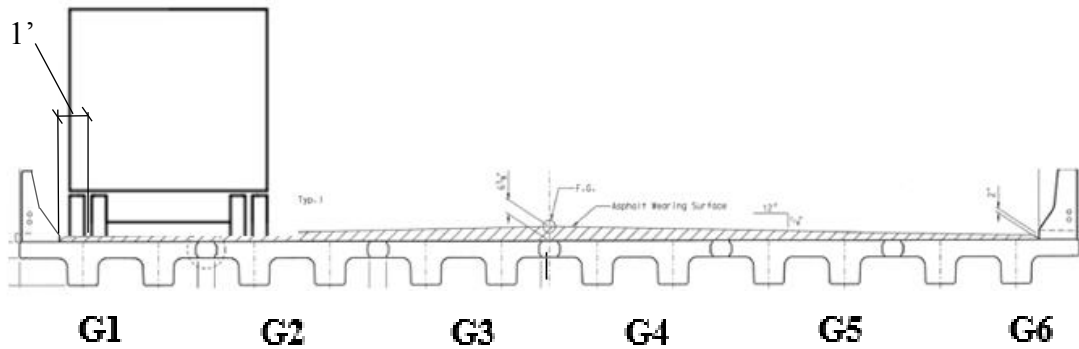
Figure 84: Load Configuration 6 (Single Truck on Exterior Girder – Symmetry with Scenario 1)
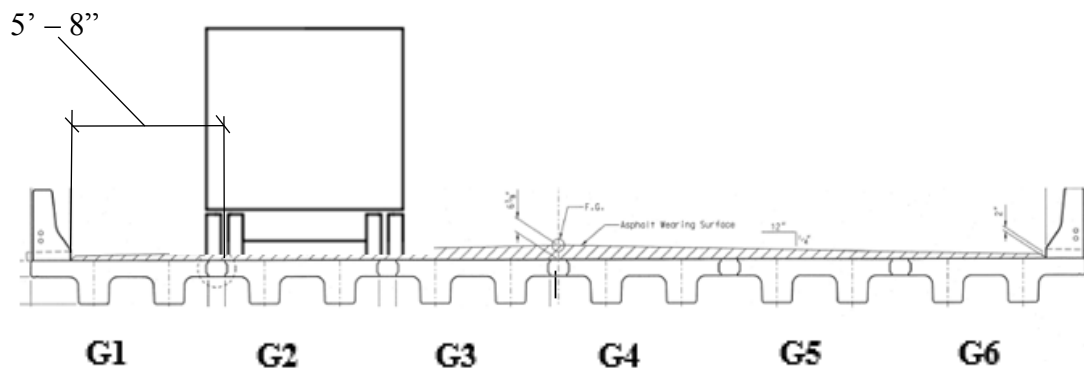
Figure 85: Load Configuration 7 (Single Truck on Interior Girder – Symmetry with Scenario 2)

3.3.6 Solid Slab Span

3.3.6.1 Strain Transducers

Sixteen strain gauges were used to measure concrete surface strain on the solid slab span. Figure 86 shows 6 strain transducers attached to solid slab girders 13 and 14, respectively.

12' – 5"
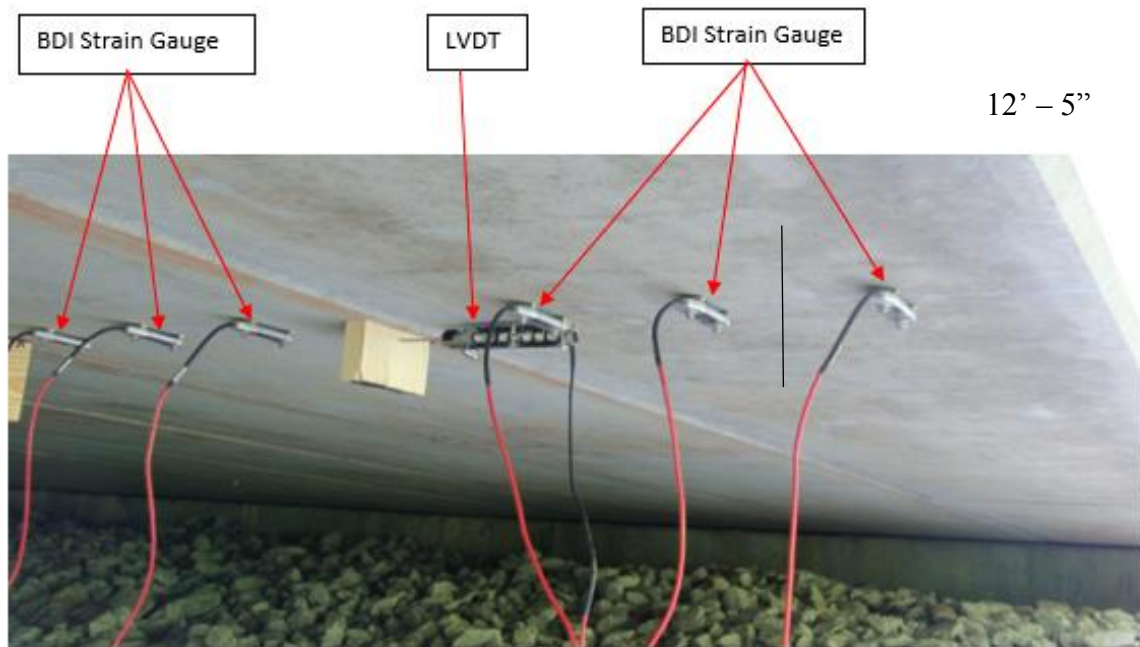
Figure 86: Strain Transducers and LVDT Rigged on Solid Slab Span

Strain transducers were mounted in the same fashion as those mounted to the NEXT D span. Figure 87 shows how the strain transducers were mounted to girders 1

through 12. Figure 88 shows how girders 13 and 14 each had 3 strain transducers

mounted.
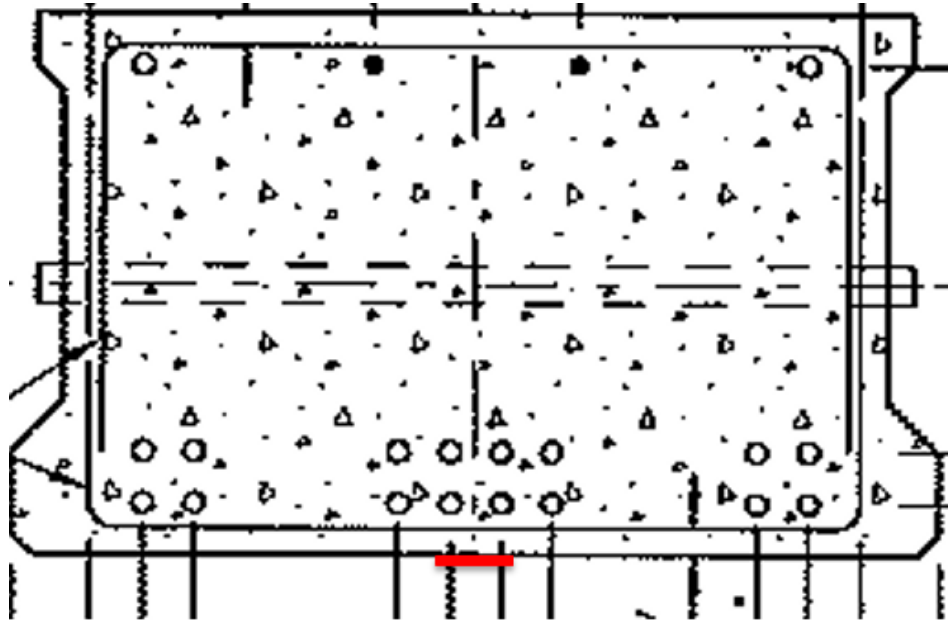
Figure 87: Schematic Drawing of Strain Gauge Mount Position on Solid Slab Girders 1 through 12
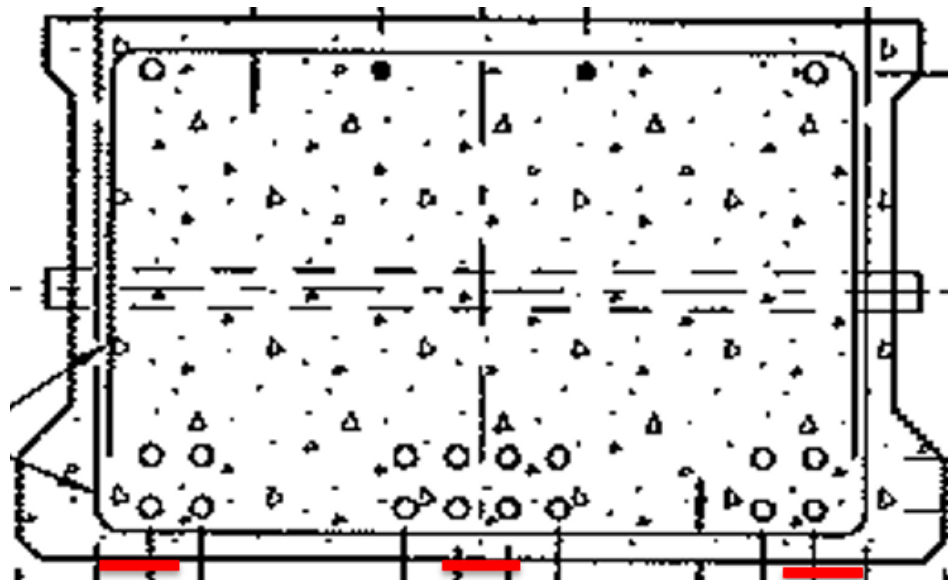
Figure 88: Schematic Drawing of Strain Gauge Mount Position on Solid Slab Girders 13 and 14

- Strain Transducer

3.3.6.2 Linear Variable Differential Transformers

Six LVDTs were instrumented and used to take horizontal joint displacements on the solid slab span. Figure 89 shows an LVDT mounted to a solid slab girder.

Figure 89: LVDT Mounted to Solid Slab

3.3.6.3 Instrumentation plans

The solid slab instrumentation plans for the BDI strain gauges and LVDT's can be seen in figures 90 and 91, respectively. Table 25 lists each strain gauge and LVDT with its corresponding BDI gauge number. In total, 16 strain gauges and 6 LVDT's were mounted to the solid slab span.
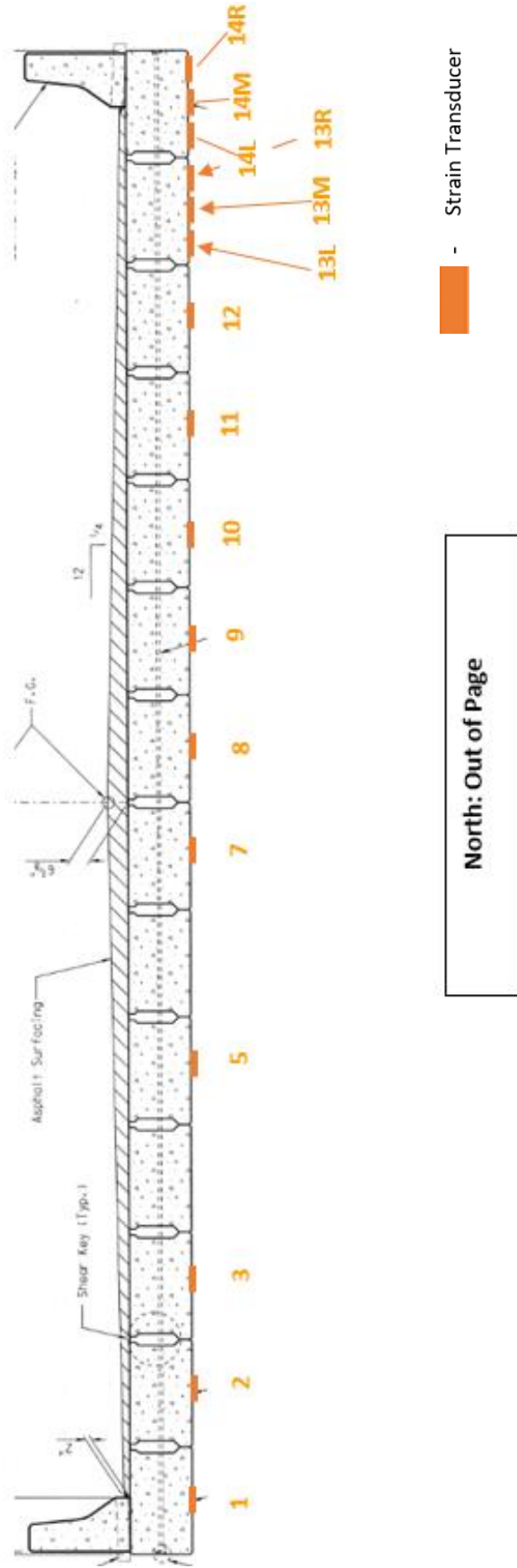
Figure 90: Solid Span Strain Gauge Sensor Layout

North: Out of Page

- Strain Transducer
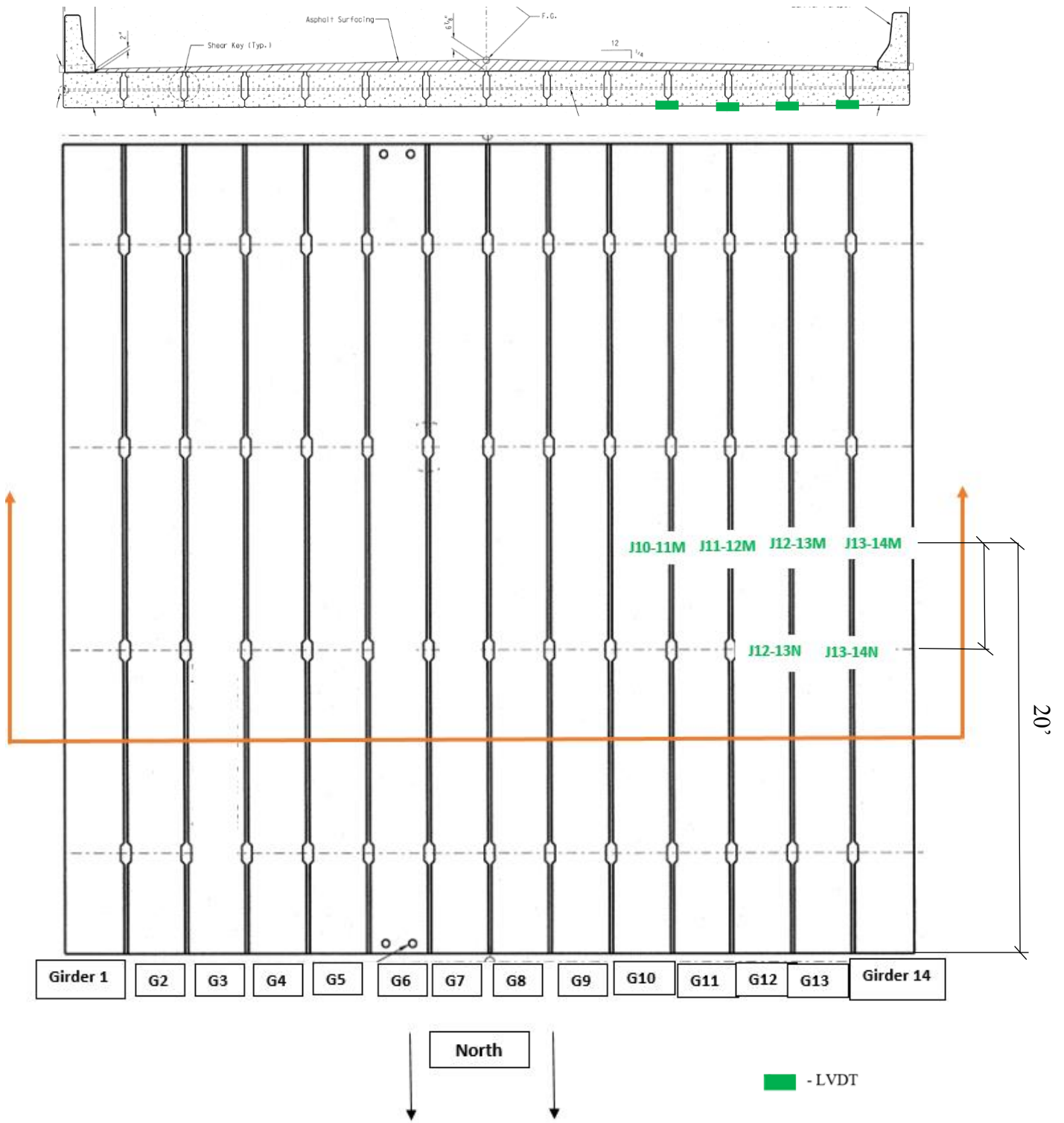
Figure 91: Solid Span LVDT Sensor Layout

Table 25: Solid Span BDI Gauge List

Instrument Layout Identifier	Sensor Type	BDI Gauge Number
1	Strain Gauge	5327
2	Strain Gauge	5326
3	Strain Gauge	5337
5	Strain Gauge	5323
7	Strain Gauge	5331
8	Strain Gauge	5332
9	Strain Gauge	5334
10	Strain Gauge	5324
11	Strain Gauge	5328
12	Strain Gauge	5336
13L	Strain Gauge	5335
13M	Strain Gauge	5338
13R	Strain Gauge	5330
14L	Strain Gauge	5329
14M	Strain Gauge	5333
14R	Strain Gauge	5325
J10-11M	LVDT	1029
J11-12M	LVDT	1027
J12-13M	LVDT	1771
J13-14M	LVDT	1028
J12-13N	LVDT	1770
J13-14N	LVDT	1030

3.3.6.4 Loading Configurations

Figures 92 through 101 show the loading scenarios on the solid span. Table 26 has a summary of the loading scenarios and their respective purposes.

Table 26: Solid Slab Span Loading Configuration Summary

Loading Scenario	Trucks Used	Trials	Truck Speed (mph)	Primary Purpose
1	Truck 2	3	< 5	Max load exterior girder and cause max response in horizontal joint displacement
2	Truck 2	3	< 5	Max load exterior girder and cause max response in horizontal joint displacement
3	Truck 2	3	< 5	Max load outermost interior girder
4	Both Trucks (Truck 2 on outside)	4	< 5	Cause max horizontal joint displacement with two trucks
5	Both Trucks (Truck 2 on outside)	3	< 5	Max load exterior girder with two trucks
6	Both Trucks (Truck 2 on outside)	3	< 5	Max load interior girder with two trucks
7	Truck 2	3	< 5	Max load exterior girder and cause max response in horizontal joint displacement (symmetry with loading 1)
8	Truck 2	3	< 5	Max load exterior girder and cause max response in horizontal joint displacement (symmetry with loading 2)
9	Truck 2	3	< 5	Max load middle interior girders
10	Truck 2	3	45	Dynamic Load Allowance
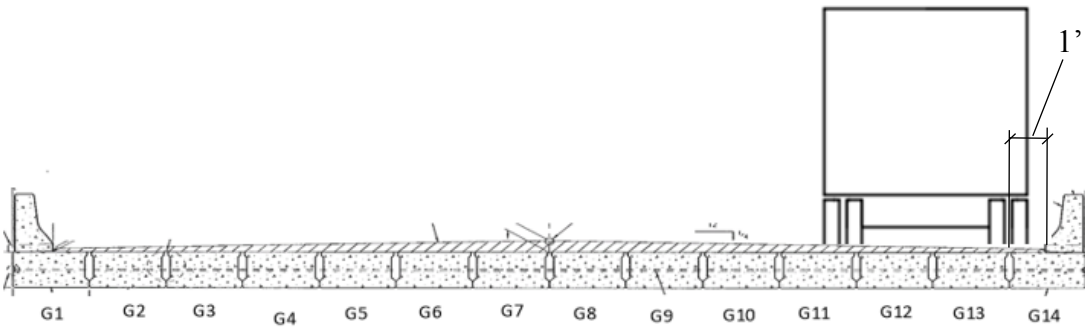
Figure 92: Load Configuration 1 (Single Truck on Exterior Girder/Joint)
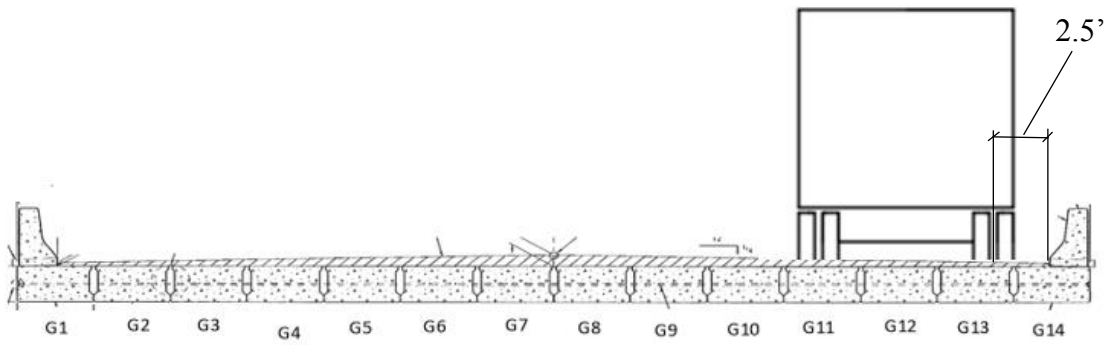
Figure 93: Load Configuration 2 (Single Truck Straddling Two Interior Joints)
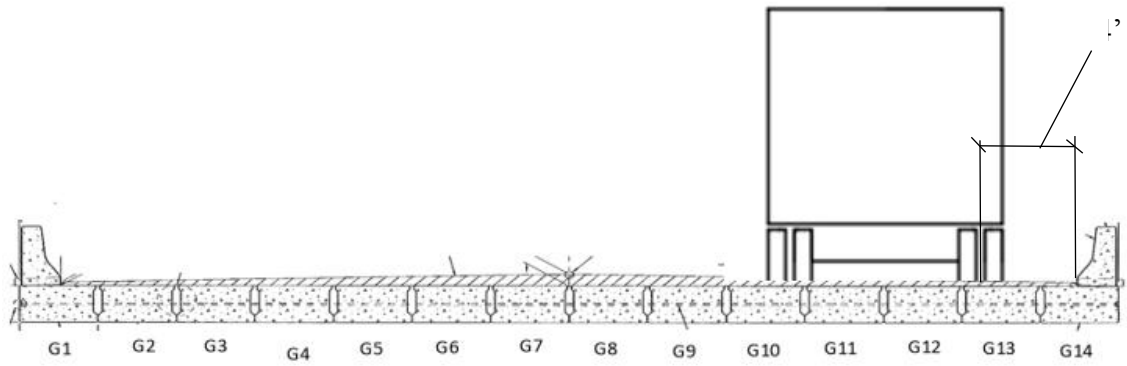
Figure 94: Load Configuration 3 (Single Truck Over Two Interior Joints)
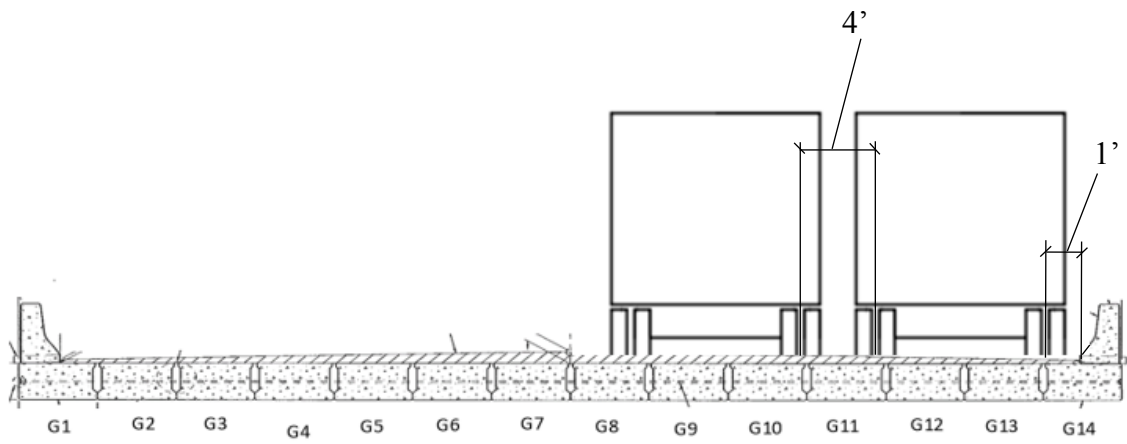
Figure 95: Load Configuration 4 (Two Trucks, each with Wheel Line Over Joint - Exterior Girder)
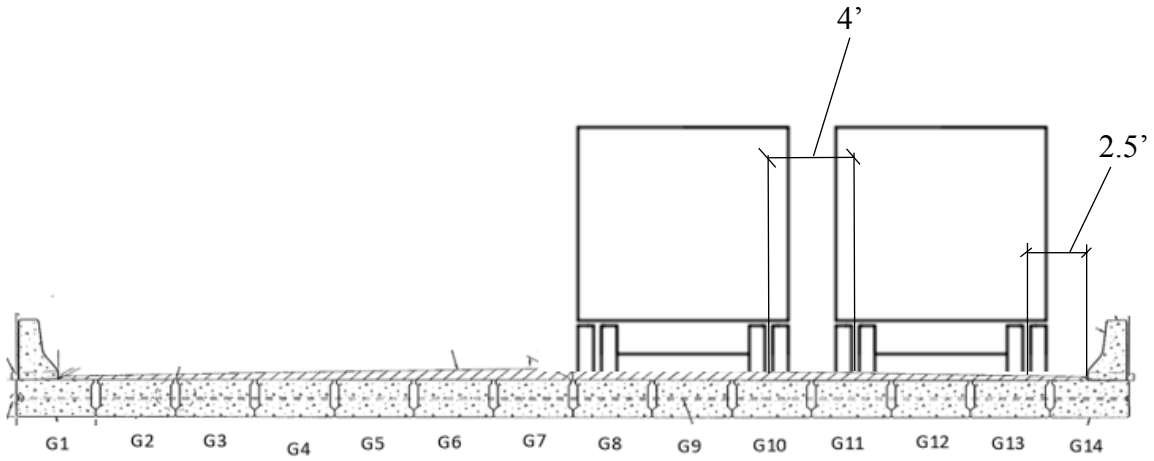
Figure 96: Load Configuration 5 (Two Trucks, offset from Joints – Interior Girders)
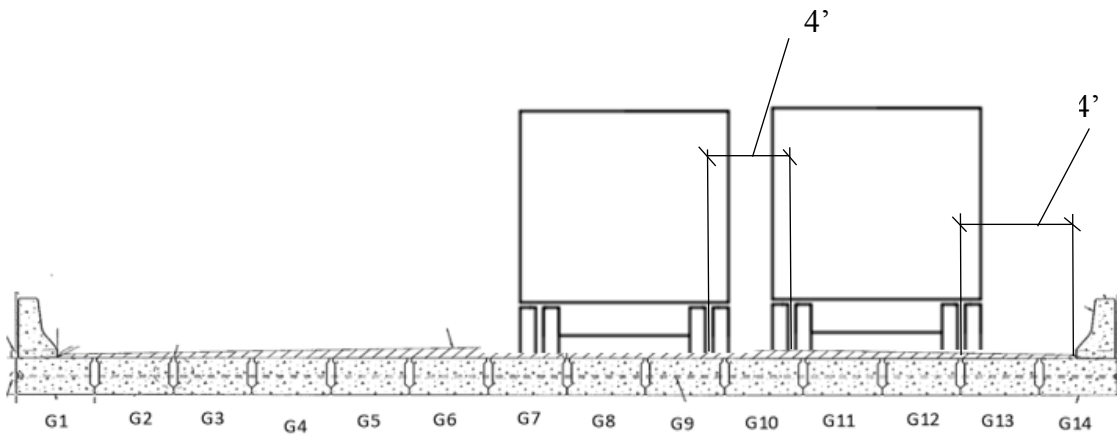
Figure 97: Load Configuration 6 (Two Trucks, each with Wheel Line Over Joint – Interior Girders)
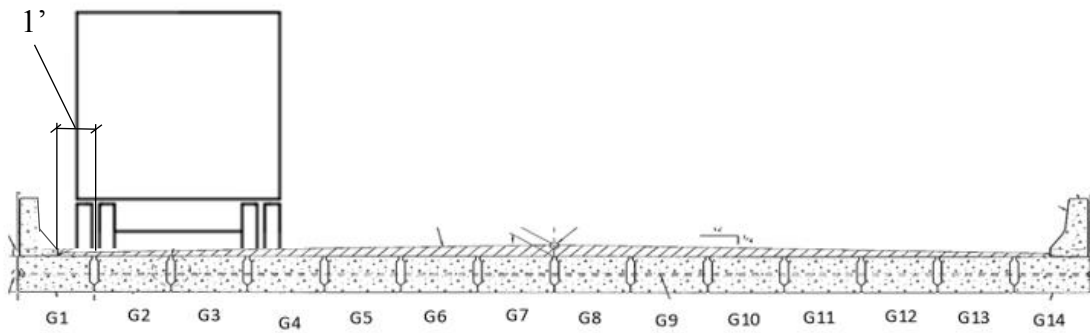
Figure 98: Load Configuration 7 (Single Truck on Exterior Girder/Joint - Symmetry with Scenario 1)
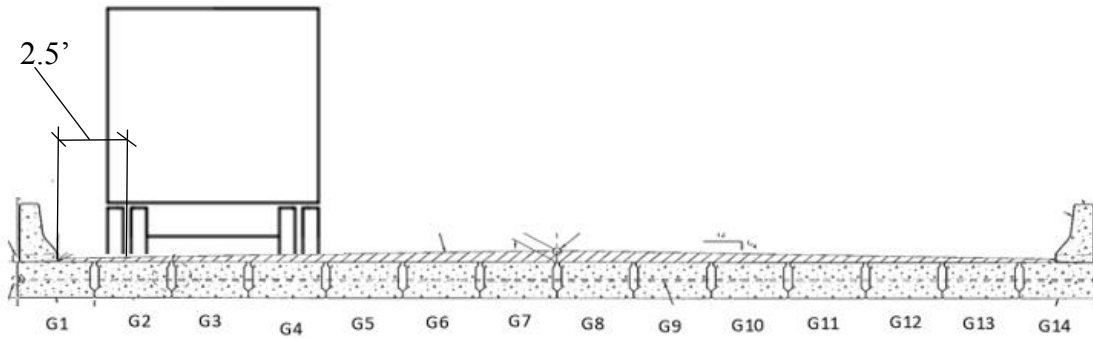
Figure 99: Load Configuration 8 ((Single Truck Straddling Two Joints – Symmetry with Scenario 2)
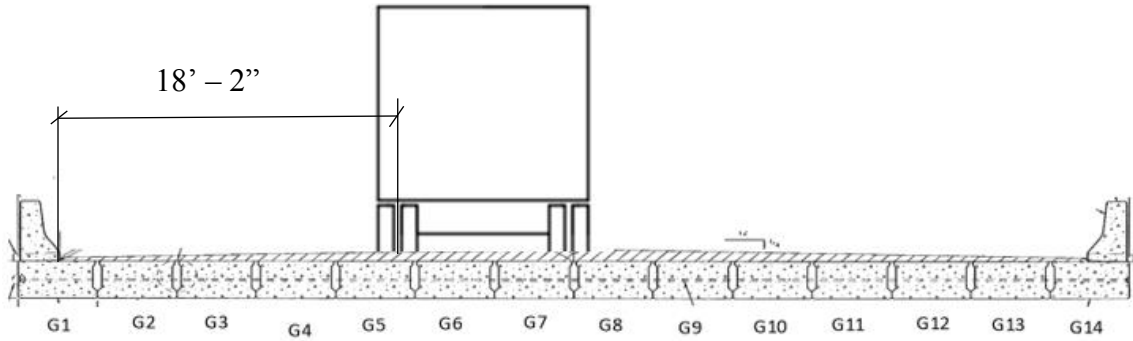
Figure 100: Load Configuration 9 (Single Truck over Middle Joint)
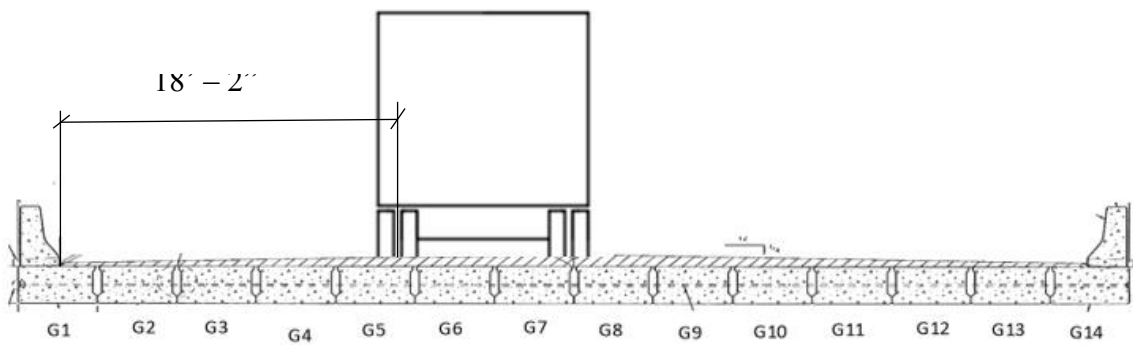
Figure 101: Load Configuration 10 (Single Truck over Middle Joint – Dynamic Case)

Chapter 4:   Results and Discussion

The project's goals were to investigate the transverse load sharing behavior of NEXT D solid slab span members, the UHPC shear key performance, and the UHPC material properties. To accomplish these goals a live load test of the Hanging Rock Creek Bridge was conducted in addition to UHPC materials testing. Specifically, the UHPC material properties were determined through material testing and the bridge transverse load distribution behavior through recorded bending strains and joint movement measured during a live load test. Results of the tests are presented in the following sections.

4.1 Material Tests Results

Results from the material tests described in chapter 3 are presented here. Materials tests were conducted to ensure that the UHPC was met the specifications established by the engineer and that the UHPC compressive, tensile, and bond strengths were typical when compared to other researchers' data sets.

4.1.1 Compressive Strength Test

Results of the Clemson UHPC compressive strength tests performed at 28 days, 90 days, and 6 months with UHPC batched on 3/20/2017 (NEXT D shear keys) are shown in table 27. No cube specimens were provided from the UHPC batched on 3/21/2017 (solid slab shear key). Table 28 contains UHPC compressive strength test results from 4 different Virginia Tech researchers [(D'Alessandro, 2013), (Halbe, 2014),

(Joyce, 2014), (Field, 2015)]. Figure 102 shows the strength gain of the UHPC over a

period of 6 months.

Table 27: Clemson University UHPC Compressive Strength Test Results

Specimen Number	Specimen Age	Compressive Stress (ksi)	Average (ksi)	Coefficient of Variation
1	28 Days	25.8	20.8	23.3%
2		20.3		
3		24.6		
4		13.5		
5		19.8		
6	90 Days	21.8	17.4	21.4%
7		13.3		
8		15.5		
9		19.1		
10	6 Months	21.1	22.5	6.7%
11		21.0		
12		23.8		
13		24.3		
14		22.3		

Table 28: Virginia Tech UHPC Compressive Strength Test Results

Researcher	Specimen ID	Specimen Age	Average Compressive Stress (ksi)	Number of Specimens Tested
Halbe	1		17.6	3
Halbe	2	13 Days	17.2	3
Field	3	7 Days	16.0	3
Field	4	28 Days	19.9	3
Joyce	5	7 Days	11.3	2
Joyce	6	11 Days	15.5	2
Joyce	7	7 Days	11.6	2
Joyce	8	11 Days	14.3	2
D'Alessandro	9	4 Days	14.5	3
D'Alessandro	10	7 Days	18.7	3
D'Alessandro	11	14 Days	19.5	3
D'Alessandro	12	21 Days	20.3	3
D'Alessandro	13	28 Days	20.8	3
D'Alessandro	14	104 Days	24.9	3

Figure 102: UHPC Compressive Strength Gain

Benjamin Graybeal states that for a concrete to be considered UHPC, it must display compressive strengths greater than or equal to 21.7 ksi (Graybeal and Russell, 2013). By the 6 month tests, three of four Clemson specimens exceeded this compressive strength.

Clemson University specimens that were tested at 28 days had high variability relative to each other, but the average compressive strength was near Graybeal's criteria. At 90 days, the specimens had high variability and for an unknown reason the average compressive decreased significantly from the 28 day compressive strength. At 6 months, the average compressive strength exceeded Graybeal's compressive strength criteria by

3.5%, and the coefficient of variation was much lower. It is believed that the low 90 day compressive strength was a fluke in the data due to small sample size of only 4 cubes.

In the Virginia Tech compressive strength tests, Halbe's, Field's, and Joyce's average compressive strengths were all significantly lower than Graybeal's specified compressive strength value of 21.7 ksi. However, D'Alessandro's average compressive strength values met Graybeal's specified compressive strength criteria by day 104.

The Clemson compressive strength test results show that the UHPC used in the Hanging Rock Creek Bridge does possess adequate compressive strength, especially when compared to typical concrete. Additionally, from the data it appears that it takes at least 28 days for UHPC to achieve its full compressive strength capabilities.

4.1.2 Splitting Tensile Test

Results of the Clemson UHPC splitting tensile strength tests performed at 28 days, 90 days, and 6 months with UHPC batched on 3/20/17 (NEXT D shear keys) and 3/21/17 (solid slab shear keys) are shown in tables 29 and 30 respectively. Table 31 contains UHPC tensile strength results from 3 different Virginia Tech researchers. [(D'Alessandro, 2013), (Halbe, 2014), (Field, 2015)]. Figure 103 illustrates the ability for UHPC to increase tensile strength over time.

Table 29: Clemson University UHPC Tensile Strength Test Results – Batched on 3/20/17

Specimen Number	Specimen Age	Tensile Strength (ksi)	Average Tensile Strength (ksi)	Coefficient of Variation
1	28 Days	3.61	3.56	5.84%
2		3.32		
3		3.72		
4		3.37		
5		3.79		
6	90 Days	3.56	3.24	13.1%
7		3.70		
8		3.11		
9		3.12		
10		2.64		
11	6 Months	3.47	3.29	7.59%
12		3.05		
13		3.58		
14		3.32		
15		3.02		

Table 30: Clemson University UHPC Tensile Strength Test Results – Batched on 3/21/17

Specimen Number	Specimen Age	Breaking Stress (ksi)	Average Tensile Strength (ksi)	Coefficient of Variation
1	28 Days	3.28	3.06	7.98%
2		3.07		
3		2.70		
4		2.96		
5		3.29		
6	90 Days	2.84	2.76	4.41%
7		2.79		
8		2.57		
9		2.73		
10		2.88		
11	6 Months	3.63	3.73	11.1%
12		3.27		
13		3.89		
14		3.49		
15		4.35		

Table 31: Virginia Tech UHPC Tensile Strength Test Results

Researcher	Specimen ID	Specimen Age	Average Tensile Strength (ksi)	Number of Specimens Tested
Halbe	1	13 Days	2.04	3
	2	13 Days	2.20	3
Field	3	7 Days	1.81	2
	4	28 Days	2.40	2
D'Alessandro	5	7 Days	2.35	3
	6	14 Days	2.79	3
	7	196 Days	3.44	2

Figure 103: UHPC Tensile Strength Gain

Benjamin Graybeal states that for a concrete to be considered UHPC, it must display tensile strengths greater than or equal to 0.72 ksi (Graybeal and Russell, 2013). Every Clemson University and Virginia Tech average tensile strength exceeded this criteria. UHPC is able to achieve this high level of tensile strength due to the steel fibers in the mix. The average tensile strength of the 3/20 and 3/21 batches were 3.36 ksi and 2.18 ksi, respectively. In both batches, average tensile strength decreased from the 28 day to 90 day test, but then increased at the 6 month test. It is believed that this scatter is due to the small sample size. Additionally, because the average tensile strength did not increase much or at all with time, it is believed that the UHPC reached its maximum tensile strength before it was 28 days old.

4.1.3 Pull Off Test

Results of the pull-off test at the specimen age of 6 months are shown in table 32. Tests were not conducted earlier due to a technical issue with the pull-off tester, causing a multiple month delay. Of the 8 specimens, 3 had failures at the UHPC to concrete interface while the remaining 5 had failures at the steel disc to epoxy interface. Results were very inconsistent. Failures in the UHPC to precast interface had a range from 120 psi to 235 psi, while failures in the steel disc epoxy interface had a range from 200 to 300 psi. The results could illustrate one or more of the following; First it is possible that that test specimen was not prepared uniformly. By roughing up the precast surface, the UHPC layer theoretically would have a stronger bond. It is possible that the surface was not uniformly rough, which would contribute to certain sections of the specimen having greater bond strength than others. Secondly, some of the specimens were tested near the

perimeter of the specimen while others were tested towards the center. It is possible that those specimens in the center of the specimen, which are surrounded by more concrete and UHPC, could have had a stronger bond strength that those at the perimeter. The minimum average bond strength independent of the failure mode was 232 psi, which is quite strong. The bond is said to be the minimum bond because it is the lower bound of the potential bond strength. This strong bond strength in addition to the UHPC tensile strength should provide a shear key that performs and remains durable for many years.

Although the pull off test results were not consistent, they are close to results that other researchers testing UHPC's bond strength have seen. Table 33 contains UHPC bond strength results from 2 different Virginia Tech researchers.

Table 32: Clemson University 6 Month UHPC Pull-Off Test Results

Specimen #	Failure Stress (psi)	Failure Mode	Bond Strength (psi)	Minimum Average Bond Strength (psi)	Coefficient of Variation
1	362	Epoxy Interface	> 362		
2	120	UHPC to Concrete Interface	= 120		
3	235	UHPC to Concrete Interface	= 235		
4	177	UHPC to Concrete Interface	= 177	232	31.8%
5	300	Epoxy Interface	> 300		
6	231	Epoxy Interface	> 231		
7	200	Epoxy Interface	> 200		
8	230	Epoxy Interface	> 230		

Table 33: Virginia Tech UHPC Pull-Off Test Results

Researcher	Specimen ID (Type)	Specimen Age	Failure Stress (psi)	Number of Specimens Tested
Halbe	1 (UHPC)	13 Days	204	6
	2 (UHPC)	13 Days	93	6
Joyce	3 (UHPC)	7 Days	180	2
	4 (UHPC)	12 Days	240	2
	5 (UHPC)	15 Days	260	2
	Average UHPC Failure Stress = 195 psi			
	6 (Grout)	7 Days	25	2
	7 (Grout)	15 Days	20	2
	Average Grout Failure Stress = 22.5 psi			

4.1.3 Summary of UHPC Tests Results

The Ductal UHPC used in the NEXT D and solid slab shear keys met or exceeded the specifications and requirements set by Benjamin Graybeal and those measured by Virginia Tech researches. After 6 months, the UHPC average compressive strength was 22.5 ksi, which exceeded Graybeal's criteria of 21. 7 ksi. After 6 months, the UHPC average splitting tensile strength in the NEXT D and Solid Slab shear keys was measured at 3.29 ksi and 3.73 ksi, respectively. Both values exceeded Graybeal's criteria of 0.72 ksi. Finally, the average bond strength of the UHPC to precast concrete was found to be at least 232 psi. This value was approximately what the Virginia Tech researchers reported for UHPC bond strength. In comparison to conventional grout's bond strength (table 32), the UHPC bond strength is far superior and in theory should facilitate a more durable shear key.

4.2 Live Load Test Results

This section of chapter 4 will focus on the results from the live load test of Hanging Rock Creek Bridge. Additionally, a comparison of experimental and theoretical values for bridge and girder characteristics is presented.

Data was recorded for live load testing of spans 1 and 4 of Hanging Rock Creek Bridge. For the NEXT D span (span 1), bridge instrumentation was attached at midspan. For the solid slab, bridge instrumentation was primarily attached at midspan with 2 additional LVDTs attached 5 feet north of midspan. Instrumentation plans can be seen in figures 77-78 and 90-91.

All deflection values have been recorded as positive for LVDT plunger extension and negative for a LVDT plunger contraction. Tensile strain is displayed as positive for tensile strain and negative for compressive strain. Recorded strains and horizontal deflections are a result of the applied live load; dead load effects are not considered in the strain and deflection data.

4.2.1 Discarded Data and Strain Gauge Noise

Each truck configuration was repeated at least 3 times to ensure a consistent data set and spot check data outliers.

For all NEXT D tests, relative horizontal data from LVDT J5-6 has been discarded. Although data was recorded, the LVDT displayed zero joint movement for every truck crossing. Figure 104 shows LVDT joint displacement data from J5-6 for load scenario 1 trial 3. The truck was directly above of LVDT J5-6, but there is no discernable joint movement.
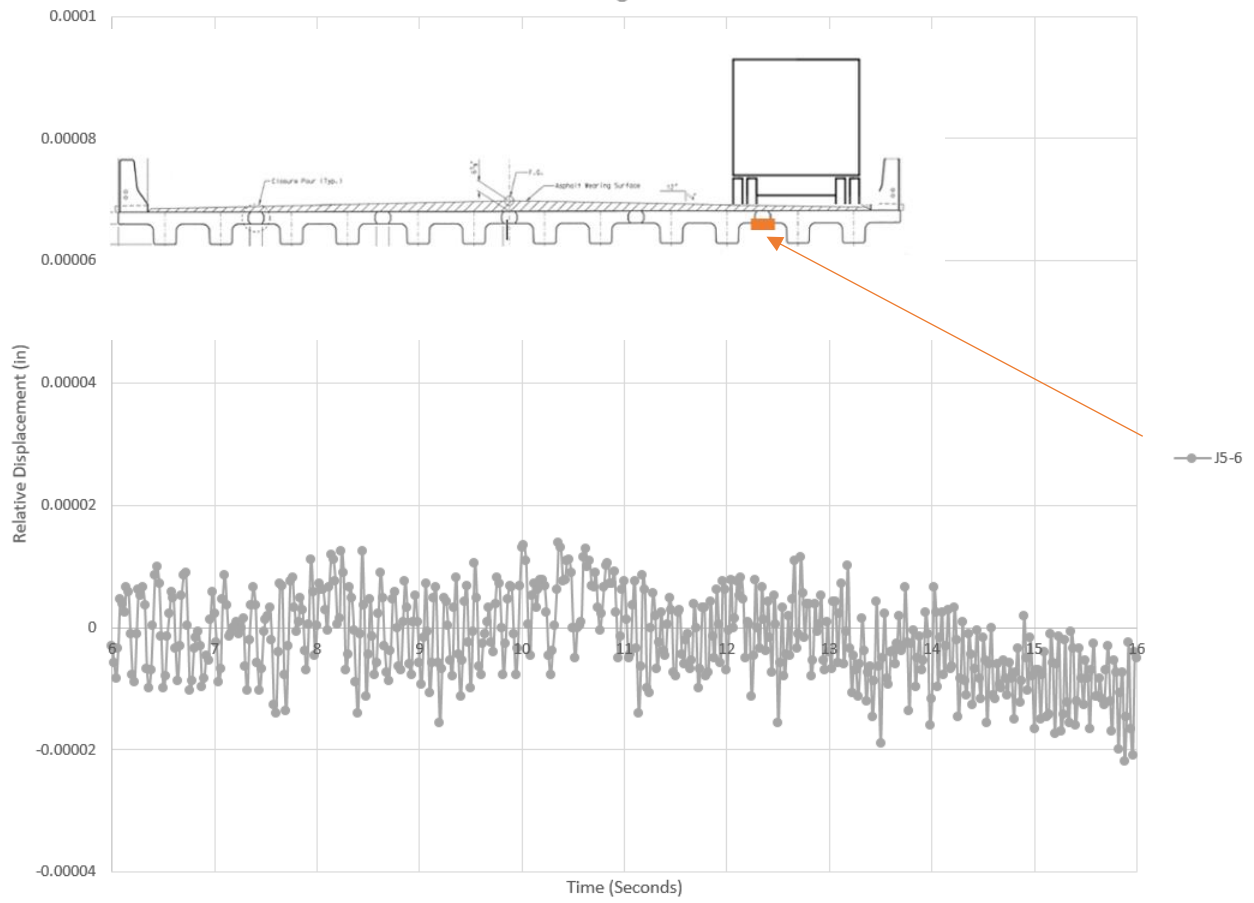
Figure 104: Load Configuration 1 Trial 3 J5-6 Data

Additionally, on both NEXT D and solid span tests, some strain data sets displayed a noticeable electronic noise as shown below in figure 105. The researchers investigated the reason for this noise, but could not determine the root cause. This noise occurred during random trials, in random strain gauges, at random times during the data recording, during single or double truck crossings and on interior and exterior girders. Since the noise was only +/- 1 microstrain and the results of the strains from tests with noise versus those without the noise was extremely consistent, all of the strain data was kept and used for the calculation of DFM values.
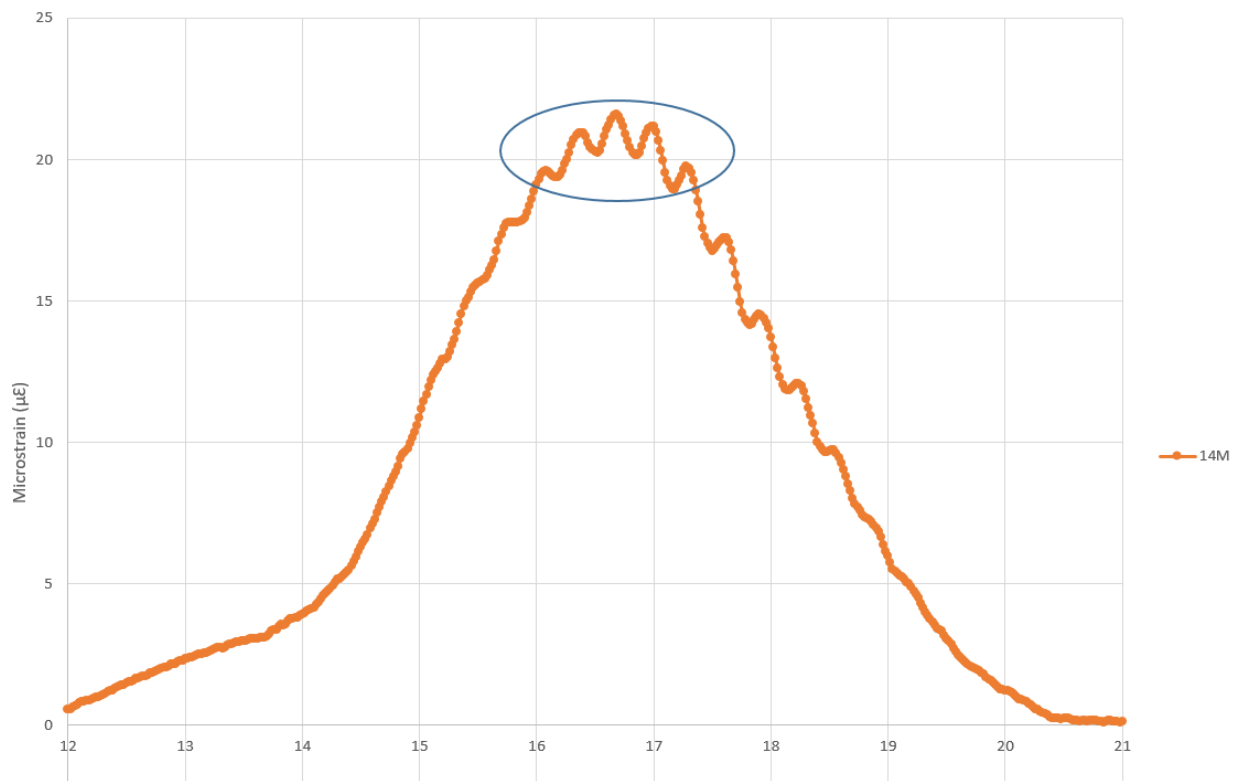
Figure 105: Strain data from Scenario 6 Trial 3 on Solid Slab – "Noise" near Peak Strain

4.2.2 NEXT D Live Load Test

4.2.2.1 Overview of Test Results

Single and side-by-side truck crossings with eight different transverse truck locations were performed on the NEXT D span of the Hanging Rock Creek Bridge. Strain data was gathered from 12 strain transducers on each truck crossing, and relative horizontal displacement data was gathered from 4 LVDTs. Bending strain in a NEXT D girder was predicted to be approximately 188 microstrain (based on a transverse load distribution 0.50 and as a simple beam-line model). Bending strains measured by the BDI system were far lower than this predicted value. It is thought that since the bridge in the plan is shaped like a square (40' long x 42' wide) and is additionally stiffened by guard rails, the bridge acts like a plate allowing for greater transverse moment distribution. This increase in transverse load distribution is consistent with the over-estimation of bending strains seen in the simple model. The bending strain calculations can be found in the appendix.

Figure 106 shows maximum girder strain data for load configuration 7 trial 3. This figure is typical of all load configurations and crossings with the largest girder strain occurring at or near the truck axles. Figure 107 shows the girder strain versus time for load configuration 7 trial 3. The girder strain rises as the front axle approaches midspan, and then peaks when the rear axle approaches midspan. The graph also illustrates that girders close to the load source receive more load, and experience greater amounts of bending strain. In the case below, the truck is almost entirely on bridge girder 2, causing strain transducers on girders 2 and 3 to register the highest bending strains.
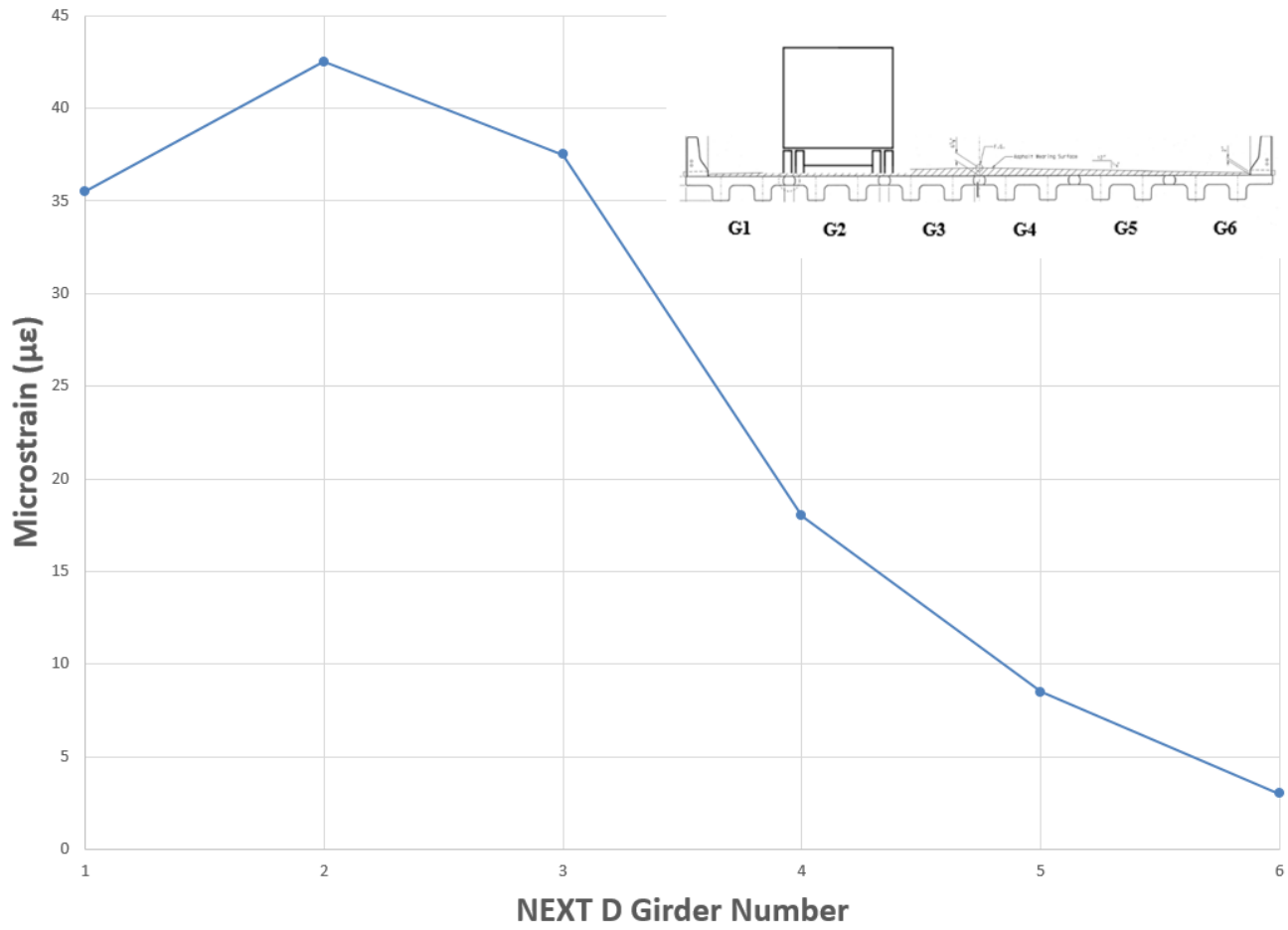
Figure 106: Cross-Section View and Strain Gauge Data for Load Configuration 7 Trial 3
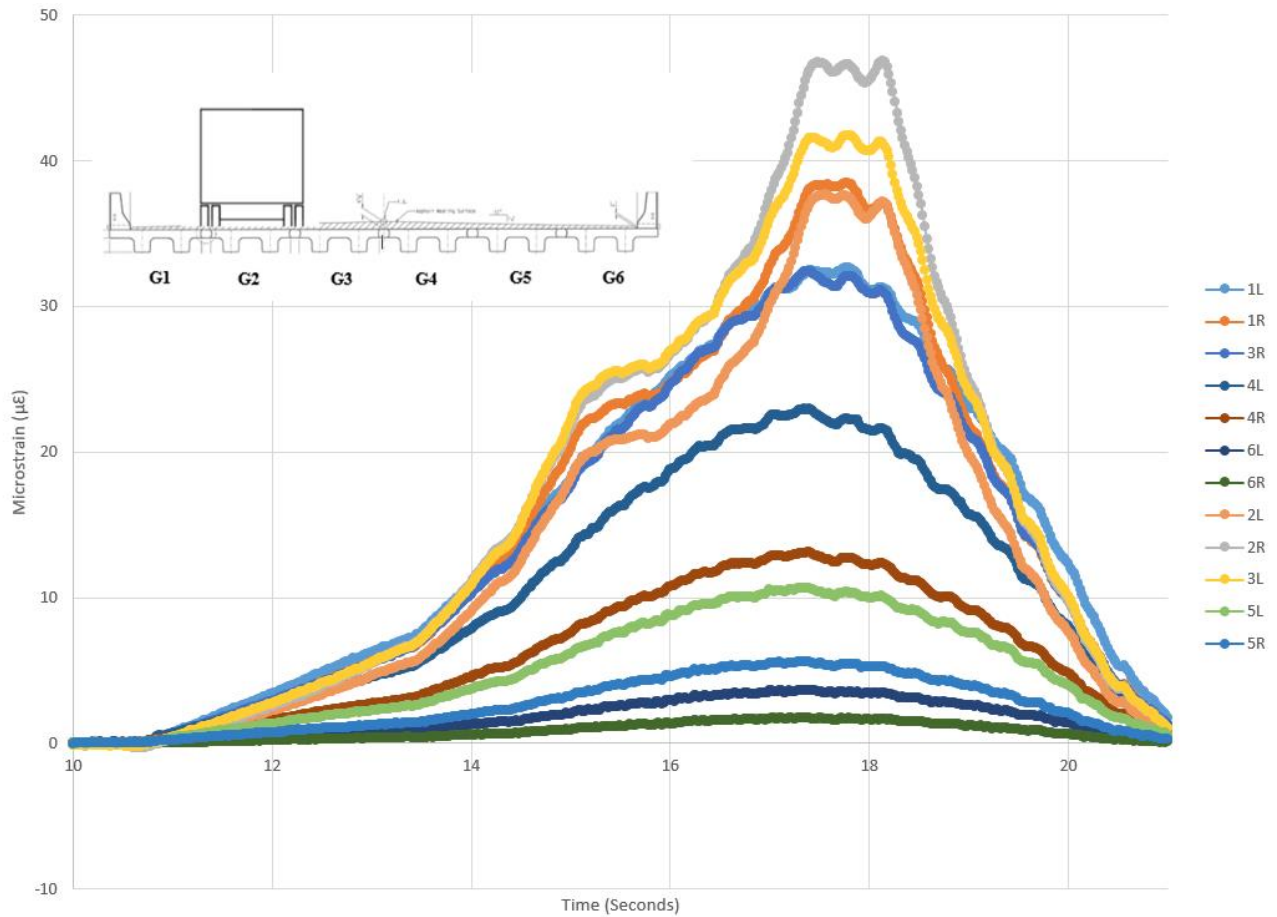
Figure 107: Strain Gauge Data from Trial 3 of Load Configuration 7 on NEXT D Span

Figure 108 shows the LVDT data from load configuration 7 trial 3. LVDTs that were closer to the load source experienced greater horizontal deflections, which in this instance was J1-2. Additionally, the plateau around 15 seconds shows when the front axle crosses over the LVDT and the peak hump at 17 seconds shows when the rear axle crosses the LVDT. Relative LVDT horizontal displacements were small in comparison to those found by Kedar Halbe (0.007 in.)(Halbe, 2014) and Sheng (0.008 in.)(Sheng et al., 2013).
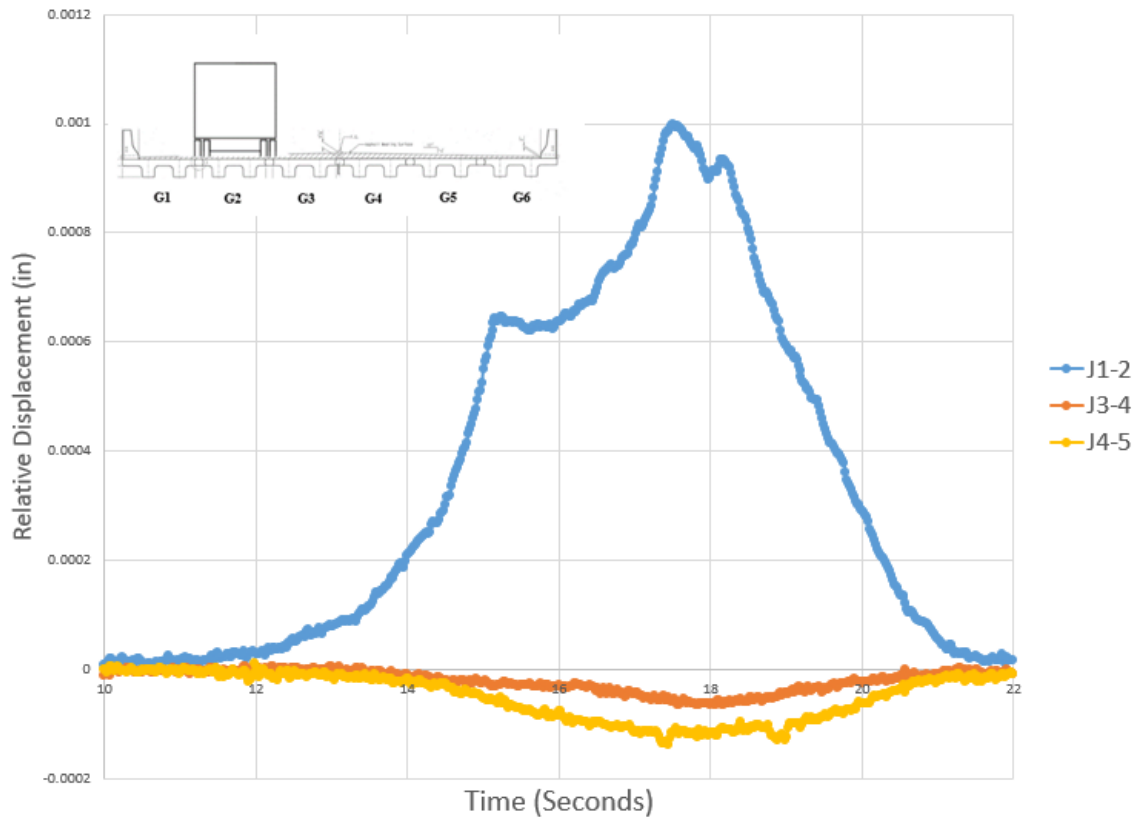
Figure 108: LVDT Data from Trial 3 of Load Configuration 7 on NEXT D Span

Using the strain gauge and LVDT data, DFMs, IM factors, and joint health were all evaluated and conclusions were made.

4.2.2.2 Strain Gauge Data and DFM Calculation

Eight different load configurations and a total of 31 separate truck crossings were performed on the NEXT D span of the Hanging Rock Creek Bridge. Strain gauge data was gathered from 12 gauges on each truck crossing. Using this strain gauge data, three different experimental distributed moment factors (DFMs) for each girder were determined per truck crossing. The methodology for determining these DFMs is

explained in the following sub-sections. After all DFMs were calculated, the maximum experimental values were found for the interior and exterior girders respectively. These values were then compared to AASHTO type i and k factors, and two separate FE model DFM values.

4.2.2.2.1 Time Independent Method

Every NEXT D girder was instrumented with two strain gauges (one per stem). To calculate the individual bridge girder DFM, a DFM was calculated for each individual stem, and then the stem values for each bridge girder were added to each other to obtain the entire bridge girder DFM value. The DFMs per stem was calculated by taking the maximum bending strain experienced by the stem and dividing it by the sum of every other bridge stems maximum bending strain value. This method is labeled as the time independent approach since not every bridge girder experienced its maximum bending strain at the same time.

4.2.2.2.2 Time Dependent Methods (a) and (b)

Each stem DFM was calculated by taking the maximum strain experienced by the stem and dividing it by the sum of the every stem's strain experienced at the time of the stem of interest experienced maximum strain, not the maximum strains experienced by all the other stems. To get the girder DFM, both stem DFMs were added to each other. Since each girder had two sensors, and each sensor experienced the maximum strain at a different time, two DFM values were determined per bridge girder. The DFM values

calculated by the time dependent approach tended to be slightly more conservative (i.e.

larger values) than the time independent values.

4.2.2.2.3 AASHTO Type i

DFMs for the AASHTO type i method were calculated in accordance with the

type i equations of AASHTO. These bridge sections are shaped like a double tee. The

physical description of this bridge is the closest match to the NEXT D span. Calculations

for this method can be found in the appendix.

4.2.2.2.4 AASHTO Type k

DFMs for the AASHTO type k method were calculated in accordance with the

type k equations of AASHTO. These bridge sections are shaped like a bulb tee, which is

similar to, but not the same as the NEXT D cross-section. Calculations for this method

can be found in the appendix.

4.2.2.2.5 NEXT-6 FE Model

DFMs for this method were taken from a Clemson University report (Sheng et al.,

2013) that modeled the NEXT beam with a 6' wide flange.

4.2.2.2.7 NEXT-8 FE Model

DFMs for this method were taken from a Clemson University report (Sheng, et

al., 2013) that modeled the NEXT beam with an 8' wide flange.

4.2.2.3 Sample DFM Calculation

This section will explain the process of calculating the DFMs for load

configuration 7 trial 3. The DFMs for all other truck configurations and crossings were

calculated in a similar fashion.

Figure 104 above is a graph showing the strain gauge data from load

configuration 7 trial 3. Table 34 displays the maximum bending strain in each web of

each girder during load scenario 7 trial 3. Using equation 9 from the literature review,

each web DFM was calculated and displayed in table 34. Since each bridge girder has

two webs and was therefore rigged with two strain gauges, the summation of the two

DFMs per stem on a girder was performed to calculate the individual girder DFM. The

data show that girder 2 has the greatest bending strain, followed by adjacent bridge

girders 1 and 3, respectively.

Table 34: Time Independent Maximum Bending Strain Values in Strain Transducers for Load Configuration 7 Trial 3

Sensor ID	Maximum Bending Strain ($\mu\varepsilon$)
1L	32.6
1R	38.5
2L	37.7
2R	46.9
3L	41.8
3R	32.4
4L	23.0
4R	13.1
5L	10.7
5R	5.63
6L	3.68
6R	1.77

Table 35: Time Independent Individual Web and Girder Calculated DFMs

Sensor ID	Girder #	Web DFM	Girder DFM
1L	1	0.113	0.247
1R		0.134	
2L	2	0.131	0.294
2R		0.163	
3L	3	0.145	0.258
3R		0.113	
4L	4	0.08	0.126
4R		0.046	
5L	5	0.037	0.057
5R		0.02	
6L	6	0.013	0.019
6R		0.006	

As stated earlier in the section, for every bridge crossing, each bridge girder received three separate DFM values, each calculated in a different fashion for comparison. Table 35 displays the time independent DFMs per girder while table 36 has the time dependent [(a) and (b)] DFMs.

Table 36: Experimental DFM Values Calculated by Time Dependent Method (a) and (b)

Girder #	Time Dependent (a) DFM	Time Dependent (b) DFM
1	0.250	0.250
2	0.298	0.301
3	0.259	0.259
4	0.126	0.126
5	0.058	0.059
6	0.021	0.019

For the load configuration 7 and trial 3, the three sets of DFM values calculated were all extremely close. This trend was present in the other load configurations and crossings as well.

For load configurations with two trucks present (load configurations 3 and 4), a similar process was used to calculated the bridge girder DFM values. There was one change, however. The DFM equation can be seen below:

$$g = distribution\ factor = \frac{M_{refined}}{n*M_{beam}}$$ **Equation 10**

$M_{refined}$ is the moment due to one truck that is carried by a single bridge girder. M_{beam} is the total moment due to one truck and n is the number of trucks present on the bridge. When two trucks are present, there is a "2" in the denominator of this equation. The researchers are intersted in using the experimental data with two trucks present to determine the DFM in terms of lanes/girder. To obtain the in terms of lanes/girder, the experimentally observed distribution factor must be multiplied by the numbers of trucks present, which is two in the case of truck configurations 3 and 4.

With 20 static bridge crossings, and 3 DFM values calculated per crossing, 60 total DFM values were experimentally calculated per bridge girder. All 60 of these values were sorted and the maximum value per girder was determined.

AASHTO LRFD calculates DFM values for both single and multiple truck lane loads. To compare experimentally determined values with AASHTO LRFD values, separate DFM values were deteremined for single and side-by-side truck crossings. The maximum DFM values experimentally determined for single and side-by-side truck loads are shown below in table 37.

Table 37: Maximum Experimentally Determined DFM Values

Girder #	Experimental DFM: Single Truck	Experimental DFM: Side-by-Side Truck
1(exterior)	0.42	0.11
2	0.30	0.23
3	0.26	0.48
4	0.31	0.53
5	0.34	0.56
6(exterior)	0.36	0.40

It should be noted that a longitudional reinforcement bar was left out during the construction of the NEXT D joint J5-6. From the data, it does not appear that the absence of the bar significantly affected the transverese moment distribution between the girders.

The maximum experimentally derived DFM is much greater in girder 6 than in girder 1 for the side-by-side truck loading. This is because the west half of the bridge receieved the majority of the different load configurations. Through bridge symmetry, it can be safely assumed that girder 1 would behave similarly to girder 6 if it experienced symmetric loadings.

In bridge engineering, typically there are two designs for bridge girders: a typical interior and typical exterior girder. As a result, a maximum DFM value was determined for the interior girder (girders 2 through 5) and for the exterior girder (girders 1 and 6) for both single truck and side-by-side truck cases. These values were then compared side by side to DFMs determined from AASHTO LRFD type i and k equations (calculations shown in appendix), respectively, as well as DFMs from NEXT-6 (flange 6' wide) and NEXT-8 (flange 8' wide) finite element models (Sheng et al., 2013), respectively. The

head-to-head comparisons for single and double truck cases can be seen in figures 109 and 110, respectively, as well as table 38.
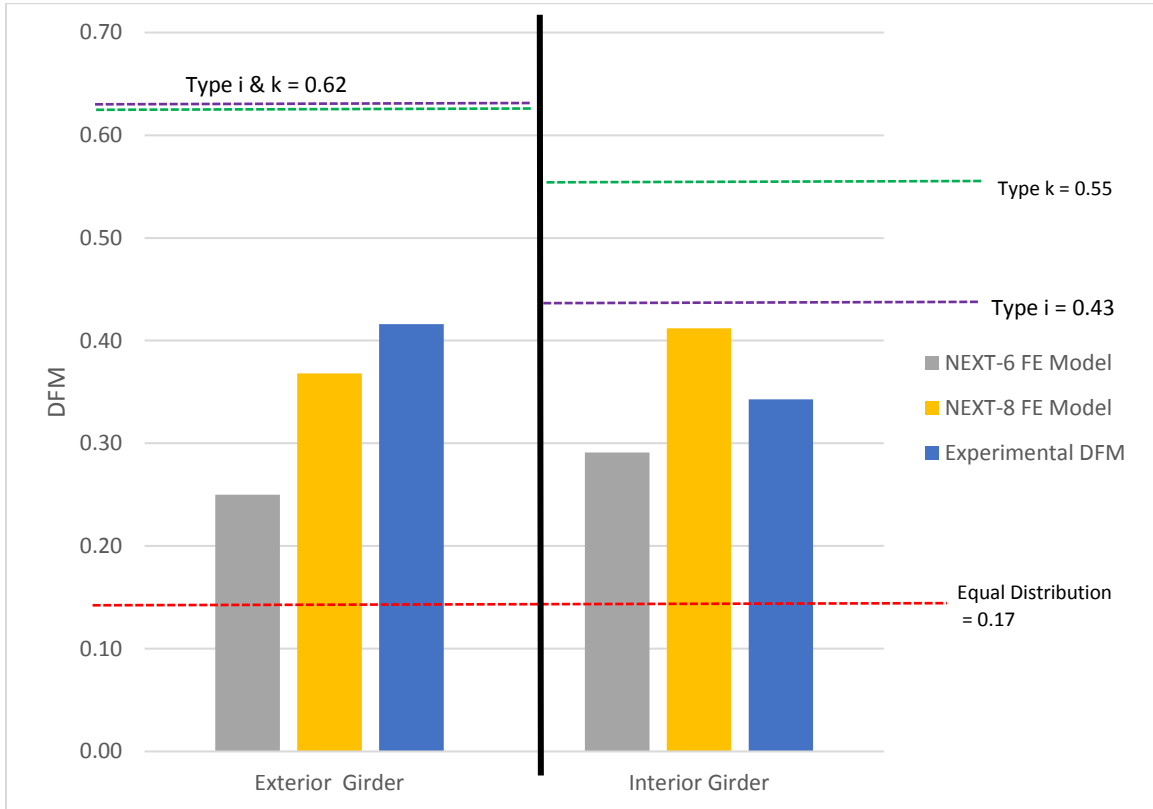
Figure 109: DFM Comparison for Single Truck Load
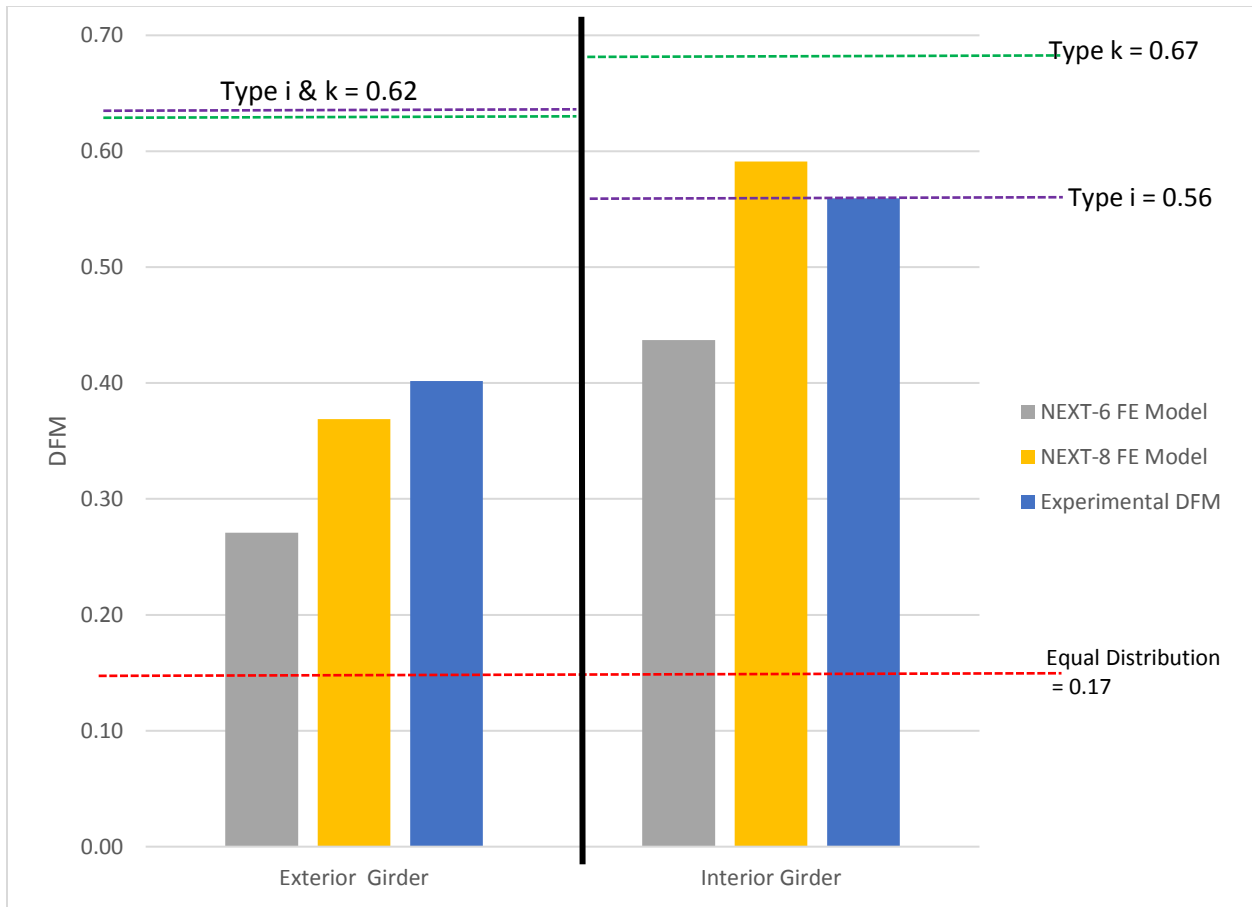
Figure 110: DFM Comparison for Side-by-Side Truck Load

Table 38: DFM Comparison for Single Truck and Side-by-Side Trucks

DFM Method	Single Truck		Side-by-Side Truck	
	Exterior Girder	Interior Girder	Exterior Girder	Interior Girder
AASHTO type k	0.62	0.55	0.62	0.67
AASHTO type i	0.62	0.43	0.62	0.56
NEXT-6 FE Model	0.25	0.29	0.27	0.44
NEXT-8 FE Model	0.37	0.41	0.37	0.59
Experimental DFM	0.42	0.34	0.40	0.56

For both single truck and side-by-side truck exterior girder cases, the AASHTO DFMs were substantially larger than the experimentally determined values. Additionally, both finite element models' DFMs were less than the experimental determined DFMs, with the NEXT-8 being more conservative (ie. larger) than the NEXT-6.

For both single truck and side-by-side interior girder cases, the AASHTO type k DFM was greater than the experimentally derived DFM value. For the single truck load, type i was also greater than the experimental DFM, but not as conservative as type k. This confirms what the original PCI technical committee had suggested. Specifically, that type k is appropriate for NEXT bridge members (Culmo and Seraderian, 2010) . For the side-by-side truck case, AASHTO type i DFM and the experimental DFM were equivalent to each other. For both single truck and side-by-side truck interior girder cases, the NEXT-6 FE model was smaller than the experimental DFM and the NEXT-8 FE model DFM was larger.

In conclusion, both AASHTO type i and k method DFMs are equal to (in one case) or greater than the experimentally derived DFMs. Type i is less conservative than type k. The author recommends that engineers continue to design NEXT beam girders in

the type k fashion because it is the most conservative. Slightly concerning is the fact that the interior girder double truck case experimental DFM is equivalent to the type i DFM.

The bridge tested is essentially brand new and no joint cracking was observed or expected. However, as a bridge ages and receives greater load cycles, shear keys tend to crack and degrade. Degraded shear keys allow less load to be transferred between girders, thus the author would expect the experimental DFM for the interior girder double truck to actually increase and become greater than the DFM calculated by the AASHTO type i method. Designing NEXT beam bridges in the AASHTO type i method could lead to a potential under-design and bridge failure.

4.2.2.4 LVDT Data

LVDT data was gathered from 4 sensors on each truck crossing. As previously discussed, one instrument (J5-6) was not working properly and its data was discarded. Relative horizontal displacement of the joints was used to observe joint behavior and see if a joint had degraded or opened up in any way. All relative horizontal displacements were averaged for each load configuration and are presented later in this section.

Figure 111 below is a graph showing the LVDT data from load configuration 7 trial 3. The graph illustrates that joints closer to the load source receive more load and experience greater amounts of relative horizontal displacement. This is attributed to the additional load going through joints closest to the trucks. In the case below, the truck is almost entirely on bridge girder 2. The joint under the left wheel load experiences significantly greater amounts of relative horizontal displacement than joints 3-4 and 4-5. Additionally, the relative horizontal displacement of joint 1-2 is positive, meaning that

143

the LVDT arm plunger is extending and that the joint is opening up slightly. The negative

displacements in joints 3-4 and 4-5 mean that those joints are closing up.
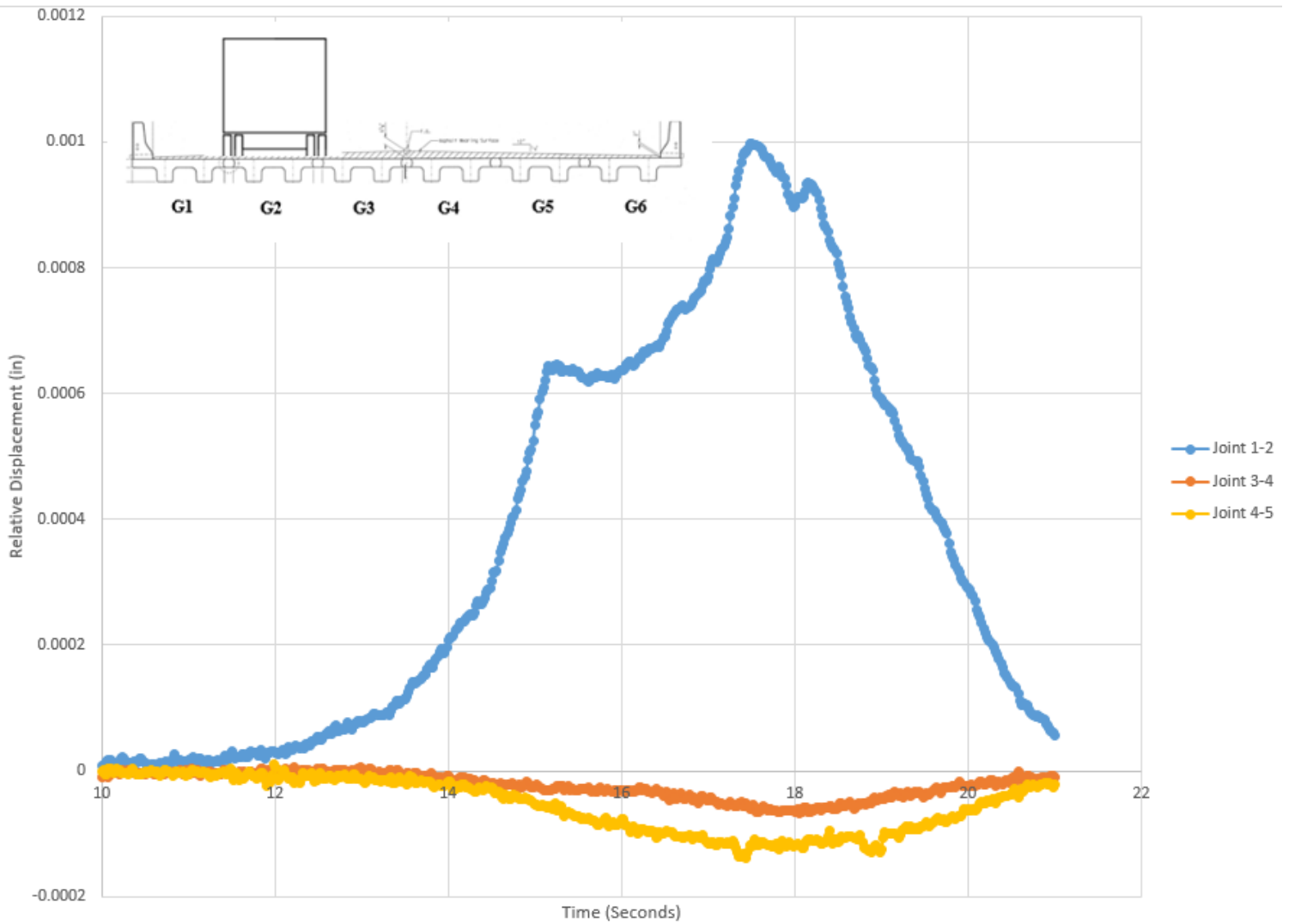
Figure 111: LVDT Data from Trial 3 of Load Configuration 7 on NEXT D Span

Table 39 displays the average LVDT horizontal displacements for each load configuration. The maximum horizontal displacements were quite small. For joints 1-2, 3-4, and 4-5, the maximum relative horizontal displacements were 0.001 in, 0.0008 in, and 0.0009 in, respectively. With such small displacements, it is believed that the UHPC joints currently have a strong bond with the precast NEXT D bridge girders and that the joints have not cracked or degraded yet. Additionally, no reflective cracks on the bridge were observed and there were no abrupt changes in the data indicating a crack initiation. One of UHPCs advantages is its bond strength, and that is illustrated by the performance of the joints during testing. In future bridge tests, it will be important to observe whether these relative horizontal displacements increase. An increase in relative horizontal displacement could be an indication that the UHPC shear key has debonded from the precast bridge girder. This would be problematic and could lead to shear key cracking, reduced transverse load distribution, and degradation of the prestressing strands via corrosive agents entering the bridge section through the wearing surface cracks.

Table 39: NEXT D Average LVDT Horizontal Displacements

		Load Configuration							
		#1	#2	#3	#4	#5	#6	#7	#8
LVDT	J4-5	0.00017	0.00090	0.00088	0.00092	0.00069	-0.000063	-0.00012	0.00078
	J3-4	-0.0001	3.31E-05	0.00068	0.00063	0.00082	-0.00010	-0.00006	0.00076
	J1-2	-0.000024	1.16E-05	-0.00015	-0.00019	-0.00013	0.00079	0.001	-0.00017

4.2.2.5 Dynamic Load Allowance

To calculate the experimental IM, bending strain values were used from all truck crossings in load configurations 5 and 8 crossings, respectively. The following equation, which was discussed in the literature review (2.2), was used to calculate the experimental IM.

$$IM = \frac{D_{dyn}}{D_{sta}} \qquad \textbf{Equation 11}$$

Each girder was rigged with two strain gauges. The maximum strains in each gauge were averaged to get a total girder strain. Each maximum average girder strain for the 3 truck crossings for load configuration 5, and 7 truck crossings for load configuration 8, were then averaged. Then the IM for each girder was calculated using static (configuration 5) and dynamic (configuration 8) responses in equation 11 above. Of the calculated data set, the maximum IM was then taken as the maximum of the experimentally determined IM. Table 40 displays the IM for three of the NEXT D bridge girders. Only girders experiencing the majority of the bending response had IM values determined. The greatest IM is 1.07, which is significantly less than AASHTOs 1.33.

Table 40: Maximum Experimentally Derived IM Values

Girder #	Load Configuration 5 Average Bending Strain (με)	Load Configuration 8 Average Bending Strain (με)	IM
3	39.0	39.6	1.02
4	51.7	51.8	1.00
5	36.8	39.4	1.07

Figure 112 is a plot of both the static and dynamic responses of strain gauge 4R. It can be seen that the dynamic crossing produces greater bending strain than the static crossing. This dynamic effect is captured in the IM factor and helps engineers design bridge components accordingly.
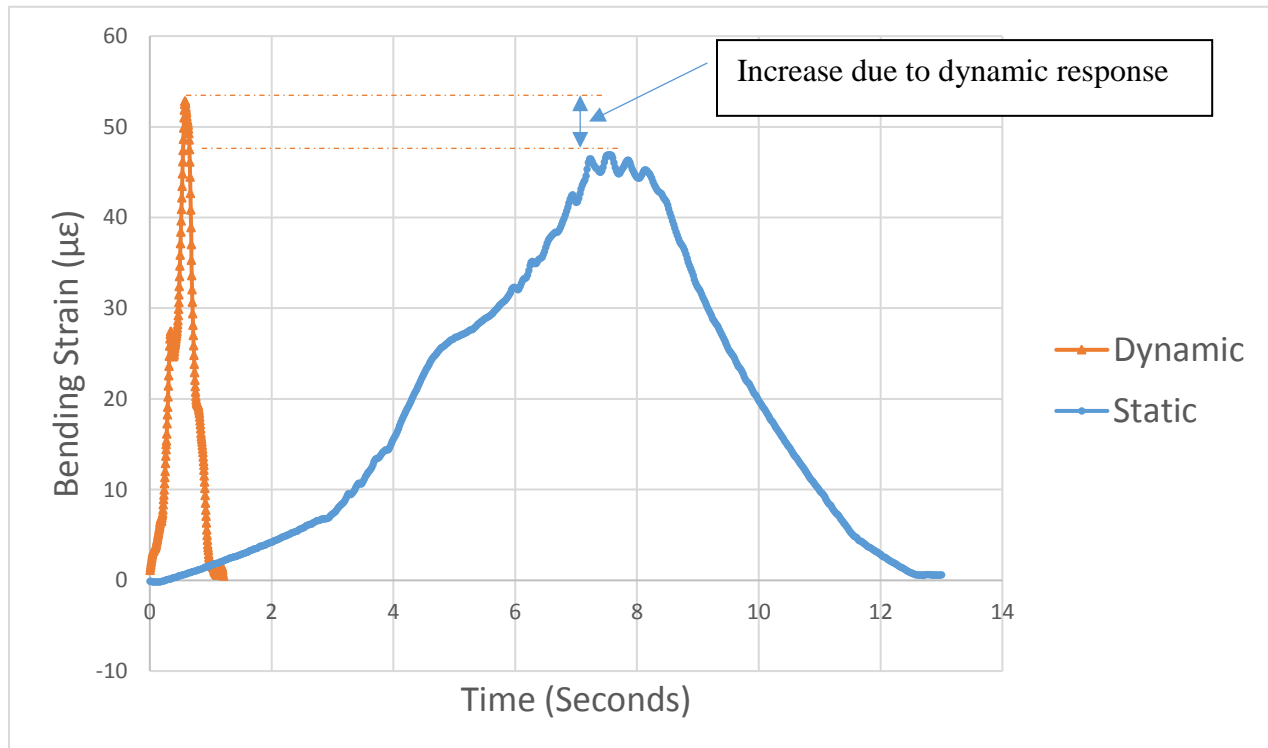
Figure 112: Dynamic vs. Static Responses in Strain Gauge 4R on NEXT D Span

The Hanging Rock Creek Bridge is newly constructed. The road surface is not rough and the approach slabs have not seen enough load to settle and create a "ramp." In future live load tests, it will be important to observe whether the IM values increase or remain constant, or decrease.

4.2.3 Solid Slab Live Load Test

4.2.3.1 Overview of Test Results

Single and side-by-side truck crossings with ten different transverse truck locations were performed on the solid slab span of the Hanging Rock Creek Bridge. Strain data was gathered from 16 strain transducers and relative horizontal displacement data was gathered from 4 LVDTs on each truck crossing. The predicted bending strain in a solid slab girder was calculated to be approximately 194 microstrain based on a transverse load factor of 0.50. In the model, the bridge was modeled as a simple span bridge, which is not how a bridge really behaves like. Bending strains measured by the BDI system were far lower than this predicted value. It is thought that since the bridge is shaped like a square (40' long x 42' wide) and is additionally stiffened by guard rails and UHPC shear keys, the bridge acts like a plate allowing for greater moment distribution both transversely and longitudinally. This increase in load distribution is thought to be culpable in the lower observed bending strain. The bending strain calculations can be found in the appendix.

Figure 113 shows maximum girder strain data for load configuration 3 trial 1. This figure is typical of all load configurations and crossings with the largest girder strain occurring at or near the truck axles. Figure 114 shows the girder strain versus time for

148

load configuration 3 trial 1. The girder strain rises as the front axle approaches midspan, and then peaks when the rear axle approaches midspan. The graph also illustrates that girders close to the load source receive more load, as evidenced by the greater amounts of bending strain. In the case below, the trucks' wheels are on the joints J10-11 and J12-13, respectively, causing strain transducers on girders 11 and 12 (inside of the wheel loads) to register the highest bending strains.
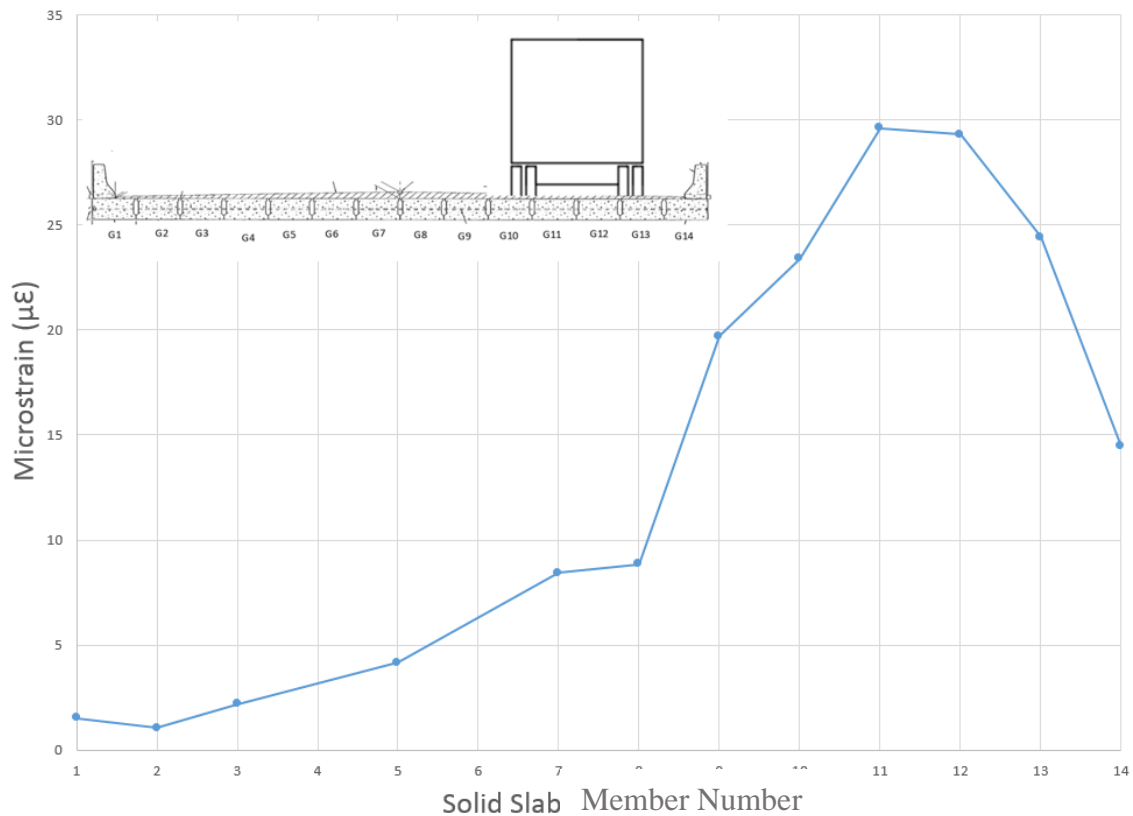
Figure 113: Cross-Section View and Strain Gauge Data for Load Configuration 3 Trial 1
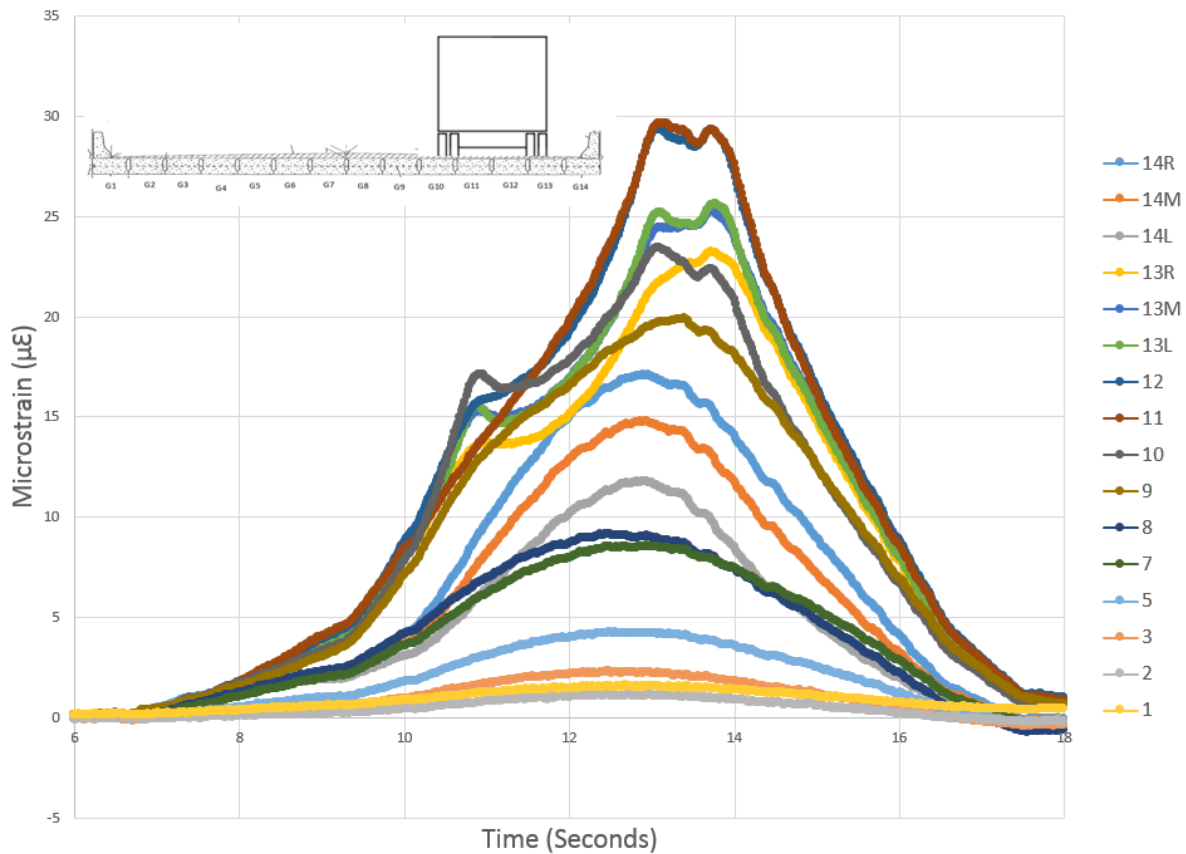
Figure 114: Strain Gauge Data from Load Configuration 3 Trial 1

Figure 115 shows the LVDT data from load configuration 3 trial 1. LVDTs that were closer to the load source experienced greater horizontal deflections, which in this instance was J10-11 and J13-14, respectively. Relative LVDT horizontal displacements were much greater in solid slab spans then the NEXT D spans. These higher displacements indicate greater joint rotation and a greater potential for joint cracking and delamination of the UHPC joint to the precast concrete. One possible explanation for these greater displacements is that the solid slab members have partial depth shear keys as opposed to the full depth shear keys of the NEXT D beam sections. Partial depth shear

keys allow for less bond between precast members and thus greater relative horizontal displacements. A second explanation of the greater displacements is that solid slab member joints are much deeper (1'-9") when compared to the NEXT D joints (8"). A similar joint rotation angle would allow for a greater relative horizontal displacement due to the deeper section.
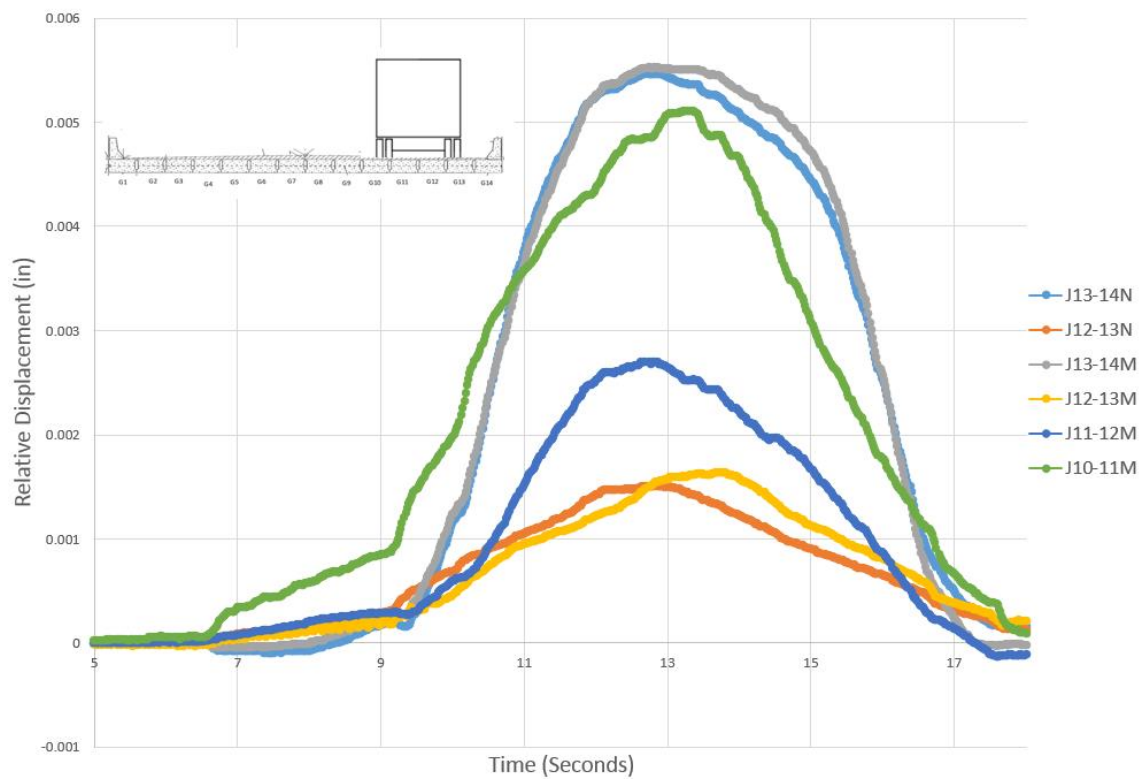
Figure 115: LVDT Data from Load Configuration 3 Trial 1 on Solid Slab Span

4.2.3.2 Strain Gauge Data and DFM Calculation

Ten different load configurations and a total of 31 separate truck crossings were performed on the solid slab span of the Hanging Rock Creek Bridge. Strain gauge data was gathered from 16 gauges on each truck crossing. Using this strain gauge data, two

different distributed moment factors (DFMs) for each girder were determined per truck crossing. The methodology for determining these DFMs is explained in the following sub-sections. After all DFMs were calculated, the maximum experimental values were found for the interior and exterior girders, respectively. These values were then compared to AASHTO type g equation factors.

4.2.3.2.1 Time Independent Method

Girders 1-3, 5, and 7-12 each were rigged with a single strain gauge. Girders 4 and 6 were not rigged with strain gauge, while girders 13 and 14 were each rigged with 3 strain gauges. Using equation 9 from the literature review, each web DFM was for the independent method calculated. When calculating the girder DFMs, maximum strains independent of the time taken were used. This method is labeled as the time independent approach since not every bridge girder experienced its maximum strain at the same time. To account for members that were not instrumented such as girder 4, this DFM was calculated by taking average DFM of girder 3 and 5, while girder 6 DFM was taken as the average of girder 5 and 7 DFM. Girders 13 and 14 had their DFMs calculated by taking the average bending strain of the given member (13 or 14) divided by the sum of the total microstrain experienced in girders 1 through 14.

4.2.3.2.2 Time Dependent Method

The time dependent method calculated the DFMs in a similar approach to the time independent method, except the maximum bending strain of a girder was divided by the sum of the all the girders at the time of the maximum bending strain rather than the sum

of the maximum bending strains. As a result, the DFM values calculated by the time

dependent approach tended to be slightly more conservative (i.e. larger values).

4.2.3.2.3 AASHTO Type g

DFMs for the AASHTO type g method were calculated in accordance with the

type g equations of AASHTO. These bridge sections are shaped like a solid slab unit.

Calculations for this method can be found in the appendix.

4.2.3.3 Sample DFM Calculation

This section will walk the reader through the process of calculating the DFMs for

load configuration 3 trial 1 of the solid slab span. The DFMs for all other load

configurations and trials were calculated in a similar fashion.

Figure 114 above is a graph showing the strain gauge data from load

configuration 3 trial 1. The data shows that girders 11 and 12 experienced the greatest

bending strain, followed closely by adjacent girders 10 and 13. Table 41 displays each

strain gauges maximum bending strain during the truck crossing. For members without

strain gauges, the strain in the table was determined by interpolating strains in adjacent

members. Using equation 9 from the literature review, each web DFM was calculated.

Girder 4 DFM was calculated by taking average of Girder 3 and 5 DFM, while girder 6

DFM was taken as the average of girder 5 and 7 DFM. Since members 13 and 14 had

multiple gauges, their DFMs were calculated by taking the average bending strain of their

gauges divided by the sum of the total microstrain experienced in girders 1 through 14.

Maximum solid slab member strains can be seen in table 41. The time independent DFMs

can be seen in table 42 and time dependent DFMs in table 43.

Table 41: Time Independent Maximum Bending Strain Values in Strain Transducers for Load Configuration 3 Trial 1

Sensor ID	Maximum Bending Strain (με)
1	1.59
2	1.22
3	2.28
5	4.23
7	8.55
8	9.13
9	19.9
10	23.4
11	29.6
12	29.4
13L	25.6
13M	25.2
13R	23.2
14L	11.8
14M	14.8
14R	17.1

Table 42: Experimental DFM Values Calculated by Time Independent Method (Method 1)

Girder #	DFM
1	0.009
2	0.007
3	0.013
4	0.018
5	0.024
6	0.036
7	0.048
8	0.051
9	0.112
10	0.131
11	0.166
12	0.165
13	0.139
14	0.082

Table 43: Experimental DFM Values Calculated by Time Dependent Method (Method 2)

Girder #	DFM
1	0.010
2	0.008
3	0.015
4	0.021
5	0.028
6	0.038
7	0.049
8	0.060
9	0.115
10	0.133
11	0.169
12	0.167
13	0.145
14	0.084

For load configuration 3 trial 1, the two sets of calculated DFMs were extremely close. This trend was present in other load scenarios and trials as well.

For load configurations with two trucks present (load scenarios 4, 5, and 6) a similar process was used to calculate the bridge girder DFM values. However, as explained before in section 4.2.2.2, the experimentally determined DFMs were multiplied by 2 to calculate the distribution value in cases when two trucks were present.

With 28 static bridge crossings and 2 DFM values calculated per crossing, 56 total DFM values were experimentally calculated per bridge girder. All 56 of these DFM values were sorted and the maximum value per girder was determined. To compare experimentally determined values with AASHTO LRFD values, separate DFM values were determined for single and side-by-side truck loads. The maximum DFM values experimentally calculated for single trucks and side-by-side trucks are shown in table 44 below.

Table 44: Maximum Experimentally Derived DFM Values

Girder #	Experimental DFM: Single Truck	Experimental DFM: Side-by-Side Truck
1(exterior)	0.16	0.03
2	0.16	0.03
3	0.17	0.06
4	0.14	0.09
5	0.14	0.11
6	0.13	0.15
7	0.12	0.19
8	0.11	0.20
9	0.12	0.25
10	0.13	0.24
11	0.18	0.27
12	0.20	0.24
13	0.20	0.21
14(exterior)	0.14	0.20

The maximum experimentally derived DFM was much greater in girder 14 than girder 1. This is because the west half of the bridge received the majority of the different load configurations. Through bridge symmetry, it can be safely assumed that girder 1 would behave similarly to girder 14 if it experienced the same load configurations.

In bridge engineering, typically there are two designs for bridge girders: a typical interior and typical exterior girder. As a result, a maximum DFM value was determined for the interior girder (girders 2 through 13) and for the exterior girder (girders 1 and 14) for both single truck and side-by-side truck crossing cases. These values were then compared side by side to DFMs determined from AASHTO LRFD type g equations. The head to head comparisons for single and double truck cases can be seen in figures 116

and 117, respectively, in addition to table 45. Calculations for the AASHTO LRFD DFM can be found in the appendix of this report.
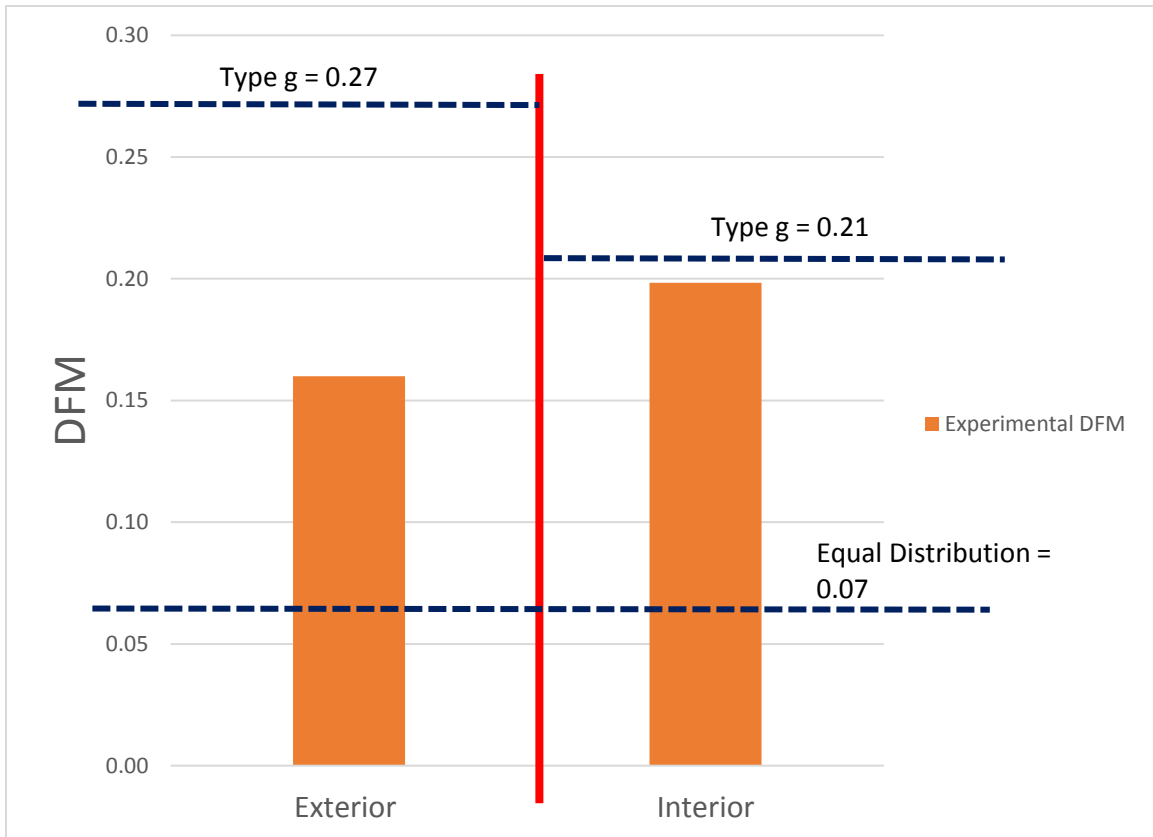
Figure 116: DFM Comparison for Solid Slab Single Truck Load
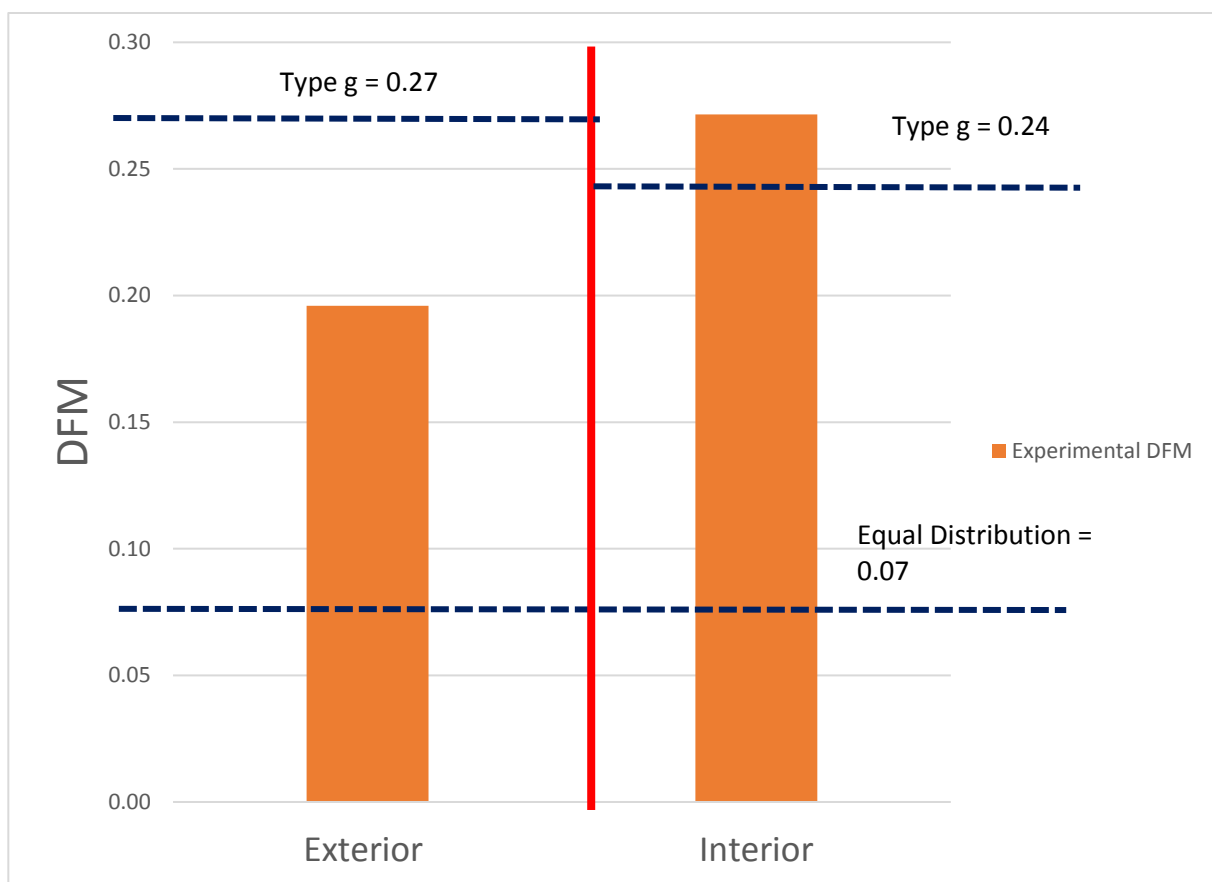
Figure 117: DFM Comparison for Solid Slab Side-by-Side Truck Load

Table 45: DFM Comparison for Solid Slab Span Single and Side-by-Side Trucks

DFM Method	Single Truck		Side-by-Side Truck	
	Exterior Girder	Interior Girder	Exterior Girder	Interior Girder
AASHTO - type g	0.27	0.21	0.25	0.24
Experimental DFM	0.16	0.20	0.20	0.27

For both single truck and side-by-side exterior girder DFMs, the AASHTO DFMs were significantly larger than experimentally derived values. For the single truck load interior girder case, the AASHTO and experimentally derived DFMs were nearly equivalent.

In 3 of the 4 comparisons, the AASHTO type g DFM is greater than, and therefore more conservative, than the experimentally derived value, with the 2 exterior girders comparisons being largely more conservative. Unexpectedly, in the side-by-side truck load, the experimentally derived DFM is greater than the AASHTO value. This is concerning because the code could allow for a bridge girder to be under-designed, thus leading to a structural failure. Experimental of verification must occur in subsequent live load tests.

4.2.3.3 LVDT Data

LVDT data was gathered from 6 sensors on each truck crossing. Relative horizontal displacement of the joints was used to observe joint behavior and see if a joint had degraded or opened up in any way. All relative horizontal displacements were averaged for each truck configuration and are presented later in this section.

Figure 118 below is a graph showing the LVDT data from load scenario 3 trial 1. The graph illustrates that joints closer to the load source experience greater amounts of relative horizontal displacement. In the case below, the truck is mostly on girders 10 and 13, respectively. The joints directly under the wheel line loads (J13-14N, J13-14M, and J10-11M) experience significantly greater amounts of relative horizontal displacement than joints 11-12 and 12-13. Additionally, all of the relative horizontal displacements of

the joints are positive, meaning that the LVDT arm plunger is extending and that the joint

is opening up.
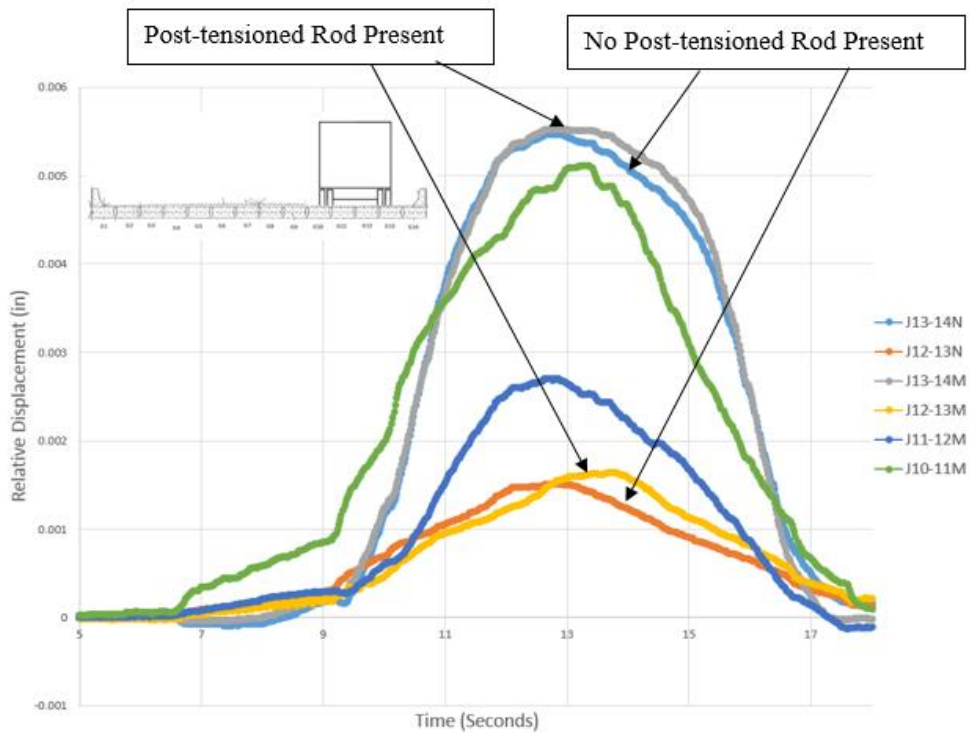
Figure 118: LVDT Data from Load Configuration 3 Trial 1 on Solid Slab Span

Table 46 displays the average LVDT horizontal displacements for each truck

configuration. The maximum horizontal displacements were quite small. For joints 10-

11, 11-12, 12-13, and 13-14 the maximum relative horizontal displacements were 0.0051

in, 0.006 in, 0.0018 in, and 0.012 in respectively. The maximum displacement (0.012 in)

was slightly greater than the displacements in comparison to those found by Kedar Halbe

(0.007 in.)(Halbe, 2014) and Sheng (0.008 in.)(Sheng et al., 2013).

With small displacements in addition to no visible cracking or abrupt in LVDT data, it is believed that the UHPC joints currently have a strong bond with the precast solid slab bridge girders and that the joints have not cracked or degraded yet. One of UHPCs advantages is its bond strength, and that is illustrated by the desirable performance of the joints during the bridge testing.

Relative horizontal displacements in the solid slab were significantly greater than those recorded in the NEXT D span. It is believed, that due to this fact, if joints were to start to crack on the Hanging Rock Creek Bridge spans, they would occur on the solid slab span before the NEXT D span. Under identical loadings NEXT D spans undergo less horizontal joint movements in comparison to the Solid slab spans, thus it is believed that these spans will experience less reflective cracking and be more durable.

In future bridge tests, it will be important to observe whether these relative horizontal displacements increase. If the relative horizontal displacement increases in the future this could be an indication that the UHPC shear key has debonded from the precast bridge girder. This would be problematic and could lead to shear key cracking, reduced transverse load distribution, and degradation of the prestressing strands via corrosive agents entering the bridge section through the wearing surface cracks.

It should be also noted that J13-14M and J13-14N have equivalent relative horizontal displacements even though J13-14N was positioned along the beam where transverse post-tensioned rod was. One would expect the relative displacement to be less at the location of the post-tensioned rod, but it was not, thus indicating that the post-tensioned rod may not be limiting joint displacement and rotation.

Table 46: Solid Slab Average LVDT Horizontal Displacements

		Load Scenario									
		#1	#2	#3	#4	#5	#6	#7	#8	#9	#10
LVDT	J10-11M	-0.00063	0.0023	0.0051	0.00054	0.0017	0.0045	-0.00011	-0.00014	-0.00036	-0.00055
	J11-12M	0.0060	0.0046	0.0027	0.0056	0.0039	0.0018	-0.00015	-0.00016	-0.00042	-0.00055
	J12-13M	0	0.00083	0.0017	0	0.00092	0.0018	0	-0.00001	-0.00005	-5.5E-05
	J12-13N	0	0.00082	0.0015	0	0.00092	0.0017	0	0	-2.3E-05	-3.5E-05
	J13-14M	0.012	0.0086	0.0053	0.012	0.0097	0.0064	-2.3E-05	-0.00003	-0.00048	-0.00055
	J13-14N	0.012	0.0085	0.0053	0.011	0.0095	0.0064	0	0	-0.00038	-0.00039

4.2.3.4 Dynamic Load Allowance

To calculate the experimental IM, bending strain values were used from all truck trials in load configurations 9 and 10, respectively. Equation 9 discussed in the literature review section 2.2, was used to calculate the experimental IM.

Maximum girder strains from the 3 trials for load scenarios 9 and 10 were averaged and used to calculate the IM factor. Then the IM for each girders 5, 6, and 7 (these were the loaded girders) were calculated using static (configuration 9) and dynamic (configuration 10) responses in equation 9 discussed above. The maximum IM between girders 5, 6, and 7 was then determined to be the experimental IM. Table 47 displays the IM for each Solid Slab bridge girder. The greatest IM is 0.80, which is much less than AASHTOs design IM of 1.33.

The data is believed to be erroneous. All of the girders have a calculated IM below 1.0. It is believed that there may have been some truck alignment variability as it crossed the solid slab span at highway speeds. This variability overloaded certain girders and under-loaded others, resulting in the IM factors shown in table 47. Additionally, the

ramping effect (Restrepo, 2002) may have affected the IM values by leading them to less than 1.0.

Table 47: Maximum Experimentally Derived IM Values on Solid Slab Span

Girder #	Load Configuration 9 Average Bending Strain (με)	Load Configuration 10 Average Bending Strain (με)	IM
5	28.3	22.8	0.80
6	26.2	20.8	0.79
7	21.3	15.8	0.74

The Hanging Rock Creek Bridge is newly constructed. The road surface is not rough and the approach slabs have not seen enough load to settle and create a "ramp." In future live load tests, it will be important to observe whether the IM values increase or remain constant.

Chapter 5:   Conclusions and Recommendations

Several bridge behaviors and UHPC properties were tested in the field live load test and material tests, respectively. A summary of these results in addition to the conclusions of the project and recommendations for the SCDOT are shown below.

5.1 Summary of Results

- After 6 months, the UHPC's average compressive, tensile, and minimum bond strength were 22.5 ksi, 3.29 ksi, and 232 psi, respectively.

- A longitudinal reinforcement bar was left out during the construction of the - NEXT D shear key J5-6. It does not appear that the absence of the bar affected the transverse moment distribution between the NEXT D girders.

- On all NEXT D live load tests, relative horizontal displacement data from LVDT J5-6 was discarded because on all load configurations and trials the joint experienced zero movement when all other LVDTs were recording some relative horizontal displacement.

- Unexplained electronic noise occurred in some strain data sets of both the NEXT D and solid slab span tests. The noise was only approximately +/- 1 microstrain, and the results of trials experiencing the noise versus not experiencing the noise were extremely consistent, therefore, none of the strain data was discarded.

- The largest bending strain recorded in the NEXT D live load test was 81 $\mu\varepsilon$ found in girder 4 of load configuration 4.

- In the NEXT D span the exterior girders maximum DFM was less than the interior girder's maximum DFM. This suggests that the guard rails stiffened the exterior NEXT D bridge girders resulting in a lower bending strain and DFM.

- Lever rule was used to determine the NEXT D exterior girder DFM. AASHTO LRFD equations for type i and k bridge sections were used to determine the interior girders.

- For the NEXT D girder single truck load case, both type i and k equations were found to produce more conservative DFMs than those experimentally calculated. In the exterior girder case, type i and k DFMs were equivalent, while in the interior girder case, type k was more conservative than i.

- For the NEXT D girder side-by-side load case, both type k equations were found to produce more conservative DFMs than those experimentally calculated, while type i was not. In the exterior girder case, type i and k DFMs were equivalent, and more conservative than those experimentally calculated. In the the interior girder case, type k was more conservative than type i, and the experimentally calculated DFM was calculated to be equivalent with type i, but more conservative than type k.

- In the NEXT D span, a maximum average relative horizontal joint displacement of 0.001 in was measured in J1-2 of load scenario 7.

- In the NEXT D span, the AASHTO impact factor of 1.33 is more conservative than those experimentally calculated.

- The largest average bending strain recorded in the solid slab live load test was 44 με found in girder 9 of load configuration 9.

- In the solid slab span, the exterior girders maximum DFM was roughly equivalent to the interior girder's maximum DFM. This suggests that the guard rails did not significantly stiffen the solid slab exterior girders.

- Lever rule could not be used to determine the solid slab span exterior girder DFM. Type g AASHTO equations were used for all solid slab span girders.

- For the solid slab girder single truck load case, type g AASHTO equations were found to produce more conservative DFMs than those experimentally calculated in both exterior and interior girders.

- For the solid slab girder side-by-side load case, AASHTO type g equations were found to be more conservative than the experimentally determined DFM for the exterior girder. However, in the interior girder case the experimentally calculated DFM was found to be greater than the AASHTO type g equation DFM.

- In the solid slab span, a maximum average relative horizontal joint displacement of 0.012 in was measured in J13-14M of load configuration 4. Solid slab displacements were greater than NEXT D span, thus cracking is more likely to occur in the solid slab joints than NEXT D joints.

- There were minimal differences in relative horizontal deflections of joints located at positions along the solid slab member where a post-tensioned rod was present versus a location where it was not present, indicating that the post-tensioned rod may not be limiting joint displacement and rotation.

- In the solid slab span, the AASHTO impact factor of 1.33 was found to be more conservative than the maximum calculated impact factor of 0.80. It is believed a truck misalignment caused erroneous data.

5.2 Conclusions

- The UHPC used in the NEXT D and solid slab span shear keys met and often exceeded the UHPC compressive, tensile, and bond strength criteria set by Benjamin Graybeal and those measured by other researchers.

- For the NEXT D span, the AASHTO type k DFM was found to be more conservative than the AASHTO type i DFM. In all cases, the type k DFM was found to be more conservative than the experimentally calculated DFM. In one case, the type i DFM was found to be equivalent with the experimentally calculated DFM.

- From visual inspection and LVDT data, it is believed that none of the NEXT D UHPC joints have cracked or delaminated at this point in time.

- In the NEXT D span, the maximum experimentally determined IM factor of 1.09 was less than the AASHTO design value of 1.33.

- For the solid slab span, the AASHTO type g DFM was found to be less conservative than the experimentally calculated DFM in the side-by-side truck load case of an interior girder.

- From visual inspection and LVDT data, it is believed that none of the solid span UHPC joints have cracked or delaminated at this point in time. However, the solid slab UHPC joints are experiencing significantly more (12 times more when

168

comparing each spans respective maximum joint movements) relative horizontal displacement in comparison to the NEXT D joints.

- Based on solid slab member LVDT data, post-tensioned rod may not be limiting joint displacement and rotation.

- In the solid slab span, the maximum experimentally determined IM factor of 0.80 was less than the AASHTO design value of 1.33. It is believed that a truck misalignment caused erroneous data.

5.3 Recommendations

- SCDOT should consider designing future bridge shear keys with UHPC. UHPC exhibits high levels of tensile strength, bond strength, and durability. Both of these qualities will limit joint cracking and reflective cracking in bridges.

- The Hanging Rock Creek Bridge is newly constructed. In the future, it is possible that joints will crack and affect the transverse load distribution capabilities. When designing NEXT D girder bridges, AASHTO type k equations should be used to calculate the design DFM since they produce more conservative results than AASHTO type i equations.

- When designing NEXT D and solid slab girder bridges, SCDOT should continue to design bridge components with a 1.33 IM factor. This factor was found to be conservative.

- Experimentally calculated DFMs for the solid span were found to be slightly greater than the AASHTO type g DFMs. The solid slab span did not exhibit as

much transverse load distribution behavior as previously thought. This conclusion should be verified in upcoming tests.

- Relative horizontal displacement was significantly greater in the solid slab span than the NEXT D span. This could be due to the wide and full depth shear key. Special attention to the displacements of both spans should be taken. If displacements significantly increase, that could be a sign of joint cracking.

- In upcoming tests, place strain gauge on both NEXT D and solid span joints to detect cracking.

- Visual inspections and documentation should be conducted during each live load test for each UHPC bridge joint. Pictures should be taken both below the bridge deck and of the wearing surface (reflective cracks).

Appendices

Appendix A: Calculations of AASHTO DFMs

This Appendix shows the calculations and processes used to evaluate the DFMs for the NEXT D beam and solid slab cross sections according to AASHTO LRFD Specifications (2012). The NEXT D beam was evaluated using both type (i) (double stem) and type (k) (single stem) cross sections, while the solid slab was evaluated as type (g). Both approaches were analyzed in order to verify the recommended procedure given by the PCI Bridge technical committee. The PCI Bridge technical committee recommends evaluating all NEXT beams as a type k bridge in order to calculate a more conservative (ie. larger) DFM value.

DFM values were calculated for both interior and exterior girders. In both cases, single and multiple lane loads were analyzed. The critical DFM value was taken as the greater of the two load cases. Section 2.2 of the literature review contains all of the equations used for calculating the DFM values for (i), (k), and (g) bridges.

A.1 NEXT D Super Structure at Hanging Rock Creek Bridge

Span 1 of the Hanging Rock Creek Bridge consists of six 40 ft. long NEXT D beams as shown in figure 118. The bridge has guard rails on the east and west sides, respectively, each with a width of 1.5 ft. The spacing between beams is 6.8 ft. and the total width of the bridge is 42 ft.
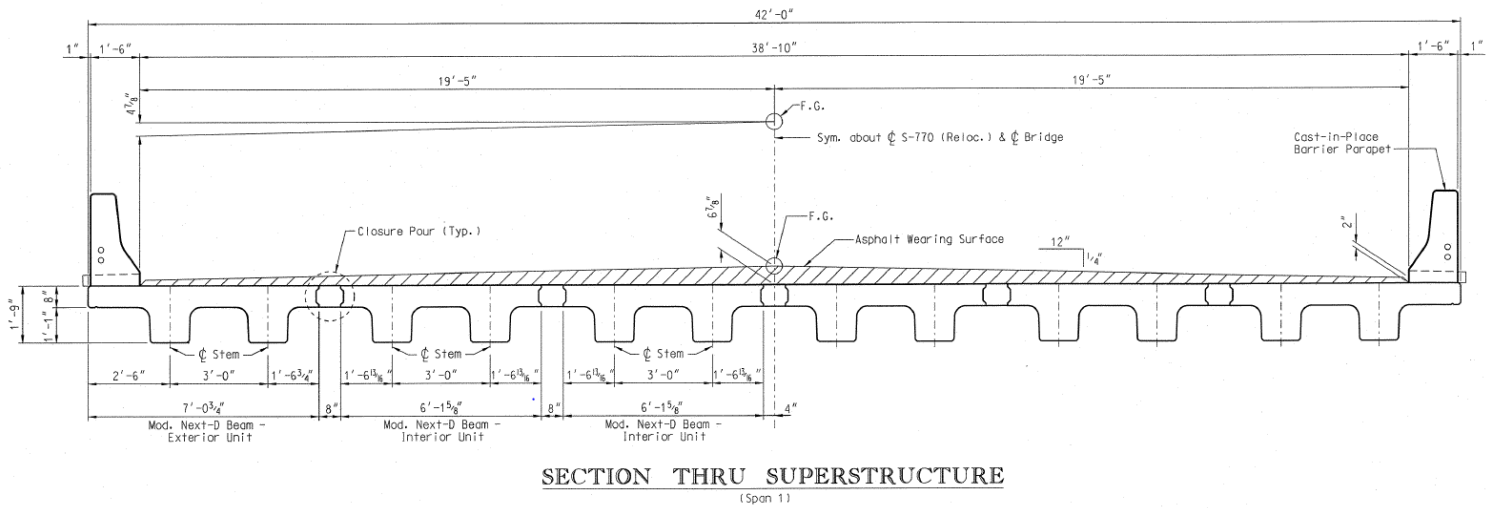
Figure 119: NEXT D Cross-Section from Hanging Rock Bridge

A.2 Single Stem Approach (SST – type k)

When evaluating a NEXT D beam as a type (k) cross section, each stem is considered as an independent girder. The calculation of the DFM takes into account the differential spacing between stems. For type (k), the spacing is taken as the average ([S1+S3]/2) of the spacing between stems in the same NEXT D beam (S1 = 3ft) and the spacing between NEXT D beams that are adjacent (S3 = 3.802 ft). These spacings are shown in figure 120. The DFM calculated using the average spacing, is then doubled to find a DFM for an entire interior NEXT D beam unit. The design interior DFM is the maximum value found from the four interior girders, while the design DFM for the exterior girder is taken as the greater of the two exterior girder calculated DFMs. Stems B2 through B11 represent interior girders, while B1 and B12 represent exterior girders.

173
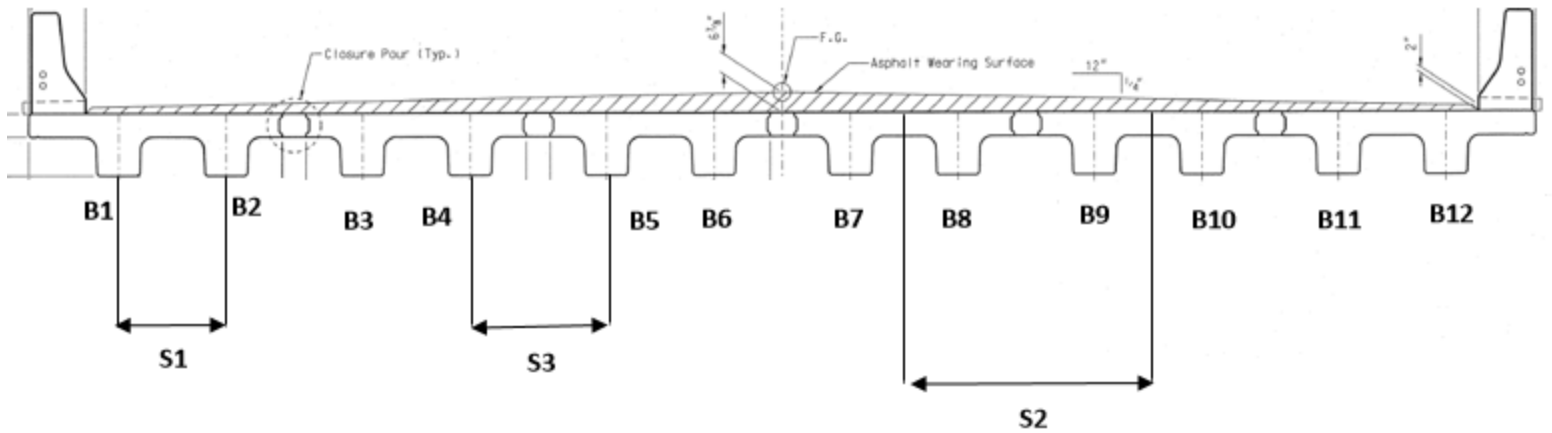
Figure 120: NEXT Beam Type k Stem Labeling Scheme

A.3 Double Stem Approach (DST – type i)

When evaluating a NEXT D beam as a type (i) cross section, each beam (consisting of two stems) is considered as a single unit. The spacing used to evaluate the DFM is taken as the distance (S2) between the centerlines of two adjacent NEXT D beams. Beams B2 through B5 are considered interior beams, while B1 and B6 are exterior beams (Figure 120). The design interior DFM is the maximum value found from the four interior girders, while the design DFM for the exterior girder is taken as the greater of the two exterior girder calculated DFMs.

174
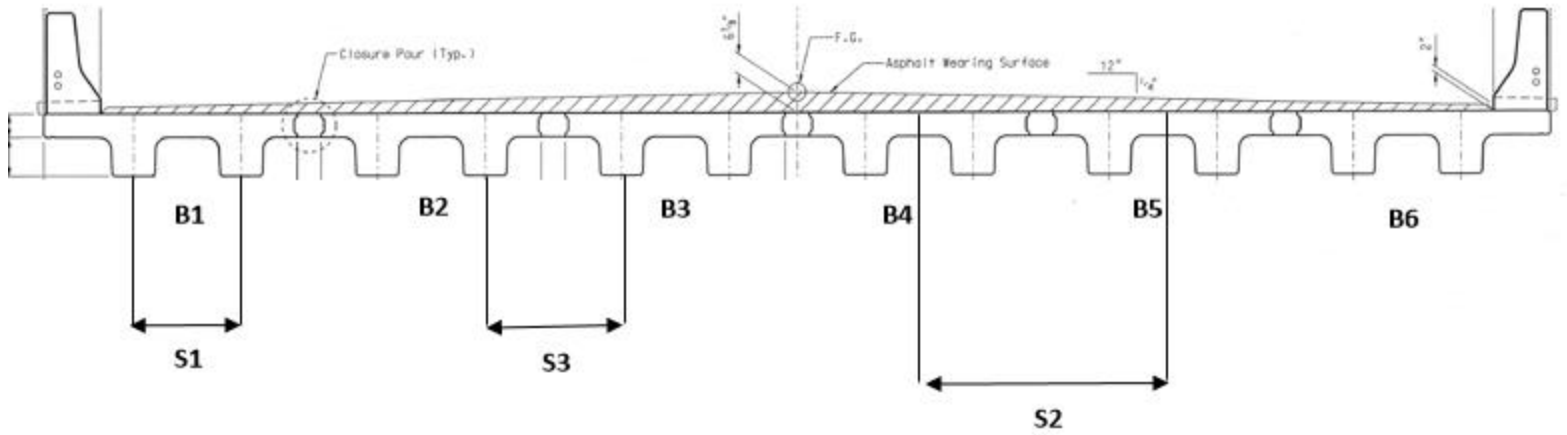
Figure 121: NEXT Beam Type i Stem Labeling Scheme

A.4 Exterior and Interior Girder DFM Calculations

A.4.1 Exterior DFM Calculation – Type (i) and (k) Approach

The width of the guard rail was taken into consideration when applying the wheel load of the HL-93 truck on the exterior bridge girder. The width of the guard rail is 1.5 ft. and the first wheel load was position 2 ft. away from the edge of the guard rail, as shown in figure 122. The second wheel load is applied to the interior beam. In order to apply lever rule, a hinge was placed at the center of the adjacent interior beam. The reaction in the exterior NEXT beam is examined at the center of the exterior unit.
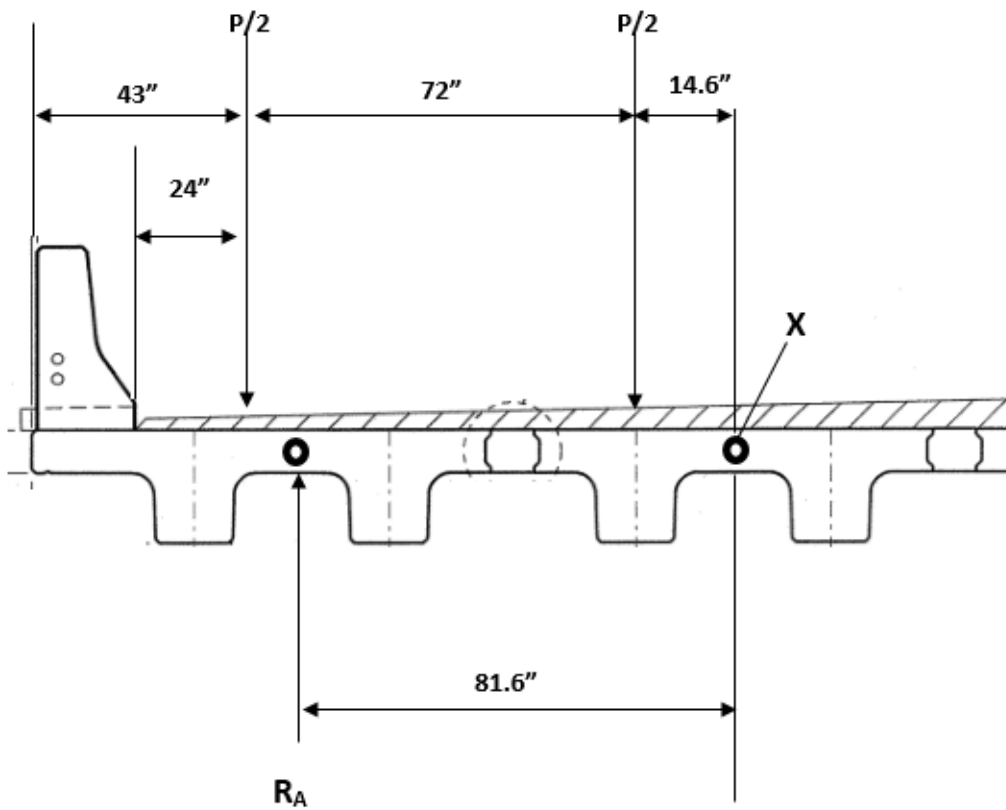
Figure 122: Type (i) and (k) Lever Rule

One Lane Loading

By summing the moments about point x, the exterior girder DFM is calculated.

$$gM_1^{e-} = 0.62$$

A.4.2 Interior DFM Calculation – Type (k) Approach

$$b_{stem} := 14in$$

$$h_{stem} := 13in$$

$$A_{bs} := b_{stem} \cdot h_{stem} = 182in^2$$

$$I_{bs} := \frac{b_{stem} \cdot h_{stem}^3}{12} = 2.563 \times 10^3 in^4$$

$$\eta := 1$$

$$e_g := 10.5in$$

$$K_g := \eta \cdot \left(I_{bs} + A_{bs} \cdot e_g^2 \right) = 2.263 \times 10^4 in^4$$

$$S := 3.4ft \qquad L := 40ft \qquad t_s := 8in$$

$$S := 3.4 \qquad L := 40 \qquad t_s := 8 \qquad K_g := 22630$$

$$InteriorDFM_{k1} := 2 \cdot \left[0.06 + \left(\frac{S}{14} \right)^{0.4} \cdot \left(\frac{S}{L} \right)^{0.3} \cdot \left[\frac{K_g}{\left(12 \cdot L \cdot t_s^3 \right)} \right]^{0.1} \right] = 0.547$$

$$InteriorDFM_{k2} := 2 \cdot \left[0.075 + \left(\frac{S}{9.5} \right)^{0.6} \cdot \left(\frac{S}{L} \right)^{0.2} \cdot \left[\frac{K_g}{\left(12 \cdot L \cdot t_s^3 \right)} \right]^{0.1} \right] = 0.669$$

A.4.3 Interior DFM Calculation – Type (i) Approach

$$A_{bs} := A_{bs} \cdot 2 = 364 \text{in}^2$$

$$I_{bs} := I_{bs} \cdot 2 = 5.126 \times 10^3 \text{in}^4$$

$$K_g := \eta \cdot \left(I_{bs} + A_{bs} \cdot e_g^2 \right) = 4.526 \times 10^4 \text{in}^4$$

$$S := 6.8 \text{ft} \qquad L := 40 \text{ft} \qquad t_s := 8 \text{in}$$

$$S := 6.8 \qquad L := 40 \qquad t_s := 8 \qquad K_g := 45260$$

$$\text{InteriorDFM}_1 := \left[0.06 + \left(\frac{S}{14} \right)^{0.4} \cdot \left(\frac{S}{L} \right)^{0.3} \cdot \left[\frac{K_g}{\left(12 \cdot L \cdot t_s^3 \right)} \right]^{0.1} \right] = 0.432$$

$$\text{InteriorDFM}_2 := 0.075 + \left(\frac{S}{9.5} \right)^{0.6} \cdot \left(\frac{S}{L} \right)^{0.2} \cdot \left[\frac{K_g}{\left(12 \cdot L \cdot t_s^3 \right)} \right]^{0.1} = 0.56$$

A.5 Solid Slab Super Structure at Hanging Rock Creek Bridge

Span 4 of the Hanging Rock Creek Bridge consists of 14 40 ft. long solid slab bridge girders as shown in figure 123. The bridge has guard rails on the east and west sides, respectively, each with a width of 1.5 ft. The solid slab girder is 3' wide and 1'9" deep. The total width of the bridge is 42 ft.
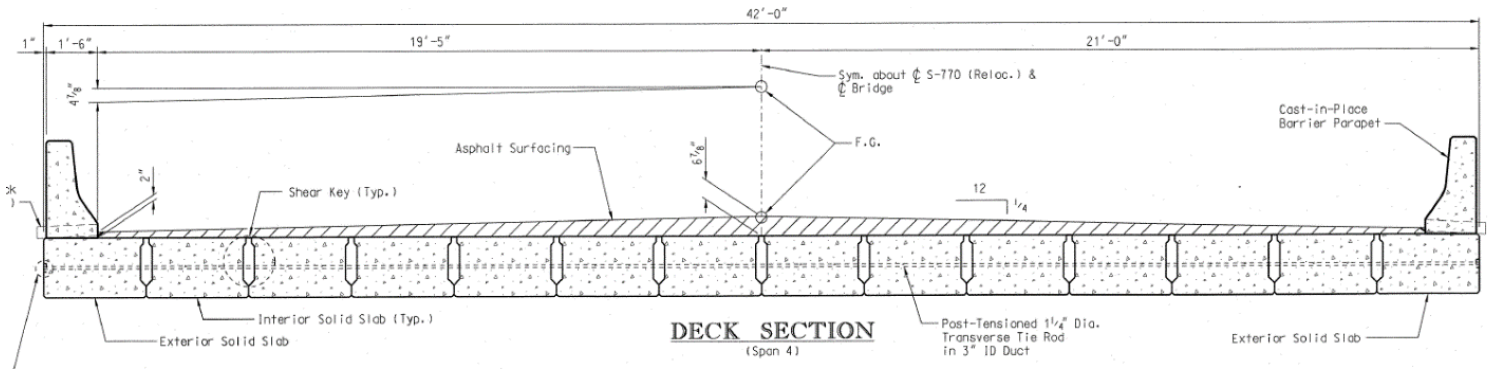
Figure 123: Solid Slab Cross-Section from Hanging Rock Bridge

A.5.1 Interior DFM Calculation – Type (g) Approach

$N_b := 14$ *# of beams

$k := 2.5 \cdot N_b^{-0.2} = 1.475$ * k must ≥ 1.5

$k := 1.5$

$b := 36$ *Width of girder

$L := 40$ *Span length

$\dfrac{I}{J}$ can be simplified using AASHTO Table 4.6.2.2.1-2

$d := 21$ *depth of girder

$x = I/J$

$x := 0.54 \cdot \left(\dfrac{d}{b} \right) + 0.16 = 0.475$

*Single Truck

$InteriorDFM_{1} := k \cdot \left(\dfrac{b}{33.3L} \right)^{0.5} \cdot (x)^{0.25} = 0.205$

*Double Truck

$InteriorDFM_{2} := k \cdot \left(\dfrac{b}{305} \right)^{0.6} \cdot \left(\dfrac{b}{12 \cdot L} \right)^{0.2} \cdot (x)^{0.06} = 0.237$

Interior DFM = 0.24

179

A.5.2 Exterior DFM Calculation – Type (g) Approach

*Single Lane Load

$d_e := 0.083$ *horizontal distance from the centerline of the exterior web to
Works Cited   exterior beam at deck level to the interior edge of curb or traffic barrier (ft)

$e := 1.125 + \dfrac{d_e}{30} = 1.128$ *d_e must ≥ 1.0

$ExteriorDFM_{e1} := e \cdot InteriorDFM_2 = 0.267$

*Double Lane Load

$e := 1.04 + \dfrac{d_e}{25} = 1.043$

$ExteriorDFM_{e2} := e \cdot InteriorDFM_2 = 0.247$

Exterior DFM = 0.27

Appendix B: Predicted NEXT D Bending Strain

Using the moving load function on SAP the max moment was found to be...

$M := 394.06 \text{kip·ft}$

$M := 0.5M$ *Assume half of truck moment goes into girder

$E := 4640.1 \text{ksi}$

$I := 35895 \text{in}^4$

$\phi := \dfrac{M}{E \cdot I} = 1.42 \times 10^{-5} \cdot \dfrac{1}{\text{in}}$

$\phi := \phi \cdot 10^6 = 14.196 \cdot \dfrac{1}{\text{in}}$

$y := 13.27 \text{in}$

$\mu\varepsilon := \phi \cdot y = 188.375$

Appendix C: Predicted Solid Slab Bending Strain

Estimated Bending Strain in Solid Slab Girders

Using the moving load function on SAP the max moment was found to be...

$M := 394.06 \text{kip} \cdot \text{ft}$

$M := 0.5M$ *Assume half of truck moment goes into girder

$f_c := 6500$ psi

$E := 57000 \cdot \sqrt{f_c} \cdot \text{psi} = 4.595 \times 10^3 \text{ksi}$

width:= 36in

depth := 21in

$I := \dfrac{\text{width} \cdot \text{depth}^3}{12} = 2.778 \times 10^4 \text{in}^4$

$\phi := \dfrac{M}{E \cdot I} = 1.852 \times 10^{-5} \cdot \dfrac{1}{\text{in}}$

$\phi := \phi \cdot 10^6 = 18.518 \cdot \dfrac{1}{\text{in}}$

$y := \dfrac{\text{depth}}{2} = 10.5 \text{in}$

$\mu\varepsilon := \phi \cdot y = 194.443$

Works Cited

AASHTO LRFD Bridge Design Specifications. Washington: AASHTO, 2010. Print.

Ahmad, Anwar S. *Bridge Preservation Guide*. London: Teach Yourself, 2003. FHWA-HIF-
    11042. *FHWA*. Aug. 2011. Web. 23 May 2017.

Bahjat, Rami, Deidre Ericson, Sergio F. Brena, and Sc A. Civjan. "Evaluation of Moment Live-
    Load Distribution of a NEXT-F Beam Bridge Through Field Load Testing and FE
    Modeling." *PCI/NBC* (2014): n. pag. 2014. Web. 23 May 2017.

Barker, Richard M., and Jay Alan. Puckett. *Design of Highway Bridges: An LRFD Approach*.
    Hoboken, N.J: Wiley, 2007. Print.

Barnes, Robert, J. Stallings, and Paul Porter. "Live-Load Response of Alabama's High-
    Performance Concrete Bridge." *Transportation Research Record: Journal of the
    Transportation Research Board* 1845 (2003): 115-24. Web.

Barnes, Robert, J. Stallings, and Paul Porter. "Live-Load Response of Alabama's High-
    Performance Concrete Bridge." *Transportation Research Record: Journal of the
    Transportation Research Board* 1845 (2003): 115-24. Web.

"Bridges." *ASCE's 2017 Infrastructure Report Card*. N.p., 2017. Web. 23 May 2017.

Cai, Chun S., and Mohsen Shahawy. "Understanding Capacity Rating of Bridges from Load
    Tests." *Practice Periodical on Structural Design and Construction* 8.4 (2003): 209-16.
    Web. 23 May 2017.

Casas, Joan R., Piotr Olaszek, Aljosa Sajna, Ales Znidaric, and Igor Lavric. *Recommendations
    on the Use of Soft, Diagnostic and Proof Load Testing*. Rep. ARCHES Project. VI EU
    Framework Prgram, 30 Aug. 2009. Web. 23 May 2017.

Chajes, Michael, Harry Shenton, and Dennis O'shea. "Bridge-Condition Assessment and Load

    Rating Using Nondestructive Evaluation Methods." *Transportation Research Record:*

    Journal of the Transportation Research Board 1696 (2000): 83-91. Web.

Chen, Wai-Fah. *Bridge Engineering Handbook, Second Edition: Construction and*

    Maintenance. N.p.: CRC, 2014. Print.

Culmo, Michael. "NEXT Beam Research Question." Message to the author. 22 Sept. 2016. E-

    mail.

Culmo, Michael P., and Rita L. Seraderian. "Development of the Northeast Extreme Tee

    (NEXT) Beam for Accelerated Bridge Construction." *PCI Journal* (2010): 86-101.

    Summer 210. Web. 23 May 2017.

D'Alessandro, Kacie. *Biaxial Behavior of Ultra-High Performance Concrete and Waffle Slab*

    Bridge Deck Design Criteria. Diss. Virginia Tech, 2013. N.p.: n.p., n.d. Print.

Deery, Daniel Patrick. *Investigation of Northeast Extreme Tee (NEXT) D Beam Bridges as an*

    Alternative to Precast Hollow Core Bridges: An Exploration of Appropriate Slab Design

    Forces. Thesis. Clemson University, 2010. N.p.: n.p., n.d. Print.

"Ductal®, Ultra-high Performance Concrete (UHPC)." *Lafarge.com*. N.p., 06 Aug. 2015. Web.

    23 May 2017.

Ei-Remaily, Ahmed, Maher K. Tadros, Takashi Yamane, and Gary Krause. "Transverse Design

    of Adjacent Precast Prestressed Concrete Box Girder Bridges." *PCI Journal* 41.4 (1996):

    96-113. Web.

Ericson, Deidre, Sergio F. Brena, Scott A. Civjan, and Abhijeet Singh. *Evaluation of Live-load*

    Distribution Factors for NEXT-F Beam Bridges. Rep. Department of Civil and

Environmental Engineering University of Massachusetts Amherst, n.d. Web. 23 May

    2017.

Field, Carrie S. *VHPC Material Characterization and Recommendations for the Buffalo Branch*

    Bridge Rehabilitation. Thesis. Virginia Tech, 2015. N.p.: n.p., n.d. Print.

Gardner, Lauren S., and Steven M. Hodgdon. "The First NEXT Beam Bridge." *PCI*

    Journal 58.1 (2013): 55-62. Winter 2013. Web. 23 May 2017.

Graybeal, Benjamin A., and Henry G. Russell. "Ultra-High Performance Concrete: A State-of-

    the-Art Report for the Bridge Community." *FHWA* FHWA-HRT-13-060 (2013): n. pag.

    June 2013. Web. 23 May 2017.

Graybeal, Benjamin A. "Behavior of Field-Cast Ultra-High Performance Concrete Bridge Deck

    Connections Under Cyclic and Static Structural Loading." *FHWA* FHWA-HRT-11-023

    (2010): n. pag. Nov. 2010. Web. 23 May 2017.

Graybeal, Benjamin A. *Material Property Characterization of Ultra-High Performance*

    Concrete. Tech. no. FHWA-HRT-06-103. N.p.: n.p., 2006. Print.

Graybeal, Benjamin. "Design and Construction of Field-Cast UHPC Connections." *FHWA* 14-

    084 FHWA.HRT (2014): n. pag. Web.

"Guidelines for Northeast Extreme Tee Beam." *PCI Northeast* (2012): n. pag. 2012. Web. 23

    May 2017.

Gunter, Robert S. *STRUCTURAL EVALUATION OF SCDOT PRESTRESSED CHANNEL*

    BRIDGES. Thesis. Clemson University, 2016. N.p.: n.p., n.d. Print.

Halbe, Kedar Ram. *New Approach to Connections between Members of Adjacent Box Beam Bridges*. Thesis. Virginia Polytechnic Institute and State University, 2014. N.p.: n.p., n.d. Print.

Hiens, C.P., and C.F. Galambos. "Highway Bridge Field Tests in the United States 1948-70." *Public Roads Journal* 36.12 (1972): n. pag. Print.

Joyce, Patrick C. *Development of Improved Connection Details for Voided Slab Bridges*. Thesis. Virginia Polytechnic Institute and State University, 2014. N.p.: n.p., n.d. Print.

Medlock, Ronnie, Kenneth C. Bauer, and Rita Seraderian. "A Next Time." *Bridge Construction* (2010): S18-20. Aug. 2010. Web. 23 May 2017.

Miller, Richard A., George M. Hlavacs, Todd Long, and Andreas Greuel. "Full-Scale Testing of Shear Keys for Adjacent Box Girder Bridges." *PCI Journal* 44.6 (1999): 80-90. Web.

Neely, W. Douglas, Thomas E. Cousins, and John J. Lesko. "Evaluation of In-Service Performance of Tomâ™s Creek Bridge Fiber-Reinforced Polymer Superstructure." *Journal of Performance of Constructed Facilities* 18.3 (2004): 147-58. Web. 23 May 2017.

"The NEXT Beam [PowerPoint]." *High Bridge Team*. Web.

Nielson, Bryant G., Scott D. Schiff, Weichiang Pang, and Huan Sheng. "Identifying a Durable and ABC Precast Alternative to Short-Span, Flat-Slab Concrete Bridges: An Overview." 2012. Lecture.

Restrepo, Edgar Salom. *Determination of AASHTO Bridge Design Parameters through Field Evaluation of the Rt. 601 Bridge: A Bridge Utilizing Strongwell 36 In. Fiber-Reinforced*

Polymer Double Web Beams as the Main Load Carrying Members. Thesis. Virginia

Polytechnic Institute and State University, 2002. N.p.: n.p., n.d. Print.

Sartor, Richard R., Michael P. Culmo, and John T. Dewolf. "Short-Term Strain Monitoring of

Bridge Structures." *Journal of Bridge Engineering* 4.3 (1999): 157-64. Web.

Seraderian, Rita L. "Developing Precast Guidelines for Accelerated Bridge Construction." *PCI*

Northeast (n.d.): n. pag. Web. 23 May 2017.

Seraderian, Rita L. "Northeast Extreme Tee Beam [Powerpoint]." *PCI Northeast* (2016): n. pag.

2 Feb. 2016. Web. 23 May 2017.

Sheng, Huan, Bryant G. Nielson, Weichiang Pang, and Scott D. Schiff. "Precast Alternative for

Flat Slab Bridges." *Home - Transport Research International Documentation - TRID*.

N.p., 30 Sept. 2013. Web. 27 June 2017.

Singh, Abhijeet Kumar. *Evaluation of Live-load Distribution Factors (LLDFs) of next Beam*

Bridges. Thesis. University of Massachusetts - Amherst, 2012. N.p.: n.p., n.d. Print.

"Ultra-High Performance Concrete UHPC." *Homeland Security Science and Technology* (n.d.):

n. pag. Web. 23 May 2017.

Zokaie, Toorak, and Roy Imbsen. "Distribution of Wheel Loads on Highway

Bridges." *NCHRP* 12.26 (1993): n. pag. Print.